

“The glory of God is intelligence, or, in
other words, light and truth.”

D&C 93:36

University of Alberta

Improving the Spectral Stability of Poly(9,9-dioctylfluorene) (PFO) Through the
use of Aromatic Ethers
by

Matthew Ron Sirtonski

A thesis submitted to the Faculty of Graduate Studies and Research
in partial fulfillment of the requirements for the degree of

Master of Science

Department of Chemistry

©Matthew Ron Sirtonski

Spring 2011
Edmonton, Alberta

Permission is hereby granted to the University of Alberta Libraries to reproduce single copies of this thesis and to lend or sell such copies for private, scholarly or scientific research purposes only. Where the thesis is converted to, or otherwise made available in digital form, the University of Alberta will advise potential users of the thesis of these terms.

The author reserves all other publication and other rights in association with the copyright in the thesis and, except as herein before provided, neither the thesis nor any substantial portion thereof may be printed or otherwise reproduced in any material form whatsoever without the author's prior written permission.

Examining Committee

Dr. Jonathan G. C. Veinot, Chemistry

Dr. Arthur Mar, Chemistry

Dr. Al Meldrum, Physics

Acknowledgements

First of all thanks are due to my supervisor, Dr. Jonathan Veinot and the Veinot Research Group. Thanks for all your help and support. Special thanks go to the polymer team (both past and present): Shaune McFarlane, Davin Piercy, Leah Coumont, Lydia Glover, Brenna Brown, Alex Dobby (Lippy), and Kale Edwards for putting up with my antics and of course for all the help. Mike Fleischauer, Ryan Tucker and Al Lalany are thanked for their assistance with the PLEDs. Rory Chisholm is thanked for training me on the AFM. Rachele Day for taking the PLM images. Adam Malcolm for doing the GPC. ACSES for the SEM, AES, and XPS analyses. In addition I would like to thank the NMR, MS, and the Analytical services laboratories for their assistance. The electronics, machine, and glass shops are also thanked for their hard work. Others that deserve thanks for a variety of reasons include Jorge Cham, Lance Holmstrom, Reuben McGill, Kevin Morais, Mark Summers, McKay White, and all my scouts.

Finally, I want to thank my family. Mom and Dad, you've always been there, especially when I needed you. Laura, I don't know how we didn't kill each other as kids, but I'm glad we survived. Lastly, I want to thank the four most important people in the entire world to me: Veronica, Zoe, Sahara, and Kirsten, you are the loves of my life. Thank you so much for all the love, support, understanding and fun. You make life worth it, and none of this would have been possible without you. I look forward to seeing what comes from all these years of schooling and where we end up.

Abstract

Aromatic ethers (AEs) have been combined with poly(9,9-dioctylfluorene) (PFO) to improve spectral stability in PFO systems. Compared to neat PFO, PFO/AE blends were found to have decreased 'g-bands' following heating in air. Some were further found to induce and maintain β -phase emission. The PFO/polyphenyl ether (PPE) blend was incorporated into polymer-light emitting diodes exhibiting blue electroluminescence and good efficiencies.

A new AE monomer (bis(4-bromophenoxy) benzene) was synthesized via iron-mediated nucleophilic aromatic substitution. Random AE/PFO copolymers were synthesized via Yamamoto (PAEFO), and Suzuki-Miyaura (PAEFO-S) cross-couplings of bis(4-bromophenoxy) benzene and 2,7-dibromo-9,9-dioctylfluorene (DOF). Another random AE/PF copolymer (PAEFO-2) was synthesized from bis(4-bromophenyl) ether and DOF via Yamamoto cross-coupling. Increasing the AE content in these polymers was found to decrease the 'g-band' and no phase changes were evidenced.

The results show PFOs spectral stability can be improved by both blending and copolymerizing with AEs.

Table of Contents

| | | |
|-------------------|---|----|
| Chapter 1: | Introduction to Polyfluorene-Based Materials | |
| 1.1 | Conductive Polymers..... | 2 |
| 1.2 | Light Emitting Polymers..... | 4 |
| 1.3 | Polymer Light Emitting Diodes..... | 5 |
| 1.4 | Polyfluorenes..... | 6 |
| 1.5 | PFO Phases..... | 7 |
| 1.6 | Origin of Green Emission in Polyfluorenes..... | 8 |
| 1.7 | Methods of Spectral Stabilization..... | 10 |
| 1.8 | Characterization Methods..... | 10 |
| 1.9 | Thesis Outline and Importance..... | 10 |
| 1.10 | References..... | 11 |
| Chapter 2: | Polyfluorene/Aromatic Ether Blends | |
| 2.0 | Introduction..... | 16 |
| 2.1 | Experimental..... | 20 |
| 2.1.1 | Materials..... | 20 |
| 2.1.2 | Film Preparation..... | 20 |
| 2.1.3 | Film Characterization..... | 21 |
| 2.1.4 | PLED Fabrication and Testing..... | 21 |
| 2.2 | Results and Conclusions..... | 22 |
| 2.2.1 | Blend Fabrication and Characterization..... | 22 |
| 2.2.2 | Thermogravimetric Analysis of the Blends..... | 22 |
| 2.2.3 | Beta-Phase Incorporation..... | 24 |
| 2.2.4 | Spectral Stability in the Presence of Oxygen..... | 27 |
| 2.2.5 | Blend Concentration Studies..... | 32 |
| 2.2.6 | Method of Stabilization..... | 36 |
| 2.2.7 | Surface/Film Structure..... | 37 |
| 2.2.8 | Polymer Light Emitting Diodes..... | 38 |
| 2.2.9 | Conclusions..... | 41 |
| 2.3 | References..... | 42 |
| Chapter 3: | Aromatic Ether-Dioctylfluorene Random Copolymers | |
| 3.0 | Introduction..... | 45 |
| 3.1 | Experimental..... | 48 |

| | | |
|------------------------------|---|-----|
| 3.1.1 | Chemicals..... | 48 |
| 3.1.2 | Procedures..... | 49 |
| 3.1.3 | Characterization..... | 49 |
| 3.1.4 | Synthesis of Bis(4-bromophenoxy) benzene..... | 49 |
| 3.1.5 | Synthesis of PAEFO..... | 50 |
| 3.1.6 | Synthesis of PAEFO-2..... | 51 |
| 3.1.7 | Synthesis of PAEFO-S..... | 51 |
| 3.2 | Results and Discussion..... | 52 |
| 3.2.1 | Monomer Synthesis..... | 52 |
| 3.2.2 | Monomer Characterization..... | 52 |
| 3.2.3 | Polymer Synthesis..... | 53 |
| 3.2.4 | Polymer Characterization..... | 54 |
| 3.2.5 | Absorption/Emission Spectra..... | 58 |
| 3.2.6 | Phase Stability..... | 61 |
| 3.2.7 | Spectral Stability in the Presence of Oxygen..... | 63 |
| 3.2.8 | Method of Spectral Improvement..... | 66 |
| 3.2.9 | Magnetism/Conductance..... | 67 |
| 3.2.10 | Conclusions..... | 68 |
| 3.3 | References..... | 68 |
| Chapter 4: Conclusion | | |
| 4.0 | Conclusion..... | 72 |
| 4.1 | Future work..... | 74 |
| 4.1.1 | Polyfluorene/Aromatic Ether Blends..... | 74 |
| 4.1.2 | Aromatic Ether-Dioctylfluorene Random Copolymers..... | 74 |
| 4.1.3 | Aromatic Ether Macrocyclic Fluorenes..... | 77 |
| 4.1.4 | Trispirobifluorene-Fluorene Random Copolymers..... | 80 |
| 4.2 | References..... | 83 |
| Appendixes | | |
| A2 | Appendix 2..... | 86 |
| A3 | Appendix 3..... | 88 |
| A4 | Appendix 4..... | 106 |

List of Tables

| | | |
|------------------|---|----|
| Table 2-1 | Weight percent concentrations of PFO and PPE in the five blends investigated..... | 33 |
| Table 3-1 | Monomer masses used and the associated monomer ratios in the Yamamoto synthesis of PAEFO | 50 |
| Table 3-2 | Monomer masses used and the associated monomer ratios in PAEFO-2 synthesis..... | 51 |
| Table 3-3 | EA calculated and found for each polymer based on fluorene:AE monomer ratios..... | 55 |
| Table 3-4 | Monomer ratios for each PAEFO and PAEFO-2 copolymer combined with molar ratios for each as determined from the integration of the ¹ H NMR spectra..... | 56 |
| Table 3-5 | Estimated average number of fluorene and AE monomer units per 2:1 PAEFO chain..... | 57 |
| Table 3-6 | Absorbance and emission spectra maxima as measured for all Polymers (emission maxima for α -phase PFO in brackets) | 59 |
| Table 3-7 | Integrated intensity ratios for each of the polymers studied..... | 64 |

List of Figures

| | | |
|--------------------|--|----|
| Figure 1-1 | Structures of PA, PPy, PT, PANI, PPP, PF, and PPV..... | 2 |
| Figure 1-2 | Structures of alkyl substituted PT, PPP, PF and PPV (R, R ₁ , R ₂ = Alkyl chain...) | 2 |
| Figure 1-3 | MO diagram for the π -bond in one repeat unit of PA, with the corresponding π -orbital overlap diagrams..... | 3 |
| Figure 1-4 | Energy levels for the π -orbitals in two repeat units of PA with corresponding π -orbital overlap diagrams..... | 3 |
| Figure 1-5 | Band diagram of conjugated polymers | 4 |
| Figure 1-6 | Structure of polycarbazole | 5 |
| Figure 1-7 | General structure of a PLED..... | 6 |
| Figure 1-8 | Structures of PEDOT and PSS..... | 6 |
| Figure 1-9 | Numbering system for PFs..... | 7 |
| Figure 1-10 | Torsion angles of α -phase (left), β -phase (right), and γ -phase (middle) regions looking along the polymer backbone (R = octyl groups)..... | 8 |
| Figure 1-11 | Structures of the four oligomers used by Chan <i>et al.</i> | 9 |
| Figure 2-1 | Structures of PF C26, TPTE, ST 755, and ST 16/7..... | 17 |
| Figure 2-2 | Structure of DFD..... | 17 |
| Figure 2-3 | Structures of PVQ and PS..... | 18 |
| Figure 2-4 | Structures of PPO, PSU, PPE, DE, m-DB, and p-DB..... | 22 |
| Figure 2-5 | TGA traces of PFO (red trace), PPO (black trace), PSU (green trace), and PPE (blue trace) under a nitrogen atmosphere at a heating rate of 10 °C/min..... | 23 |
| Figure 2-6 | Normalized UV-vis absorbance spectra of a representative 100 nm thick PFO thin film. Films were prepared by spin coating chloroform solutions containing 1% w/v PFO onto quartz substrates. Pristine film (—) and film annealed in nitrogen at 140 °C for 2 hours (---)..... | 25 |
| Figure 2-7 | Normalized UV-vis absorbance spectra of a representative 1-1 PFO-PPE composite thin film of nominally 100 nm thickness prior to annealing (—) and following annealing in nitrogen at 140 °C for 2 hours (---)..... | 26 |

| | |
|--------------------|---|
| Figure 2-8 | Normalized photoluminescence spectra of PFO (A-red traces) and PFO-PPE blend (B-blue traces) thin films (<i>ca.</i> 100 nm) measured prior to (—) and following (---) annealing in nitrogen ($\lambda_{\text{ex}} = 350$ nm).....27 |
| Figure 2-9 | Normalized PL spectra of thin films cast from solutions of PFO (red trace), PFO-PPO (black trace), PFO-PSU (green trace), and PFO-PPE (blue trace) measured prior to (A) and following (B) heating in air ($\lambda_{\text{ex}} = 350$ nm).....29 |
| Figure 2-10 | Normalized PL spectra of thin films cast from solutions of PFO (red trace), PFO-DE (green trace), PFO-m-DB (black trace), PFO-p-DB (cyan trace) and PFO-PPE (blue trace) measured prior to (A) and following (B) heating in air ($\lambda_{\text{ex}} = 350$ nm).....31 |
| Figure 2-11 | Normalized PL spectra of thin films spin-cast (blue trace) and drop-cast (cyan trace) from PFO-PPE solution measured following heating in air for one hour ($\lambda_{\text{ex}} = 350$ nm).....32 |
| Figure 2-12 | PFO-PPE blend composition dependence of absorbance spectra of thin films (<i>ca.</i> 100 nm) spin-coated from these blend solutions (1-1: blue, 3-1: black, 5-1: green, 8-1: orange, PFO: red).....33 |
| Figure 2-13 | Normalized photoluminescence spectra of PFO-PPE blend thin films (<i>ca.</i> 100 nm), spin-coated from their respective solutions (I: 1-1, II: 3-1, III: 5-1, IV: 8-1, V: PFO), measured prior to (—) and following (---) annealing in air ($\lambda_{\text{ex}} = 350$ nm).....34 |
| Figure 2-14 | Normalized photoluminescence spectra of thin films (<i>ca.</i> 100nm) cast from solutions of the PFO-PPE blend (A) and PFO (B) measured prior to (black) and following annealing in air for one hour (blue), three hours (green), five hours (orange), twenty-two hours (pink), and twenty-five hours (red) ($\lambda_{\text{ex}} = 350$ nm).....35 |
| Figure 2-15 | Normalized photoluminescence spectra of air-annealed PFO film (green), re-annealed in air (red), and re-annealed in air with PPE on top (blue) ($\lambda_{\text{ex}} = 350$ nm).....37 |
| Figure 2-16 | (A) Current versus voltage and (B) light output versus voltage for devices made from the 1-1 blend (blue) and PFO (red).....39 |
| Figure 2-17 | (A) External quantum efficiency versus voltage and (B) normalized electroluminescence spectra of devices made from the 1-1 blend (blue) and PFO (red).....41 |
| Figure 3-1 | Structures of PFO, PFH, LPPP, and PIF.....46 |
| Figure 3-2 | TGA curves of PTE, MTE and DOF monomers in N ₂ and air atmospheres. Samples were heated at 10 °C/min.....58 |
| Figure 3-3 | Normalized UV-vis absorbance spectra of a representative PFO film (red trace), representative PAEFO films (2:1 blue trace, 7:1 purple trace, and 13:1 orange |

| | | |
|-------------------|---|----|
| | trace), representative PAEFO-2 films (2:1 cyan trace, and 11:1 green trace), and a representative PAEFO-S film (black trace)..... | 59 |
| Figure 3-4 | Normalized PL spectra of representative PFO (red trace), PAEFO (2:1 blue trace, 7:1 purple trace, and 13:1 orange trace), PAEFO-2 (2:1 cyan trace, and 11:1 green trace), and PAEFO-S (black trace) films ($\lambda_{\text{ex}} = 350 \text{ nm}$)..... | 61 |
| Figure 3-5 | Normalized UV-vis absorbance spectra of representative PFO (red trace), PAEFO (2:1 blue trace, 7:1 purple trace, and 13:1 orange trace), PAEFO-2 (2:1 cyan, and 11:1 green trace), and PAEFO-S (black trace) films all measured following heating at 140 °C in a nitrogen environment..... | 62 |
| Figure 3-6 | Normalized PL spectra of representative PFO (A-red traces) and PAEFO (B-blue traces) thin films (ca. 100 nm) measured prior to (—) and following heating for 1 hour (---), and 20 hours (···) in nitrogen ($\lambda_{\text{ex}} = 350 \text{ nm}$)..... | 63 |
| Figure 3-7 | Normalized PL spectra of representative PFO (red trace), PAEFO (2:1 blue trace, 7:1 purple trace, and 13:1 orange trace), PAEFO-2 (2:1 cyan trace, and 11:1 green trace), and PAEFO-S (black trace) films measured following heating for 1 hour in air ($\lambda_{\text{ex}} = 350 \text{ nm}$)..... | 64 |
| Figure 3-8 | Normalized PL spectra of representative PFO (red trace), PAEFO (2:1 blue trace, 7:1 purple trace, and 13:1 orange trace), PAEFO-2 (2:1 cyan trace, and 11:1 green trace), and PAEFO-S (black trace) films measured following heating for 5 hours in air ($\lambda_{\text{ex}} = 350 \text{ nm}$)..... | 65 |
| Figure 3-9 | Normalized PL spectra of representative 2:1 PAEFO (blue trace), 2:1 PAEFO-2 (cyan trace), and PAEFO-S (black trace) films measured following heating for 20 hours in air ($\lambda_{\text{ex}} = 350 \text{ nm}$)..... | 66 |
| Figure 4-1 | UV-vis absorbance of PEDOT:PSS (blue trace) and PAEFO (black trace)..... | 75 |
| Figure 4-2 | Structures of BPA, BP, 4,4-diphenoxy diphenyl ether, CAEF-1, CAEF-2, and CAEF-3..... | 78 |
| Figure 4-3 | Proposed structures of some of the main actual products obtained from the attempted synthesis of CAEF-2 (See Figure A4-5 for MALDI-TOF MS)..... | 79 |
| Figure 4-4 | Structures CAE-1, CAE-2, and CAE-3..... | 80 |
| Figure 4-5 | MALDI-TOF MS of CAE-1 with macrocycle repeat unit in the inset..... | 80 |
| Figure 4-6 | Trispirobifluorene..... | 81 |
| Figure 4-7 | PL spectra of PSFO measured in CHCl_3 solution (blue trace) and thin film (red trace) ($\lambda_{\text{ex}} = 350 \text{ nm}$)..... | 82 |
| Figure 4-8 | Spirobifluorene..... | 83 |

| | | |
|---------------------|---|-----|
| Figure A2-1 | Stacked AES spectra measured at four different points on thin film cast from 1-1 blend, showing carbon peak at ca. 260 nm, and a weak oxygen peak at ca. 510 nm (highlighted by the grey oval/dotted line)..... | 86 |
| Figure A2-2 | Stacked AES spectra measured at four different points on thin film cast from PFO, showing a carbon peak at ca. 260 nm, and no oxygen peak (highlighted by the grey oval)..... | 87 |
| Figure A3-1 | EI MS of bis(4-bromophenoxy) benzene..... | 88 |
| Figure A3-2 | FTIR spectrum of bis(4-bromophenoxy) benzene..... | 88 |
| Figure A3-3 | ¹ H NMR spectrum of bis(4-bromophenoxy) benzene..... | 89 |
| Figure A3-4 | ¹³ C-NMR spectrum of bis(4-bromophenoxy) benzene..... | 90 |
| Figure A3-5 | HMQC 2D NMR spectrum of bis(4-bromophenoxy) benzene..... | 91 |
| Figure A3-6 | Bis(4-bromophenoxy) benzene with ¹³ C NMR assignments shown. ¹ H NMR assignments are as follows: a protons are bonded to C ₃ 's, b protons are bonded to C ₄ 's, and c protons are bonded to C ₅ 's..... | 91 |
| Figure A3-7 | ¹ H NMR spectrum of 2:1 PAEFO..... | 92 |
| Figure A3-8 | ¹³ C-NMR spectrum of 2:1 PAEFO..... | 93 |
| Figure A3-9 | MALDI-TOF MS of 2:1 PAEFO..... | 93 |
| Figure A3-10 | GPC of 2:1 PAEFO..... | 94 |
| Figure A3-11 | ¹ H-NMR spectrum of 7:1 PAEFO..... | 95 |
| Figure A3-12 | ¹³ C-NMR spectrum of 7:1 PAEFO..... | 96 |
| Figure A3-13 | MALDI-TOF MS of 7:1 PAEFO..... | 96 |
| Figure A3-14 | ¹ H NMR spectrum of 13:1 PAEFO..... | 97 |
| Figure A3-15 | ¹³ C NMR spectrum of 13:1 PAEFO..... | 98 |
| Figure A3-16 | MALDI-TOF MS of 13:1 PAEFO..... | 98 |
| Figure A3-17 | ¹ H NMR spectrum of 2:1 PAEFO-2..... | 99 |
| Figure A3-18 | ¹³ C NMR spectrum of 2:1 PAEFO-2..... | 100 |
| Figure A3-19 | MALDI-TOF MS of 2:1 PAEFO-2..... | 101 |
| Figure A3-20 | ¹ H NMR spectrum of 11:1 PAEFO-2..... | 101 |
| Figure A3-21 | ¹³ C NMR spectrum of 11:1 PAEFO-2..... | 102 |

| | | |
|---------------------|---|-----|
| Figure A3-22 | MALDI-TOF MS of 11:1 PAEFO-2..... | 102 |
| Figure A3-23 | ¹ H NMR spectrum of PAEFO-S..... | 103 |
| Figure A3-24 | ¹³ C NMR spectrum of PAEFO-S..... | 104 |
| Figure A3-25 | MALDI-TOF MS of PAEFO-S..... | 104 |
| Figure A3-26 | Photograph demonstrating the magnetic properties in PAEFO..... | 105 |
| Figure A3-27 | XPS of 11:1 PAEFO-2 showing region for Ni(0) in the inset..... | 105 |
| Figure A4-1 | MALDI-TOF MS of PAEFO synthesized without the use of a microwave..... | 106 |
| Figure A4-2 | ES MS of CAEF-1..... | 106 |
| Figure A4-3 | ES MS of CAEF-2..... | 107 |
| Figure A4-4 | ES MS of CAEF-3..... | 107 |
| Figure A4-5 | MALDI-TOF MS of CAEF-2..... | 108 |
| Figure A4-6 | ES MS of CAE-1..... | 108 |
| Figure A4-7 | ES MS of CAE-2..... | 109 |
| Figure A4-8 | ES MS of CAE-3..... | 109 |
| Figure A4-9 | MALDI-TOF MS of PSFO..... | 110 |

List of Schemes

| | | |
|-------------------|---|----|
| Scheme 3-1 | a) Generalized Suzuki-Miyaura cross-coupling reaction, and b) Generalized Yamamoto cross-coupling reaction, where Ar = aromatic group, X = halogen, 1 = oxidative addition, 2 = transmetalation, and 3 = reductive elimination (ligands not directly involved have been omitted for clarity)..... | 47 |
| Scheme 3-2 | Synthesis of (bis(4-bromophenoxy) benzene)..... | 52 |
| Scheme 3-3 | Synthetic route to PAEFO..... | 53 |
| Scheme 3-4 | Synthetic route to PAEFO-2..... | 54 |
| Scheme 3-5 | Synthetic route to PAEFO-S..... | 54 |
| Scheme 4-1 | Synthesis of MIBC..... | 78 |
| Scheme 4-2 | Synthesis of trispirobifluorene monomer..... | 81 |

List of Abbreviations and Symbols

| | |
|------------------------|---|
| ΔG_m | free energy of mixing |
| ΔH_m | enthalpy of mixing |
| ΔS_m | entropy of mixing |
| λ | wavelength |
| λ_{abs} | absorption wavelength |
| λ_{ex} | excitation wavelength |
| π | molecular bonding orbital formed from overlap of two p orbitals |
| π^* | molecular antibonding orbital formed from two p orbitals |
| ^{13}C NMR | carbon nuclear magnetic resonance spectroscopy |
| ^1H NMR | proton nuclear magnetic resonance spectroscopy |
| 2D | two dimensional |
| Å | angstrom |
| AO | atomic orbital |
| AE | aromatic ether |
| AES | auger electron spectroscopy |
| AFM | atomic force microscopy |
| amu | atomic mass units |
| AR | aromatic group |
| a.u. | arbitrary units |
| B_{ij} | binary interaction parameter |
| BP | biphenyl |
| BPA | bisphenol-A |
| BPY | bipyridyl |
| CAE | cyclic aromatic ether |
| CAEF | aromatic ether macrocycle fluorene |
| CDCl_3 | deuterated chloroform |
| CIE | Commission Internationale de l'Eclairage |
| COD | 1,5-cyclooctadiene |
| Cp | cyclopentadienyl |
| DE | diphenyl ether |
| DFD | 2,7-bis[2-(4- <i>tert</i> -butylphenyl)-1,3,4-oxadiazol-5-yl]-9,9-dihexylfluorene |
| DMF | dimethylformamide |
| EA | elemental analysis |
| ECL | effective conjugation length |
| E_g | band-gap |
| EI | electron impact |
| EL | electroluminescence |
| EQE | external quantum efficiency |
| ES | electrospray |
| ETMs | electron transporting materials |
| eV | electron volts |

| | |
|-----------|---|
| FTIR | fourier-transform infrared spectroscopy |
| g | gram |
| 'g-band' | green emissive band seen in oxidized PFs |
| GPC | gel permeation chromatography |
| HIL | hole injection layer |
| HMQC | heteronuclear multiple quantum coherence |
| HOMO | highest occupied molecular orbital |
| HRMS | high resolution mass spectrometry |
| HTMs | hole-transporting molecules |
| ICP | inductively coupled plasma |
| ITO | indium tin oxide |
| KHz | kilohertz |
| LEDs | light-emitting diodes |
| LPPP | ladder-type poly(para-phenylene) |
| LUMO | lowest unoccupied molecular orbital |
| M | moles/liter |
| MALDI-TOF | matrix-assisted laser-desorption time-of-flight |
| m-DB | 1,3-diphenoxy benzene |
| MHz | mega hertz |
| MIBC | meta-intermediate-bimetallic-complex |
| min | minutes |
| ml | millilitre |
| M_n | number-average molecular weight |
| MO | molecular orbital |
| MS | mass spectrometry |
| M_w | weight-average molecular weight |
| nm | nanometer |
| PA | polyacetylene |
| PAEFO | bis(4-bromophenoxy) benzene-dioctylfluorene copolymer |
| PAEFO-2 | bis(4-bromophenyl) ether-dioctylfluorene copolymer |
| PAEFO-S | PAEFO synthesized using Suzuki-Miyaura cross-coupling |
| PANI | polyaniline |
| p-DB | 1,4-diphenoxy benzene |
| PDI | polydispersity index |
| PEDOT-PSS | poly(3,4-ethylenedioxythiophene)-poly(styrene sulfonate) |
| PF | polyfluorene |
| PF C26 | poly(2,7-(9,9-bis(2-ethylhexyl))co-(9,9-bis((3S)-3,7-dimethyloctyl))fluorene) |
| PFH | poly(9,9-dihexylfluorene) |
| PFO | poly(9,9-dioctylfluorene) |
| PIF | polyindenofluorene |
| PL | photoluminescence |
| PLEDs | polymer light-emitting diodes |

| | |
|---------|--|
| PLM | polarizing light microscopy |
| PPE | polyphenyl ether |
| PPO | poly(2,6-dimethyl-1,4-phenylene oxide) |
| PPP | poly(para-phenylene) |
| PPV | poly(para-phenylenevinylene) |
| PPy | polypyrrole |
| PS | polystyrene |
| PSFO | trispirobifluorene-dioctylfluorene copolymer |
| PSU | polysulfone |
| PT | polythiophene |
| PVQ | poly(vinyldiphenylquinoline) |
| RF | radiofrequency |
| RIE | reactive ion etching |
| rpm | revolutions per minute |
| SANS | small-angle neutron scattering |
| SEM | scanning electron microscopy |
| ST 16/7 | N,N'-diphenyl- N,N'-bis- α -naphthylbenzidine |
| ST 755 | starburst amine |
| TGA | thermogravimetric analysis |
| TPTE | triphenylamine tetramer |
| UV-vis | ultraviolet and visible |
| w/v | weight per volume |
| XRD | x-ray diffraction |

Chapter 1

Introduction

1.0 Introduction

1.1 Conductive Polymers

In 1977 Alan Heeger, Alan G. MacDiarmid, and Hideki Shirakawa discovered that doped polyacetylene (PA) exhibits nearly metallic conductivity.¹ Although it was known that some polymers were semiconductors or conductors when doped,²⁻⁴ their ‘discovery’ pushed this knowledge into the mainstream, starting a revolution in polymer science, and leading to these men receiving the Nobel Prize for Chemistry in 2000.⁵ Because of the limited processability and instability of PA in air, early work focused on finding alternative materials.⁶ Generally, these candidate materials maintained the fundamental PA structure of alternating single and double bonds extended through the polymer chain, and included polypyrrole (PPy),⁷ polythiophene (PT),⁸ polyaniline (PANI),⁹ poly(para-phenylene) (PPP),¹⁰ polyfluorene (PF),¹¹ and poly(para-phenylenevinylene) (PPV) (Figure 1-1).¹² All of these polymers exhibit improved stability compared to PA, but retain its poor processability. To render these polymers solution processable various functional groups (typically alkyl chains) have been added as pendant chains on the polymer backbone; unfortunately this often compromised electrical conductivity (*vide infra*).¹³ A dramatic breakthrough was realized with the development of 3-alkyl substituted PTs, when researchers were able to combine solubility with a conductivity of up to 100 S/cm (Figure 1-2).¹⁴ Following this advancement other soluble conductive polymers were synthesized including alkyl substituted PPPs,¹⁵ PPVs,¹⁶ and PFs (Figure 1-2).¹⁷ PFs are particularly promising as substitution at the methylene bridge will have little, if any, effect on the conjugation.¹³

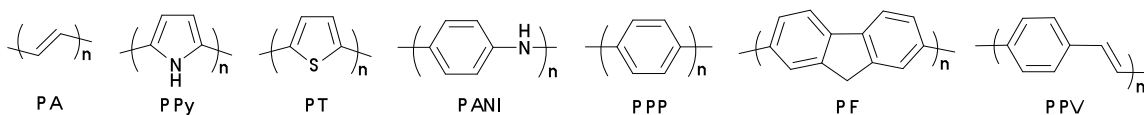


Figure 1-1 Structures of PA, PPy, PT, PANI, PPP, PF, and PPV.

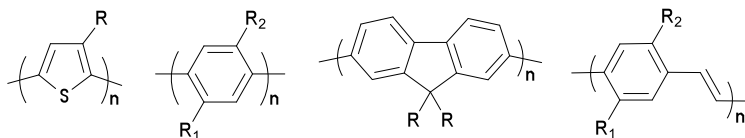


Figure 1-2 Structures of alkyl substituted PT, PPP, PF and PPV (R, R₁, R₂ = Alkyl chain).

As all these polymers are based on the PA structure of alternating single and double carbon-carbon bonds, PA will be used to explain how these polymers can be conductive. Starting with

one repeat unit of PA, and only looking at the π -electrons, we get a molecular orbital (MO) diagram as seen in Figure 1-3.

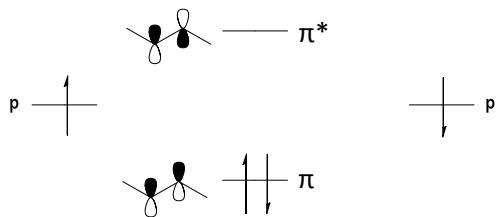


Figure 1-3 MO diagram for the π -bond in one repeat unit of PA, with the corresponding π -orbital overlap diagrams.

This interaction gives a filled bonding π -orbital and an unfilled anti-bonding π^* -orbital. The difference in energy between these two levels is often referred to as the energy gap (E_g), or HOMO-LUMO gap. This basic structure can now be built up by looking at two repeat units (Figure 1-4). With four atomic orbitals (AOs) there are now four MOs, two filled bonding orbitals and two unfilled anti-bonding ones, leading to a decrease in the E_g compared to one repeat unit.

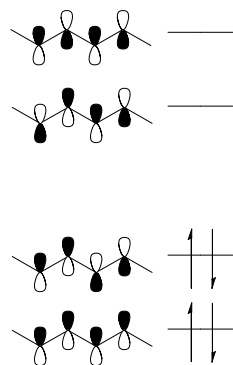


Figure 1-4 Energy levels for the π -orbitals in two repeat units of PA with corresponding π -orbital overlap diagrams.

As this system is continuously built up, more and more MOs are added, and the E_g continues to get smaller. While the E_g continues to get smaller with each MO added, the change in E_g also decreases. Thus there becomes less of a difference between each bonding orbital (same for the anti-bonding orbitals) and the energy levels in the MO diagram resemble bands (Figure 1-5). Analogous to inorganic semiconductors, these two bands are often called the valence band (filled lower energy band) and the conduction band (unfilled higher energy band) with the difference in energy now referred to as the band gap (E_g). In such a band structure, π -electrons can be viewed

as being delocalized along the entire chain. Of course the preceding, simplified discussion assumes the π -orbitals are all in the same plane and neglects the effects of any backbone twisting caused by steric repulsions from functional groups on the polymer chain. Any such twisting would be detrimental to in-chain conductance (*vide supra*), as each twist would break the conjugation. Each conjugated polymer has a different E_g , as the structure will determine the size and location of the valence and conduction bands.¹⁸ As such, the E_g can be tailored by functionalization of the monomer units.

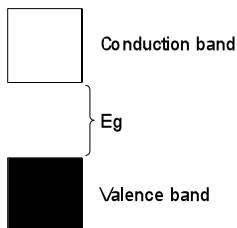


Figure 1-5 Band diagram of conjugated polymers.

From the preceding discussion it is evident how the electrons are delocalized along the polymer chain; however, these conjugated polymers are still not conductive, but rather semi-conductive, as the electrons have nowhere to go within the fully filled valence band. Doping, either oxidatively (p-doped) or reductively (n-doped),¹⁹ is then used to make these conjugated polymers truly conductive.²⁰ Oxidation leads to “holes” in the valence band, with holes defined as the absence of an electron. These holes then allow for the movement of electrons, or in other words, electrical conduction. Such p-doped materials are often called hole injectors as they can “inject” holes into neighbouring materials by oxidizing them.²¹ On the other hand, reduction places electrons into the conduction band, allowing for electrons to travel along the chain. Thus p-doped materials conduct electrons through the valence band, while n-doped materials use the conduction band.

1.2 Light-Emitting Polymers

In the early years of conductive polymer research it was also discovered that some of the polymers, including PPP, PPV and PF, were luminescent.²² This, combined with their other polymeric properties is likely part of what Heeger was thinking of when he said in his Nobel lecture that “conducting polymers... offer a unique combination of properties not available from any other known materials”.¹⁸ Green emitting PPV was first incorporated into a electroluminescent device in 1990,²³ with poly(9,9-dihexylfluorene) (PFH) following one year later.²⁴

The colour emitted by these luminescent polymers is dependent on their E_g . After an electron is placed in the conduction band (either through excitation or reduction) it can relax down to the valence band, emitting a photon with an energy corresponding to the E_g . The larger the E_g , the higher the energy of the emitted photon, and the shorter its wavelength. As tailoring of the monomer unit can affect the size of the E_g (*vide supra*) then it can also be used to tailor the colour of light emitted. A wide variety of luminescent polymers can be found in the literature, including PF,¹³ PPP,²² PPV,²⁵ PT,²⁶ and polycarbazole,²⁷ (Figure 1-6) among others.^{22, 28}

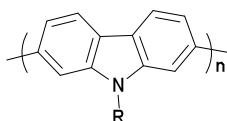


Figure 1-6 Structure of polycarbazole.

1.3 Polymer Light-Emitting Diodes

Light-emitting diodes (LEDs) are devices which utilize electrical energy to produce light. Polymer LEDs (PLEDs) are then LEDs in which a polymer is used as the luminescent material. A typical PLED consists of five layers; a transparent substrate, a transparent conductive anode, a hole injection layer (HIL), an EL layer, and a cathode (Figure 1-7). For prototype devices such as those presented in Chapter 2, indium tin oxide coated glass is often used as the substrate and transparent conductive anode. While this is the most common anode for PLEDs and was used here, poly(ethylenedioxythiophene)-poly(styrene sulfonate) (PEDOT:PSS) can also be used. PEDOT:PSS overcomes ITOs limitations of inflexibility and high cost of production, and by varying the PSS content the conductivity can be varied as desired.²¹ The HIL (also called the hole transport layer) used for the devices presented herein was (PEDOT:PSS) (Figure 1-8). Negatively charged PSS is used here to balance the positive charge of the already oxidized PEDOT, making it water soluble.²⁹ Aluminum is used as the cathode in these devices, although many reports in the literature involve using calcium as the cathode, with aluminum deposited as a protective cap.²⁸

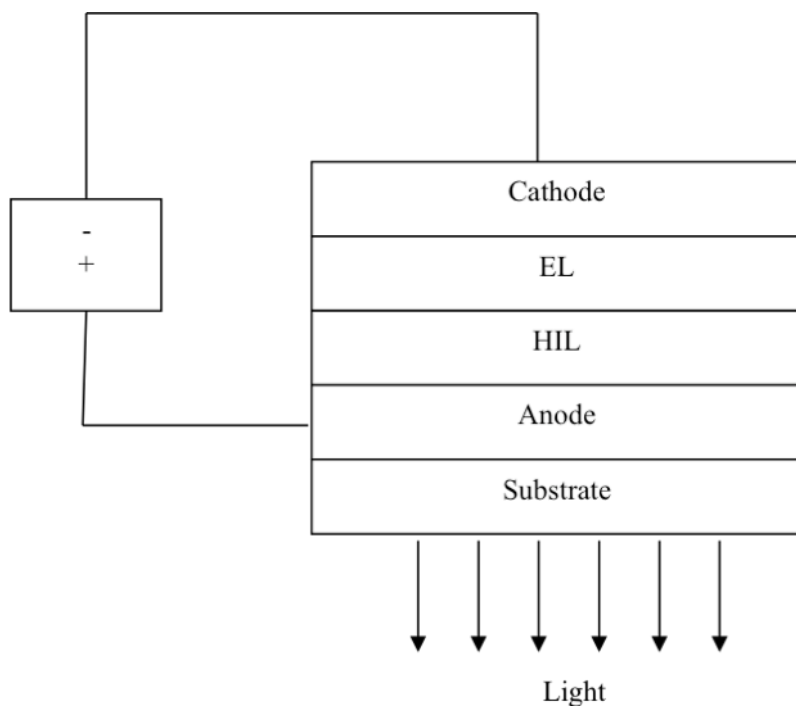


Figure 1-7 General structure of a PLED.

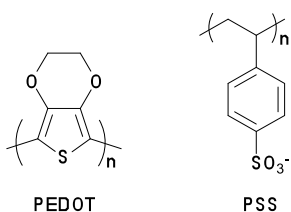


Figure 1-8 Structures of PEDOT and PSS.

When a positive bias is applied to the ITO, holes are injected into this layer which then can then travel to the ITO-PEDOT:PSS boundary. These holes then oxidize PEDOT:PSS, creating holes within this layer which then migrate under the influence of the applied field and are injected into the EL layer where they reside in the valence band (or HOMO). At the other side of the device, electrons are injected from the cathode into the conduction band (or LUMO) of the EL layer. These electrons can then relax into the holes in the HOMO, emitting a photon of light.

1.4 Polyfluorenes

Polyfluorenes are an attractive candidate for use as a blue emitter in light-emitting applications for a variety of reasons. First, they exhibit high photo- and electroluminescent (PL and EL)

quantum efficiencies.³⁰ In addition their properties are tunable through functionalization at the bridgehead carbon (or 9-position; see Figure 1-9) without decreasing the conductivity/luminescence.¹³

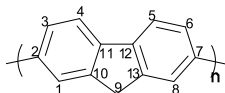


Figure 1-9 Numbering system for PFs.

1.5 PFO Phases

Some alkyl substituted PFs have multiple structural “phases” manifested in their absorption and luminescent spectra. In 1997 the Bradley group discovered a new feature in the absorption spectrum of poly(9,9-dioctylfluorene) (PFO) when a “weaker” solvent (i.e., a solvent that is less able to solvate the solute) was used.³¹ It was proposed this new peak arose from polymer aggregation arising from the limited solubility in a solvent of “weaker” solvating power. While a variety of nomenclature has been used to describe the aggregated and non-aggregated regions, the term “phases” has come to dominate the terminology used in the literature. Generally, it is accepted that three phases of PFO form, the common α -phase, the aggregated β -phase, and the less common γ -phase. While β -phase incorporation leads to the addition of a new absorption feature that is relatively small, it also exhibits a better defined, red-shifted emission spectrum.³¹ It is believed β -phase regions act as energy traps, and so only a small amount is needed to dominate the materials emissive properties. The spectral characteristics of β -phase PFO have lead some to consider it to be the most promising organic polymer for lasing applications.³⁰ Because of this much effort has been expended to find new ways to introduce β -phase regions. A variety of methods including thermal cycling of PFO films,³² employing “weak” solvents,^{33, 34} solvent mixtures,³⁵ solution aging,³⁶ and exposure to solvent vapours are all promising methods for preparing PFO β -phase.^{37, 38} While the majority of PF phase studies have been done with PFO, it has been found that β -phase regions can also be found, though to a lesser extent, in diheptyl- and dinonyl- substituted PF.³⁴

In 2005 the Winokur group showed that the structure of these three phases could be predicted computationally.³⁹ They more appropriately referred to these “phases” as conformational isomers, labelling them C_α , C_β , and C_γ , however the “phases” terminology will continue to be used for clarity. The torsion angle, or degree of rotation between monomer units along the polymer

backbone, was found to dictate the phase. The computationally predicted absorbance and emission spectra for different torsion angles were compared to the experimentally observed spectra. Torsion angles of 135° , 150° , and 160° were found to correspond to the α -phase, γ -phase and β -phase, respectively (Figure 1-10). As the torsion angle is increased there is an overall increase in planarity along the polymer chain. This increased planarity leads to better interchain interaction, lowering the E_g from $3.1 \pm .1$ eV (α -phase) to $2.94 \pm .04$ eV (β -phase). This also leads to greater aggregation, showing that the Bradley group was not far off in their original hypothesis as to the cause of β -phase emission.³¹

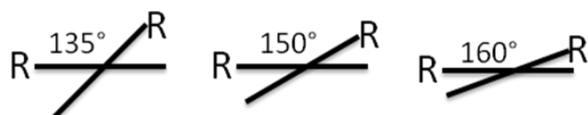


Figure 1-10 Torsion angles of α -phase (left), β -phase (right), and γ -phase (middle) regions looking along the polymer backbone (R = octyl groups).

1.6 Origin of Green Emission in Polyfluorenes

The most significant limitation to using PFs as blue emitters in light-emitting applications is their colour instability.⁴⁰ While in the presence of oxygen, either heating and/or device operation will cause the desired blue emission to be quickly overcome by a new undesired green emissive band or ‘g-band’. Originally it was believed that ‘heating induced aggregation’ led to the formation of excimers¹ between polymer chains.^{41,42} It forms between two molecules, one of which being in an excited electronic state, and the other molecule in its ground electronic state. When close enough for electronic interaction they share electron density, decreasing the HOMO-LUMO gap. For luminescent materials like PFs this will lead to a bathochromic shift in emission.

It was later shown that the ‘g-band’ came from the incorporation of fluorenone defects within the PF chain.⁴⁰ Becker *et al.* employed single molecule spectroscopy to further show the absence of intermolecular interactions in leading to the ‘g-band’.⁴³ To isolate single PF molecules they dispersed the polymers in a zeonex matrix and spin-coated from toluene. However they failed to address a few key assumptions: First is the assumption that no chain folding occurs, allowing for interchain interactions within one chain. More importantly is the assumption that no phase

¹ An excimer, or more appropriately an exciplex, is a short-lived excited state complex.

separation occurs. Even small amounts of phase separation would lead to multiple PF chains together, and so no insight would be gained.

In studying the effects of photo-oxidation of PFO the Bradley group proposed a new theory to explain the appearance of the ‘g-band’.⁴⁴ They demonstrated that while fluorenone is clearly necessary, interchain interactions must also be involved in the formation of the ‘g-band’. In this context they proposed that fluorenone-fluorenone excimers formed leading to low energy green emission. Their argument brought both theories (excimer and fluorenone) together; however it was refuted by the Becker *et al.*⁴³ single molecule study. While Scherf and co-workers continue to promote the monomolecular nature of the ‘g-band’,⁴⁵ the Bradley group has put forward some compelling evidence.⁴⁶ More recently, Chan *et al.* used oligomers to show the possibility of fluorenone-fluorenone excimer formation.⁴⁷ They synthesized four different oligomers (Figure 1-11), consisting of one fluorenone unit and from one to four dialkylfluorene units. They showed that even with a fluorenone moiety on every chain, the ‘g-band’ could be completely removed by lowering the concentration in solution. It was further determined that solvent nature has an effect on the ‘g-band’ emergence. At a concentration of 10^{-12} M in chloroform, no ‘g-band’ was evident. However after taking some of this solution and diluting it ten-fold with toluene (new concentration of 10^{-13} M) the ‘g-band’ appears. This ‘g-band’ could be removed again by diluting ten-fold with chloroform to get a concentration of 10^{-14} M. X-ray diffraction (XRD) of the fluorenone centered trimer shows inverted molecular pairs with the fluorenones aligning cofacially with an intermolecular distance of 3.50 Å. While this does not necessarily directly relate to packing of polymer chains in a thin film, it does show the tendency for fluorenone moieties to interact. Combining the solution studies with the XRD measurements it seems clear that there is more involved in the ‘g-band’ appearance than just monomolecular fluorenone defects.

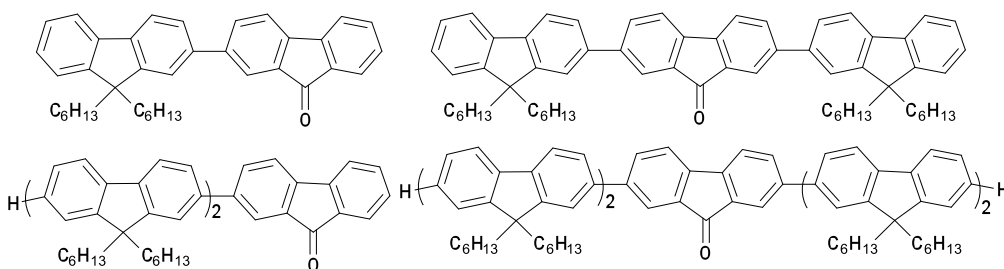


Figure 1-11 Structures of the four oligomers used by Chan *et al.*⁴⁷

1.7 Methods of Spectral Stabilization

Numerous approaches toward achieving color purity have appeared throughout the literature including, but not limited to, monomer purification,⁴⁸ polymer blending,⁴⁹⁻⁵¹ nanoparticle doping,^{52, 53} copolymerization,^{54, 55} incorporation of sterically demanding groups,^{56, 57} and functionalization with thermally stable,^{58, 59} and/or spiro-moieties.⁶⁰⁻⁶²

The most common of these methods has been functionalization at the 9-position with groups that are sterically demanding and/or thermally stable.⁶³ Previously in the Veinot group, aromatic ether groups were incorporated at the 9-position of PF.^{64, 65} Aromatic ethers were chosen for their good thermal, chemical and oxidative stability.⁶⁶

1.8 Characterization methods

Materials described in the following Chapters were characterized with Fourier-Transform Infrared spectroscopy (FTIR), ¹H and ¹³C nuclear magnetic resonance spectroscopy (NMR), Elemental analysis (EA), electron impact mass spectrometry (EI MS), electrospray (ES) MS, matrix-assisted laser-desorption ionization time of flight (MALDI-TOF) MS, thermogravimetric analysis (TGA), gel permeation chromatography (GPC), and UV-vis, PL, and EL spectroscopy.

1.9 Thesis outline and importance

PF based materials are considered to be the best candidate for light-emitting materials.²² However, they exhibit deleterious changes to their emission spectrum upon thermal stressing and/or device operation.²² Many strategies have been employed to prevent these spectral changes (*vide supra*), and tend to focus on the perceived cause of change. The perceived cause has changed over time from excimer formation, to ketonic defects, to fluorenone-fluorenone excimer formation. When Becker *et al.*⁴³ showed it was monomolecular fluorenone that led to the so called 'g-band', the focus shifted from techniques used to prevent aggregation to those focused on preventing oxidation. Da Como *et al.* summed this shift up when they stated that "synthetic strategies for reaching a blue stable emission in PF-based [PLEDs] should therefore concentrate on formulating protective groups, rather than on spacers to control intermolecular interactions".⁴⁵ However, this shift may have been premature as the recent report by Chan *et al.* shows while fluorenone is necessary for green emission in PFs, interchain interactions are also required.⁴⁷

Among the recent reports discussing stabilization of the optical properties of PFs are two reports detailing AE functionalization.^{64, 65} This functionalization was shown to drastically improve the

spectral stability of PF. This Thesis presents work utilizing other methods to incorporate AEs with PFs to achieve spectral stability. PFO-AE blends, which were found to exhibit decreased ‘g-bands’ relative to PFO after thermal treatments in air are discussed in Chapter 2. Some of these blends also exhibit improved phase stability with β -phase emission being introduced upon spin-casting thin films and remaining after thermal treatments. Chapter 3 discusses PF-AE copolymers which also exhibit improved spectral stability, both in terms of ‘g-band’ and phase stability. At high enough AE content, these copolymers were found to have smaller ‘g-bands’ than the PFO-AE blends after identical thermal stressing. Finally, Chapter 4 summarizes the work and the conclusions found. It also presents areas of future work that can be explored.

1.10 References

1. C. K. Chiang, C. R. Fincher, Y. W. Park, A. J. Heeger, H. Shirakawa, E. J. Louis, S. C. Gau and A. G. MacDiarmid, *Phys. Rev. Lett.*, 1977, **39**, 1098-1101.
2. J. H. Lupinski and K. D. Kopple, *Science*, 1964, **146**, 1038-1039.
3. H. Hoegl, *J. Phys. Chem.*, 1965, **69**, 755-766.
4. R. B. Seymour, *Polym. Eng. Sci.*, 1976, **16**, 817-820.
5. Nobelprize.org, The Nobel Prize in Chemistry 2000, http://nobelprize.org/nobel_prizes/chemistry/laureates/2000/, Accessed Dec. 21, 2010.
6. N. Hall, *Chem. Commun.*, 2003, 1-4.
7. A. F. Diaz, K. K. Kanazawa and G. P. Gardini, *J. Chem. Soc. Chem. Commun.*, 1979, 635-636.
8. G. Tourillon and F. J. Garnier, *J. Electroanal. Chem.*, 1982, **135**, 173-178.
9. A. F. Diaz and J. A. Logan, *J. Electroanal. Chem.*, 1980, **111**, 111-114.
10. L. W. Shacklette, H. Eckhardt, R. R. Chance, G. G. Miller, D. M. Ivory and R. H. Baugman, *J. Chem. Phys.*, 1980, **73**, 4098-4102.
11. R. J. Waltman and J. Bargon, *J. Electroanal. Chem.*, 1985, **194**, 49-62.
12. D. R. Gagnon, J. D. Capristan, F. E. Karasz and R. W. Lenz, *Polym. Bull.*, 1984, **12**, 293-298.
13. M. Leclerc, *J. Polym. Sci. Part A: Polym. Chem.*, 2001, **39**, 2867-2873.
14. M. A. Sato, S. Tanaka and K. Kaeriyama, *J. Chem. Soc. Chem. Commun.*, 1986, 873-874.
15. M. Rehahn, A. D. Schluter, G. Wegner and W. J. Feast, *Polymer*, 1989, **30**, 1060-1062.
16. S. Shi and F. Wudl, *Macromolecules*, 1990, **23**, 2119-2124.
17. M. Fukada, K. Sawada and K. Yoshino, *Jpn. J. Appl. Phys.*, 1989, **28**, L1433.

18. A. J. Heeger, Semiconducting and Metallic Polymers: The Fourth Generation of Polymeric Materials, http://nobelprize.org/nobel_prizes/chemistry/laureates/2000/heeger-lecture.pdf, Accessed Dec. 21, 2010.
19. S. G. Robinson, D. H. Johnston, C. D. Weber and M. C. Lonergan, *Chem. Mater.*, 2010, **22**, 241-246.
20. A. J. Epstein, in *Conjugated Polymers: Theory, Synthesis, Properties, and Characterization*, eds. T. A. Skotheim and J. R. Reynolds, CRC Press, 2007.
21. J. C. Simpson, K. Rueter and S. Kirchmeyer, in *Conjugated Polymers: Theory, Synthesis, Properties, and Characterization*, eds. T. A. Skotheim and J. R. Reynolds, CRC Press, 2007.
22. A. C. Grimsdale, K. L. Chan, R. E. Martin, P. G. Jokisz and A. B. Holmes, *Chem. Rev.*, 2009, **109**, 897-1091.
23. J. H. Burroughes, D. D. C. Bradley, A. R. Brown, R. N. Marks, K. Mackay, R. H. Friend, P. L. Burn and A. B. Holmes, *Nature*, 1990, **347**, 539-541.
24. Y. Ohmori, A. Uchida, K. Muro and K. Yoshino, *Jpn. J. Appl. Phys.*, 1991, **30**, L1941-L1943.
25. A. B. Holmes and A. C. Grimsdale, in *Conjugated Polymers: Theory, Synthesis, Properties, and Characterization*, eds. T. A. Skotheim and J. R. Reynolds, CRC Press, 2007.
26. Y. Ohmori, M. Uchida, K. Muro and K. Yoshino, *Jpn. J. Appl. Phys.*, 1991, **30**, L1938-L1940.
27. I. Levesque, P.-O. Bertrand, N. Blouin, M. Leclerc, S. Zecchin, G. Zotti, C. I. Ratcliffe, D. D. Klug, X. Gao, F. Gao and J. S. Tse, *Chem. Mater.*, 2007, **19**, 2128-2138.
28. L. Akcelrud, *Prog. Polym. Sci.*, 2003, **28**, 875-962.
29. J. Huang, P. F. Miller, J. C. de Mello, A. J. de Mello and D. D. C. Bradley, *Synth. Met.*, 2003, **139**, 569-572.
30. A. Monkman, C. Rothe, S. King and F. Dias, *Adv. Poly. Sci.*, 2008, **212**, 187-225.
31. D. D. C. Bradley, M. Grell, X. Long, H. Mellor, A. Grice, M. Inbasekaran and E. P. Woo, *Proc. SPIE*, 1997, **3145**, 254-258.
32. A. J. Cadby, P. A. Lane, M. Wohlmenannt, C. An, Z. V. Vardeny and D. D. C. Bradley, *Synth. Met.*, 2000, **111-112**, 515-518.
33. F. B. Dias, J. Morgado, A. L. Macanita, F. P. da Costa, H. D. Burrows and A. P. Monkman, *Macromolecules*, 2006, **39**, 5854-5864.

34. D. W. Bright, F. B. Dias, F. Galbrecht, U. Scherf and A. P. Monkman, *Adv. Funct. Mater.*, 2009, **19**, 67-73.
35. P. Blondin, J. Bouchard, S. Beaupre, M. Belletete, G. Durocher and M. Leclerc, *Macromolecules*, 2000, **33**, 5874-5879.
36. S. Guha, M. Arif and C. Volz, *Mater. Res. Soc. Symp. Proc.*, 2006, **916**, 3-13.
37. H. Azuma, T. Kobayashi, Y. Shim, N. Mamedov and H. Naito, *Organic Electronics*, 2007, **8**, 184-188.
38. M. Ariu, M. Sims, M. D. Rahn, J. Hill, A. M. Fox, D. G. Lidzey, M. Oda, J. Cabanillas-Gonzalez and D. D. C. Bradley, *Phys. Rev. B*, 2003, **67**, 195333.
39. W. Chunwaschirasiri, B. Tanto, D. L. Huber and M. J. Winokur, *Phys. Rev. Lett.*, 2005, **94**, 107402.
40. E. J. W. List, R. Guentner, P. S. de Freitas and U. Scherf, *Adv. Mater.*, 2002, **14**, 374-378.
41. U. Lemmer, S. Heun, R. F. Mahrt, U. Scherf, M. Hopmeier, U. Siegner, E. O. Gobel, K. Mullen and H. Bassler, *Chem. Phys. Lett.*, 1995, **240**, 373-378.
42. S. Jenekhe, A and J. A. Osaheni, *Science*, 1994, **265**, 765-768.
43. K. Becker, J. M. Lupton, J. Feldmann, B. S. Nehls, F. Galbrecht, D. Gao and U. Scherf, *Adv. Funct. Mater.*, 2006, **16**, 364-370.
44. M. Sims, D. D. C. Bradley, M. Ariu, M. Koeberg, A. Asimakis, M. Grell and D. G. Lidzey, *Adv. Funct. Mater.*, 2004, **14**, 765-781.
45. E. Da Como, K. Becker and J. M. Lupton, in *Adv. Polym. Sci.*, eds. U. Scherf and D. Neher, Springer-Verlag, Berlin, 2008, pp. 293-318.
46. T. A. M. Ferenczi, M. Sims and D. D. C. Bradley, *J. Phys.: Condens. Matter*, 2008, **20**, 045220.
47. K. L. Chan, M. Sims, S. I. Pascu, M. Ariu, A. B. Holmes and D. D. C. Bradley, *Adv. Funct. Mater.*, 2009, **19**, 2147-2154.
48. M. R. Craig, M. M. De Kok, J. W. Hofstraat, A. P. H. J. Schenning and E. W. Meijer, *J. Mater. Chem.*, 2003, **13**, 2861-2862.
49. A. P. Kulkarni and S. Jenekhe, A, *Macromolecules*, 2003, **36**, 5285-5296.
50. D. Sainova, T. Miteva, H. G. Nothofer, U. Scherf, I. Glowacki, J. Ulanski, H. Fujikawa and D. Neher, *Appl. Phys. Lett.*, 2000, **76**, 1810-1812.
51. J. H. Ahn, C. Wang, I. F. Perepichka, M. R. Bryce and M. C. Petty, *J. Mater. Chem.*, 2007, **17**, 2996-3001.

52. J. H. Park, Y. T. Lim, O. O. Park, J. K. Kim, J.-W. Yu and Y. C. Kim, *Chem. Mater.*, 2004, **16**, 688-692.
53. C.-H. Yang, C. J. Bhongale, C.-H. Chou, S.-H. Yang, C.-N. Lo, T.-M. Chen and C.-S. Hsu, *Polymer*, 2007, **48**, 116-128.
54. U. Giovanella, M. Pasini, S. Destri, W. Porzio and C. Botta, *Synth. Met.*, 2008, **158**, 113-119.
55. F.-I. Wu, D. S. Reddy and C.-F. Shu, *Chem. Mater.*, 2003, **15**, 269-274.
56. S. Setayesh, A. C. Grimsdale, T. Weil, V. Enkelmann, K. Mullen, F. Meghdadi, E. J. W. List and G. Leising, *J. Am. Chem. Soc.*, 2001, **123**, 946-953.
57. J. Lee, H.-J. Cho, B.-J. Jung, N. S. Cho and H.-K. Shim, *Macromolecules*, 2004, **37**, 8523-8529.
58. G. Kwag, E. Park and S. N. Lee, *J. Appl. Polym. Sci.*, 2005, **96**, 1335-1340.
59. J. Liu, J. Zou, W. Yang, H. Wu, C. Li, B. Zhang, J. Peng and Y. Cao, *Chem. Mater.*, 2008, **20**, 4499-4506.
60. N. Cocherel, C. Poriel, L. Vignau, J.-F. Bergamini and J. Rault-Berghelot, *Org. Lett.*, 2010, **12**, 452-455.
61. Y.-H. Tseng, P.-I. Shih, C.-H. Chien, A. K. Dixit, C.-F. Shu, Y.-H. Liu and G.-H. Lee, *Macromolecules*, 2005, **28**, 10055-10060.
62. D. Katsis, Y. H. Geng, J. J. Ou, S. W. Culligan, A. Trajkovska, S. H. Chen and L. J. Rothberg, *Chem. Mater.*, 2002, **14**, 1332-1339.
63. S. Kappaun, C. Slugovc and E. J. W. List, in *Adv. Polym. Sci.*, eds. U. Scherf and D. Neher, Springer-Verlag, Berlin, 2008.
64. S. L. McFarlane, L. S. Coumont, D. G. Piercey, R. McDonald and J. G. C. Veinot, *Macromolecules*, 2008, **41**, 7780-7782.
65. S. L. McFarlane, D. G. Piercey, L. S. Coumont, R. T. Tucker, M. D. Fleishauer, M. J. Brett and J. G. C. Veinot, *Macromolecules*, 2009, **42**, 591-598.
66. R. J. Cotter, *Engineering Plastics: A Handbook of Polyarylethers*, Gordon and Breach Science Publishers, Basel, 1995.

Chapter 2

Polyfluorene/Aromatic Ether Blends

2.0 Introduction

As described in Chapter 1, alkyl-substituted fluorene-based polymers (PFs) such as poly(9-9-dioctylfluorene) (PFO) have significant spectral stability problems. Although not the most common method for ameliorating these issues, blending PFO with another material has been used. Reports of blending PFs with hole-transporting molecules (HTMs),¹ electron transporting materials (ETMs),² and other blue-emitters³ are found in the literature.

Sainova *et al.* blended poly(2,7-(9,9-bis(2-ethylhexyl)co-(9,9-bis((3S)-3,7-dimethyloctyl))fluorene) (PF C26) with several HTMs at a weight ratio of 1: 0.03 (PF C26:HTM).¹ The hole-transporters used were a triphenylamine tetramer (TPTE), starburst amine (ST 755), and N,N'-diphenyl- N,N'-bis- α -naphthylbenzidine (ST 16/7) (Figure 2-1). This blending approach accomplished two things: First the luminance efficiency increased relative to pure PF C26 and second, there was a sharp decrease in the intensity of the 'g-band' in the electroluminescence (EL) spectrum. The authors attribute both outcomes to the hole-transporting nature of these materials proposing the blended HTMs competed for hole-trapping with the defect sites leading to a minimizing of green defect emission. Furthermore, the observed increased intensity of the characteristic blue emission was proposed to arise from the once defect trapped holes becoming "detrapped" and recombining with electrons on a nearby PF chain. Unfortunately, this work does not mention anything about the long-term spectral stability of the blends. While these blends offer immediate improvement of spectral properties, it is unclear if they will improve the spectral stability when under oxidative conditions and/or device operation.

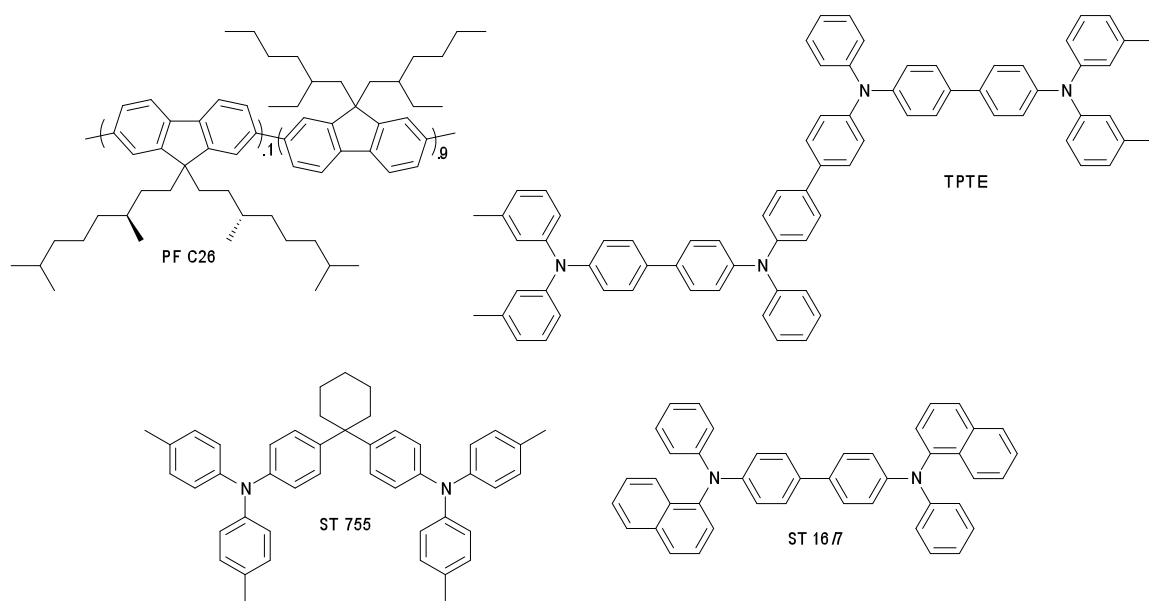


Figure 2-1 Structures of PF C26, TPTE, ST 755, and ST 16/7.

Ahn *et al.* reported improved colour purity and efficiency through blending PFO with an ETM.² The electron transporting 2,7-bis[2-(4-*tert*-butylphenyl)-1,3,4-oxadiazol-5-yl]-9,9-dihexylfluorene (DFD) (Figure 2-2) was found to improve both device efficiency and spectral stability of PFO. Several proposals were made to account for these observations. DFD has a higher electron affinity than PFO and so would be the predominant electron carrier in the blended film. As a result, it is reasonable the lower number of electrons being carried by PFO would make the PFO less prone to oxidation and therefore less likely to form fluorenone defects. In addition, it was proposed that, especially at high DFD concentrations, DFD microencapsulates the PFO, protecting it from the Ca cathode, which has been shown to strongly catalyze the oxidation of PF.⁴ Finally the authors proposed blended films would exhibit fewer interchain interactions between the PFO chains, thus reducing any excimer emission.

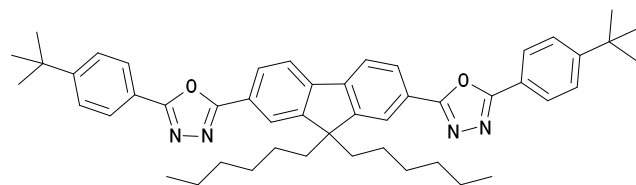


Figure 2-2 Structure of DFD.

Kulkarni *et al.* reported blending PFO with polystyrene (PS), an insulating polymer, and poly(vinyl diphenylquinoline) (PVQ), a blue-emitting polymer (Figure 2-3).³ Blending with PS

led to substantial phase separation and no impact in spectral stability. While no mention is made of phase separation, a decrease in the 'g-band' was noted when PFO was blended with PVQ. As the PVQ content of the film was increased, (and the PFO content equivalently decreased - See Appendix A2) the 'g-band' intensity decreased. However, in light of the blue emitting properties of PVQ it was clear the authors did nothing more than replace one blue-emitter with another. It was also noted that because PVQ is less conductive, its blends showed a decrease in EL efficiency, to the point that at 50 % PVQ there was no measureable EL.

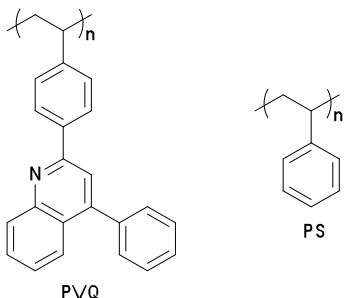


Figure 2-3 Structures of PVQ and PS.

When working with blends there are three fundamental requirements that must be met if they are to be useful in device applications.⁵ If these requirements are met the blend is referred to as a composite. First there should be two or more blend components that are physically distinct and mechanically separable. Second, it must be possible to prepare the composite by mixing the components. Third, the composite must possess properties which are superior to the properties of the individual components. While the first two requirements are straightforward, the third is not. One factor that relates to this qualification is miscibility. A miscible polymer blend has been defined as a blend in which the free energy of mixing (ΔG_m) is less than or equal to zero.⁶ Immiscible polymer blends are then blends with ΔG_m greater than zero. Because the entropy of mixing (ΔS_m) is generally very small for polymer blends, an exothermic enthalpy of mixing (ΔH_m) is generally required for two polymers to be miscible.⁷ Depending on the application, there may be a need for varying degrees of miscibility. While most composites require good miscibility to achieve optimal performance, some degree of heterogeneity is necessary to maintain individual properties.⁸ Alternatively some materials, like bulk heterojunction solar cells, use inherent immiscibility of the two components to create phase separated regions that allow for better charge separation.⁹ While it is reasonable that intermolecular forces (vide infra) may be used to predict component miscibility, there are numerous independent factors that also play a role. These factors

include temperature, concentration, pressure, molecular weight, polydispersity index (PDI) and preparation method.⁶

Numerous intermolecular forces will affect miscibility independently and in combination, including London dispersion forces, ion-ion interactions, dipole-dipole interactions, hydrogen bonding, and π - π stacking. For conjugated organic systems π - π stacking is the main interacting force. When blending with PFO for example, π - π stacking is the dominant force, but the pendant alkyl chains will also affect miscibility. In addition, the presence of ketonic defects (see detailed discussion in Chapter 1) can play a role. In the Polymer Blends Handbook, Utracki compiled binary interaction parameters (B_{ij}) for key functional groups.⁶ While these values were determined from small molecules, it is expected that they can be extended to predict polymer miscibility. By definition, when B_{ij} is negative the two functional groups in question are attractive, increasing the likelihood of material miscibility. Alternatively, if B_{ij} is positive the functional groups hinder good miscibility. For example, -CH₂- and C₆H₅-O- have a B_{ij} of 8.34 cal/ml, showing that, as expected, they are repulsive. While still positive, the B_{ij} is lowered when methyl groups are introduced to the C₆H₅-O- group. In contrast, C₆H₅-O- groups have negative B_{ij} values with C₆H₅- and -CO- groups. While alkyl chains on PFO will hinder miscibility with aromatic ethers (AEs), the two materials may still be miscible because of the attractive interactions between the conjugated backbone of PFO and the AE repeat units. Ketonic defects should also increase miscibility between these two components, though this may only be a factor if the defects are present prior to film preparation, which is unlikely in pristine PFO.

The way the independent factors affect miscibility can depend upon the intermolecular forces present. Increasing the mixing temperature usually improves miscibility due to the increased disorder. However, higher temperatures can have the opposite effect when the two blend components have strong attractive interactions. For example, while C₆H₅- and -CO- groups have a B_{ij} of -36.9 cal/ml at 80 °C, their B_{ij} is 15.1 cal/ml at 90 °C.⁶ Thus, by increasing the temperature with a system containing these two functional groups on different polymer chains, phase separation will increase. Miscibility tends to decrease with high molecular weight components because, when everything else is constant, blends of higher molecular weight polymers will have less entropy, so the ΔS_m for that blend will be smaller. Increasing pressure increases the magnitude of ΔH_m through increasing the effect of the intermolecular forces present. Thus miscibility will increase when ΔH_m is negative, and decrease when ΔH_m is positive.⁶

The blend preparative method also impacts miscibility. Polymer blends involving PFO are typically evaluated as thin films. There can be a dramatic difference in the properties of drop-cast and spin-cast films. Drop-cast films are prepared by placing drops of solution on a substrate and allowing the solvent to slowly evaporate off, leaving a film behind. Spin-cast films are prepared by placing drops of solution on a substrate, and then spinning said substrate at a high speed to remove the solvent and leave behind a more uniform film. When two components of a blend are dissolved they are considered completely miscible because dissolution minimizes interchain interactions (i.e., the solvent is separating individual chains).⁶ Compared to drop-cast films, those prepared by spin-casting are more miscible as they have less time for polymer separation to occur. However, as was seen by Kulkarni *et al.*, spin-coating thin films does not guarantee that a miscible blend will result.³

In the following chapter a new composite material prepared by blending commercially available PFO with a number of other polymers and molecules is described. Blending PFO with polyphenyl ether (PPE), provided a straightforward method toward minimizing and even reversing the appearance of the ‘g-band’. In addition, this blend was found to induce β -phase domains within the PFO film. With these superior properties this polymer blend can be designated as a composite.

2.1 Experimental

2.1.1 Materials

Chloroform (Caledon), PFO (ADS129BE: American Dye Source, Inc), PPE (OS-124, Santovac fluids LLC), poly(2,6-dimethyl-1,4-phenylene oxide) (PPO), polysulfone (PSU), diphenyl ether (DE), 1,3-diphenoxy benzene (m-DB), 1,4-diphenoxy benzene (p-DB), and poly(3,4-ethylenedioxythiophene)/(polystyrenesulfonate) (PEDOT:PSS) (Aldrich), and Optical Grade Fused Quartz substrates (ESCO products) were used as received.

2.1.2 Film Preparation

All solutions were prepared by simultaneously dissolving predetermined quantities of PFO and one of the other polymers/molecules in chloroform. These solutions were heated slightly to ensure full dissolution of PFO. All solutions contained PFO concentrations of 1 % w/v and, unless specified, the blend component also had a concentration of 1 % w/v. Spin coating of thin films from these solutions was carried out using a Laurell Technologies Corporation model WS-

400B-6NPP/LITE/AS spinner. Spinning started at 500 rpm for 5 seconds, followed by 1000 rpm for 10 seconds and finally 4000 rpm for 40 seconds.

2.1.3 Film Characterization

Spin-coating yielded thin films of *ca.* 100 nm thicknesses as measured with a 50 kHz Olympus tip (Asylum Research) using a Digital Instruments Dimension 3100 Atomic Force Microscope. This measurement was done by first scraping the polymer film away with the AFM tip in contact mode, and then using tapping mode to measure the change in height between the undisturbed area and the scraped away area. UV-vis measurements were obtained using a Hewlett Packard 8453 UV-VIS DAD Spectrophotometer, while photoluminescence (PL) data was recorded with a Varian Cary Eclipse Fluorescence Spectrophotometer ($\lambda_{\text{ex}} = 350$ nm, slit width parameter = 2.5 nm). Ratios of the absolute intensities of the green and blue spectral regions were determined by integrating over the 500 – 600 nm range (green) and dividing by the integrated 400 – 500 nm range (blue). Atomic force microscopy (AFM) images of the films were obtained in tapping mode with a 285 kHz Arrow-NCR Nanoworld tip (Asylum Research) using a Digital Instruments Dimension 3100 Atomic Force Microscope. Polarizing light microscopy (PLM) was done on a Nikon ECLIPSE E400 POL Polarizing Microscope. Scanning electron microscopy (SEM) and auger electron spectroscopy (AES) were done using a JAMP 9500F Scanning Auger Microprobe.

2.1.4 PLED Fabrication and Testing

Indium-tin oxide (ITO)-coated glass substrates (8-12 Ω /sq, Delta Technologies) were pre-cleaned by sonicating three times each in detergent (Sparkleen 1), distilled water, methanol, acetone and 2-propanol. The clean dry substrates were then exposed to an oxygen plasma using a Plasmalab MicroEtch RIE for one minute (parameters: oxygen flow = 80%, oxygen pressure = 150 mTorr, radiofrequency (RF) power = 75%). A PEDOT:PSS layer was spin-coated using a Head-way resist spinner at 500 rpm for 5 seconds, followed by 1000 rpm for 10 seconds and finally 4000 rpm for 45 seconds. This thin film (*ca.* 60 nm measured by SEM) was annealed at 60°C in air for ten minutes in a class 10 cleanroom. The emissive layer was prepared by spin-coating either PFO or the 1-1 blend from CHCl_3 (using the same protocol described above). An aluminum cathode was subsequently thermally evaporated onto the organic layered structure in a vacuum deposition system housed in a Nitrogen filled MBraun glovebox. Electroluminescent (EL) measurements were taken at 0.1 mA current with a Gigahertz-Optik X4-OLED Light Analyzer, and a Varian Cary Eclipse Fluorescence Spectrophotometer (slit width parameter = 2.5 nm); IV curves were recorded with a Gigahertz-Optik X4-OLED Light Analyzer using a computer-controlled Keithley

A version of this chapter has been published. Sirtonski et al., 2010, J. Mater. Chem., 20:8147-8152. 21

2400 source. The current was measured as voltage was increased by 0.1 volts/step from 0 to 10 volts, holding for 0.5 seconds at each step.

2.2 Results and Discussion

2.2.1 Blend Fabrication and Characterization.

PFO was blended with three different polymers and three other molecules. The polymers used were PPO, PSU, and PPE. PPO and PSU are thermoplastics, and while PPE is actually an oligomer, it is used as a high temperature lubricant.¹⁰ The other three molecules (DE, m-DB, and p-DB) were chosen for their structural similarity to PPE (See: Figure 2-4). As thermoplastics, both PPO and PSU are known to exhibit high thermal and oxidative stability.^{11, 12} Similarly, PPEs have high thermal and oxidative stability, with the all meta-substitution showing a slightly higher degradation temperature.¹⁰ When comparing PPEs of varying chain length (from two to six rings), the five-ring PPE (referred to as just PPE in this Chapter) shows the highest thermal stability as determined by isoteniscope.¹⁰

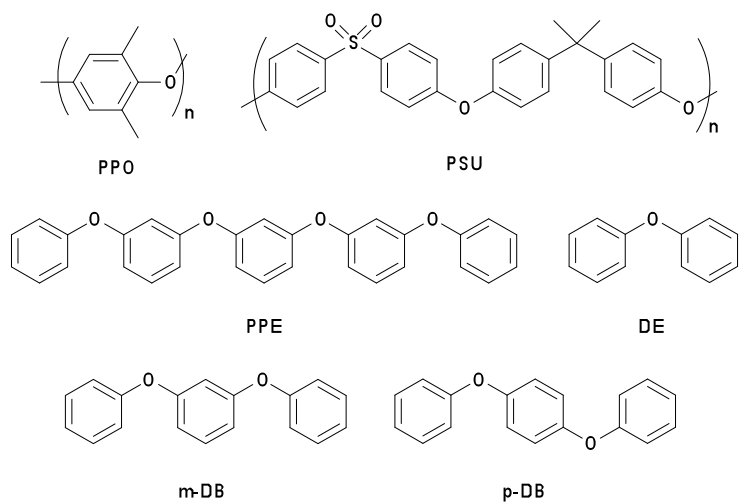


Figure 2-4 Structures of PPO, PSU, PPE, DE, m-DB, and p-DB.

2.2.2 Thermogravimetric Analysis of the Polymers

Thermogravimetric analysis (TGA) of the four polymers was done at a heating rate of 10 °C/min in nitrogen (Figure 2-5). Weight loss can be due to either decomposition or evaporation, although thermal degradation does not always lead to weight loss. While this is usually the case, some decomposition mechanisms may not lead to weight loss. For example when PFO is heated in air ketonic defects are formed. While this would lower the polymer weight, if the alkyl chains remain

in the film no weight loss would be detected. Still, TGA is a good starting place for polymer characterization. PPE starts showing weight loss at 300 °C, which is about 100 °C lower than PFO. This is likely due to PPE being an oligomer, rather than a polymer. The drop in weight percent of PPE to zero suggests that evaporation is the cause, but PPE has a boiling point of 476 °C,¹³ so it is possible that while PPE starts to decompose at a 300 °C, the cause of weight loss shifts to evaporation at higher temperatures. It could also be a combination of both processes occurring together. Despite this, 300 °C is still much higher than what would be seen in any device operation. Unlike PPE, PFO, PPO and PSU don't progress to zero weight percent suggesting that the TGA shows degradation temperatures in these instances. PPO begins to degrade at about 450 °C (~50 °C higher than PFO), but shows a steeper curve than PFO. Combining these two observations suggests that PPO has similar thermal stability to PFO. PSU on the other hand has a much higher degradation temperature, with weight loss not appearing until after 500 °C.

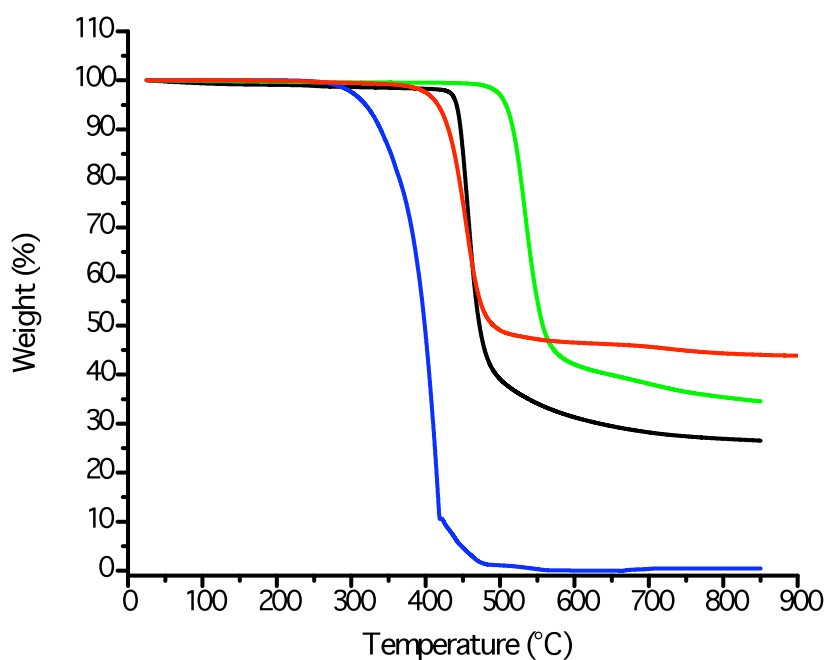


Figure 2-5 TGA traces of PFO (red trace), PPO (black trace), PSU (green trace), and PPE (blue trace) under a nitrogen atmosphere at a heating rate of 10 °C/min.

2.2.3 Beta-Phase Incorporation

It was found blending with PPE, DE, and both DB compounds led to the formation of β -phase regions within the PFO. This does not occur when blending PFO with other materials reported here (i.e., PPO, PSU) and suggests that only PPE, DE and the DBs substantially influence the solution properties of the blend. Interestingly, the spectral signature of the PFO β -phase disappears from the PFO-DE blend following heating for one hour in air – the photoluminescent response becomes characteristic of γ -phase emission. Because DE is a liquid at room temperature, it is reasonable that while it had an effect upon the solvating power of the chloroform, it was spin-coated off and did not blend into the film. Films from the PFO-m-DB blend and the PFO-p-DB blend were cloudy (i.e., not transparent), and so were not characterized further. Despite this, it is clear from the PL of both of the PFO-DB blends that β -phase regions are formed. The opacity of these two films suggests substantial phase separation because opacity arising from scattering is generally only seen in blends when the size of the heterogeneity is larger than 100 nm and the refractive index difference between them is more than 0.01.⁶ On the other hand the size of heterogeneity in the PFO-PPE blend can be expected to be less than 100 nm since PFO and PPE have refractive indices of 1.7¹⁴ and 1.630,¹⁵ respectively (i.e., different by more than 0.01), yet the PFO-PPE blend shows no opacity.

UV-vis absorption spectra were acquired for thin films of neat PFO prepared by spin-coating chloroform solutions containing 1% w/v PFO onto quartz substrates (Figure 2-6). A characteristic broad absorption feature at ca. 390 nm attributed to α -phase domains is clearly evident. Thermal annealing of these films in a nitrogen atmosphere for one hour at ca. 140 °C leads to the appearance of a low energy shoulder (ca. 420 nm) consistent with structural changes leading to the formation of γ -phase domains.¹⁶

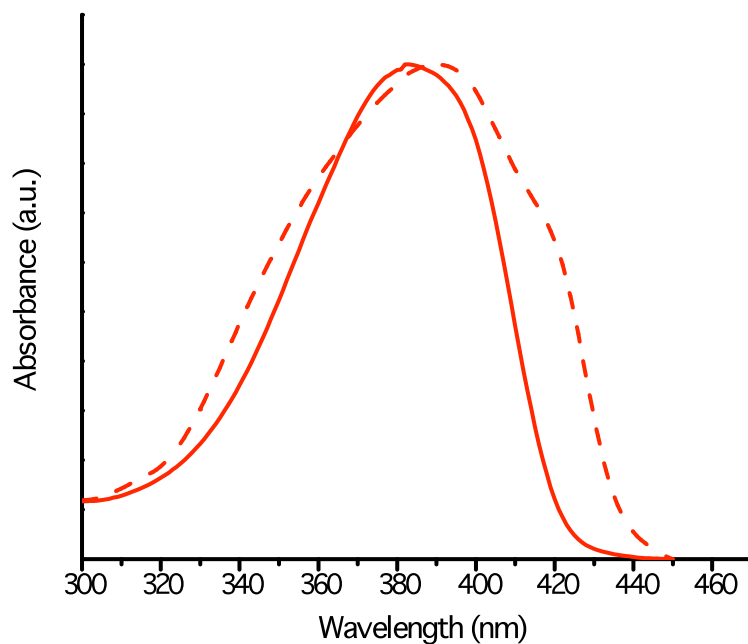


Figure 2-6 Normalized UV-vis absorbance spectra of a representative 100 nm thick PFO thin film. Films were prepared by spin coating chloroform solutions containing 1% w/v PFO onto quartz substrates. Pristine film (—) and film annealed in nitrogen at 140 °C for 2 hours (---).

In contrast, equivalent films spin coated from chloroform solutions containing 1% w/v PFO and 1% w/v PPE show a new, narrow UV-vis band at 435 nm (Figure 2-7). These bands have previously been attributed to β -phase domains.¹⁷ It appears the addition of PPE has caused PFO to adopt β -phase conformations in the thin film. It is reasonable PPE reduces the solvating power of CHCl_3 toward PFO resulting in β -phase domain formation. This is consistent with analogous observations noted for studies involving mixtures containing weak and strong solvating agents.¹⁸ ¹⁹ Thermal annealing of composite films in nitrogen at *ca.* 140 °C only increases the intensity of the β -phase absorption feature (Figure 2-7), while the same thermal annealing of pristine PFO films resulted in much more dramatic spectral changes (See Figure 2-6). Clearly, once the PFO-PPE composite is laid down as a thin film, minimal changes to its optical properties occur under thermal stressing.

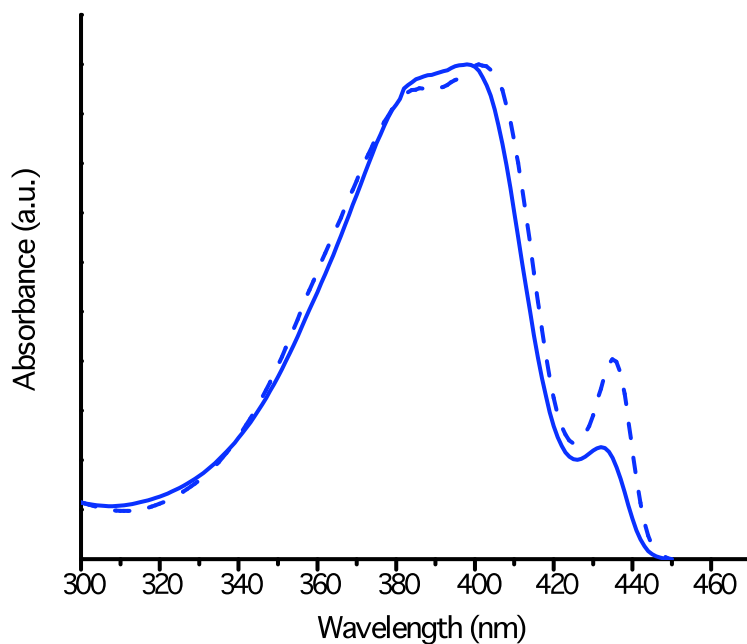


Figure 2-7 Normalized UV-vis absorbance spectra of a representative 1-1 PFO-PPE composite thin film of nominally 100 nm thickness prior to annealing (—) and following annealing in nitrogen at 140 °C for 2 hours (---).

Photoluminescence (PL) spectra of PFO and PFO-PPE composite thin films (Figure 2-8 A and B) were evaluated prior to and following annealing for 2 hours at *ca.* 140 °C in a nitrogen atmosphere. The pre-annealed PL spectrum of PFO (Figure 2-8A, solid trace) shows an emission maximum at 435 nm suggesting the presence of β -phase domains in the PFO film, however, the vibronic structure is not clearly resolved;²⁰ furthermore, emission bands characteristic of the theoretical α -phase remain at *ca.* 426 nm and 455 nm. These observations and the absence of a β -phase shoulder in the absorption spectrum, suggest the β -phase domains within the film are small in size and/or few in number. Following annealing, the PFO PL spectrum red-shifts and three resolved vibronics (Figure 2-8A) emerge. The red-shift is consistent with polymer structural changes, however, the emission maxima appear 5-10 nm lower than expected for β -phase domains.²¹ Spectral signatures similar to those shown in Figure 2-8A have been attributed to γ -phase conformational isomer domains.¹⁶

Upon first inspection, the PL spectrum of the as prepared PFO-PPE blend thin film (Figure 2-8B) appears similar to that exhibited by the annealed PFO film (Figure 2-8A); however, its vibronic

structure is red-shifted indicating the presence of β -phase domains.²¹ Annealing the blended film in a nitrogen atmosphere (Figure 2-8B) produces no detectable variation in peak positions and only minor changes to the relative intensities of the vibronics, suggesting minimal polymer chain reordering.²²

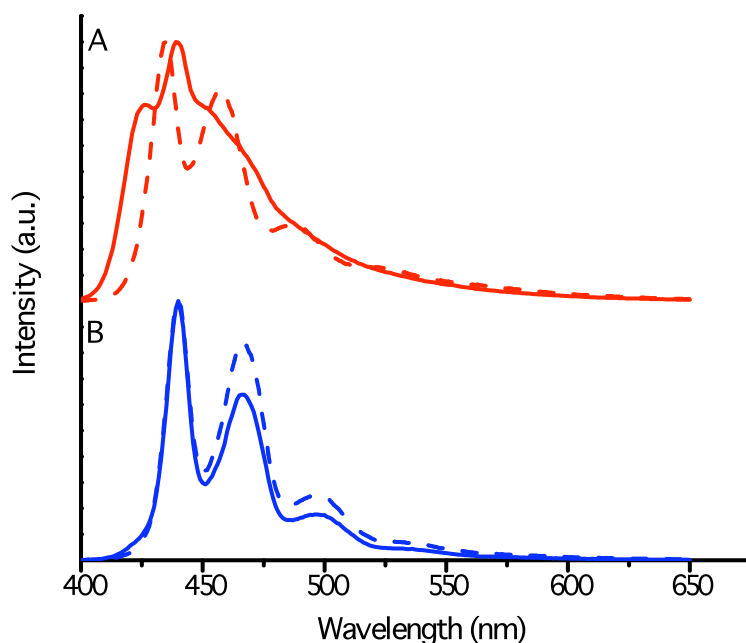


Figure 2-8 Normalized photoluminescence spectra of PFO (A-red traces) and PFO-PPE blend (B-blue traces) thin films (*ca.* 100 nm) measured prior to (—) and following (---) annealing in nitrogen ($\lambda_{\text{ex}} = 350$ nm).

2.2.4 Spectral Stability in the Presence of Oxygen

Thin films of PFO, PFO-PPO, PFO-PSU and PFO-PPE were spin-cast from chloroform solutions containing 1% w/v of each particular component. As noted previously, PL of the PFO-PPE blend shows clear β -phase emission (Figure 2-9 A). The PL spectra of PFO and the PFO-PPO and PFO-PSU blends show a maximum at 435 nm reminiscent of β -phase emission, however the vibronic structure is not clearly resolved (Figure 2-9 A).²⁰ It is likely while β -phase regions exist in these films they are too small and/or too few in number for their properties to dominate the spectrum. All these films were subsequently heated at 140 °C for one hour in air and PL measurements were retaken (Figure 2-9 B). As expected, the PL spectrum obtained from PFO shows a shift to γ -phase

emission combined with the emergence of the typical large 'g-band'. The PFO-PSU blend exhibited a spectral signature nearly identical to that of PFO, suggesting PSU has little or no effect on the spectral stability of the blend and suggests blending PFO with PSU results in phase segregated regions. This observation is similar to those made for a PFO-PS blend reported by Kulkarni.³ While the PFO-PPO blend shows γ -phase emission similar to PFO and the PFO-PSU blend, annealed films show a substantial decrease in 'g-band' luminescent intensity. The PFO-PPE blend shows the lowest 'g-band' emission intensity while maintaining β -phase emission. These results suggest miscibility is important for spectral stability improvement. While the methyl groups of PPO may increase miscibility with alkyl chains of PFO, they will hinder miscibility with the PFO backbone. Clearly, the PFO-PPE blend exhibits the most stable spectral response and shows promise for device application thereby warranting further investigation.

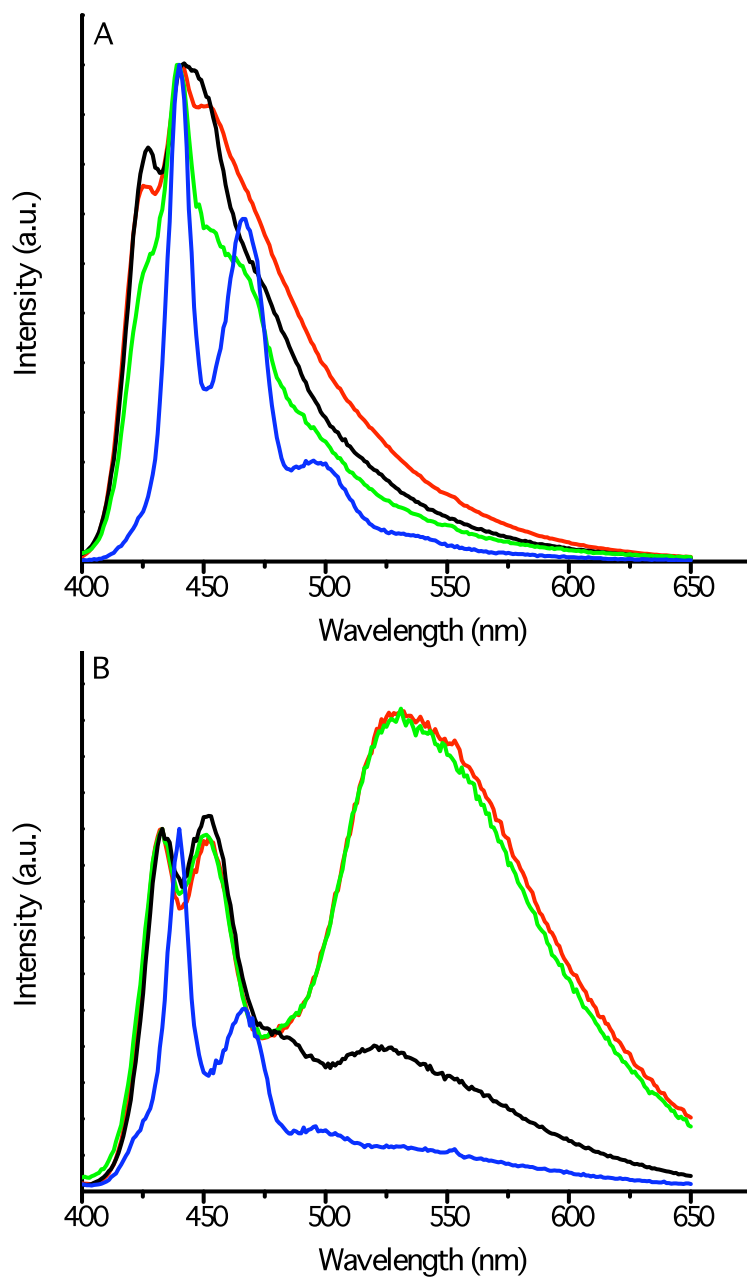


Figure 2-9 Normalized PL spectra of thin films cast from solutions of PFO (red trace), PFO-PPO (black trace), PFO-PSU (green trace), and PFO-PPE (blue trace) measured prior to (A) and following (B) heating in air ($\lambda_{\text{ex}} = 350$ nm).

To further investigate the influence of PPE on the spectral stability of PFO, thin films of PFO-DE, PFO-p-DB, and PFO-m-DB blends were made similarly to those of the other blends and

compared to new PFO and PFO-PPE films. As mentioned earlier PL measurements of these four blend thin films all show β -phase emission (Figure 2-10 A). Heating for one hour at 140 °C in air led to some significant differences between the different blend films (Figure 2-10 B). As noted previously the PFO-DE blend shifts from β -phase to γ -phase emission. In addition, its 'g-band' is equivalent to the one for the PFO film. This suggests that only PFO remains in this film. While the β -phase emission remains with the other three blends, once again the PFO-PPE blend shows the smallest 'g-band'. The PFO-m-DB and PFO-p-DB blends on the other hand have a 'g-band' that is intermediate to that seen for PFO and the PFO-PPE blend. This is likely due to the increased phase separation in these two blends compared to the PFO-PPE blend. While likely a coincidence, it is further interesting to note that the order of increased spectral stability of the blends corresponds to the order of increased thermal stability of the AE used.¹⁰ Because of the increased stability of the PFO-PPE blend over all the other blends, it will be the focus of the rest of this chapter.

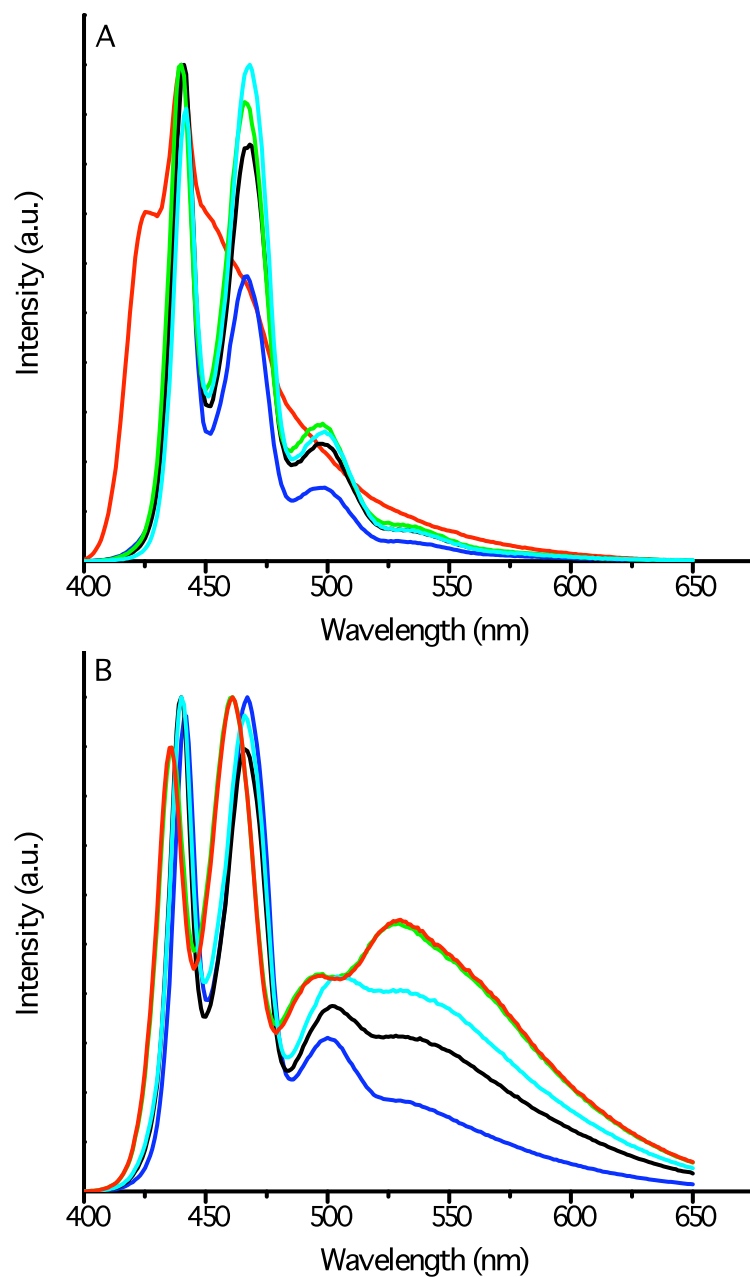


Figure 2-10 Normalized PL spectra of thin films cast from solutions of PFO (red trace), PFO-DE (green trace), PFO-m-DB (black trace), PFO-p-DB (cyan trace) and PFO-PPE (blue trace) measured prior to (A) and following (B) heating in air ($\lambda_{\text{ex}} = 350$ nm).

If blend miscibility is a factor in the improvement of PFO spectral stability, the relative intensity of the ‘g-band’ emission in the spectrum acquired from a drop-coated film should be greater than

that observed for a spin-coated film.⁶ This is exactly what is observed in Figure 2-11. Drop-cast PFO-PPE films show a substantially more intense ‘g-band’ emission compared to their spin-cast counterparts. Drop-coating also appears not to influence the formation of β -phase domains, showing that this property is entirely due to solution properties, rather than deposition method.

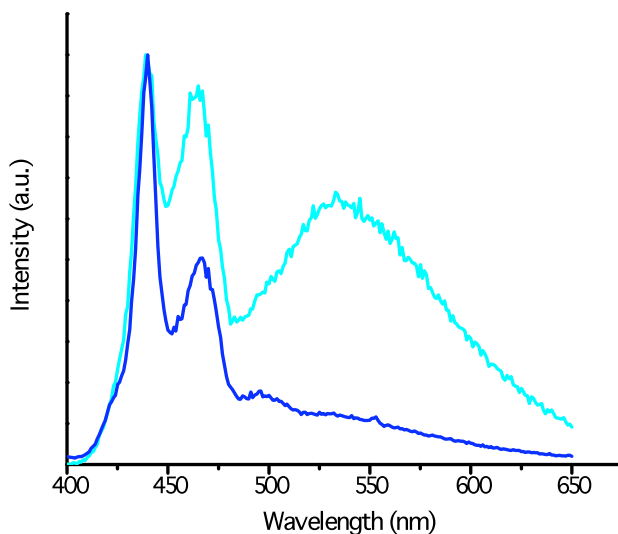


Figure 2-11 Normalized PL spectra of thin films spin-cast (blue trace) and drop-cast (cyan trace) from PFO-PPE solution measured following heating in air for one hour ($\lambda_{\text{ex}} = 350$ nm).

2.2.5 Blend Concentration Studies

To further elucidate the stabilizing influence of PPE on β -phase formation we have systematically investigated the dependence of β -phase formation on the PFO-PPE composite composition. Chloroform solutions containing 1% w/v PFO and predetermined concentrations of PPE (0 to 1% w/v) (Table 2-1) were prepared and spin-coated onto quartz substrates. The UV-vis spectra obtained from thin films of the polymer blends (Figure 2-12) clearly show an increase in the β -phase absorption feature with higher PPE concentration, concurrent with a slight red shift in the α -phase absorption peak. Higher PPE concentrations than those presented yielded no detectable changes in the optical spectra.

Table 2-1 Weight percent concentrations of PFO and PPE in the five blends investigated.

| Blend | 1-1 (%) | 3-1 (%) | 5-1 (%) | 8-1 (%) | PFO (%) |
|--------------------------------|---------|---------|---------|---------|---------|
| PFO] (w/v CHCl ₃) | 1 | 1 | 1 | 1 | 1 |
| [PPE] (w/v CHCl ₃) | 1 | 0.33 | 0.20 | 0.125 | 0 |

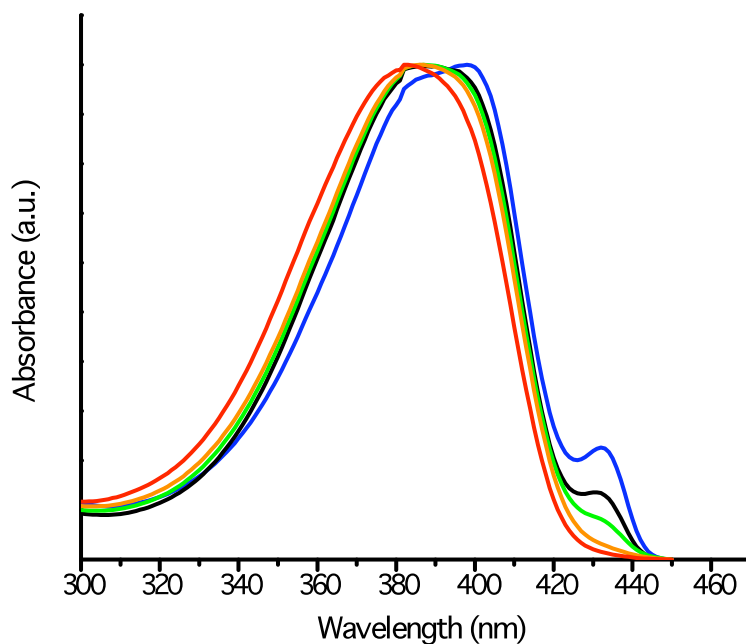


Figure 2-12 PFO-PPE blend composition dependence of absorbance spectra of thin films (*ca.* 100 nm) spin-coated from these blend solutions (1-1: blue, 3-1: black, 5-1: green, 8-1: orange, PFO: red).

To evaluate the influence of PPE on the optical response of PFO, PL spectra of neat PFO and 1-1, 3-1, 5-1, and 8-1 PFO-PPE composite thin films were acquired prior to and following annealing in air for one hour at *ca.* 140 °C (Figure 2-13). Annealing a pristine neat PFO film in air gives rise to the well-established low energy ‘g-band’ (*ca.* 530 nm). This observation is similar to other reports of PFO air annealing and is commonly attributed to ketonic defect formation and more recently the formation of fluorenone-fluorenone dipole mediated stacking (See Chapter 1).²³⁻²⁷ To provide a semi-quantitative measure of the ‘g-band’ intensity, the ratio of integrated intensities for the green and blue spectral regions was compared (See: Section 2.1.1).

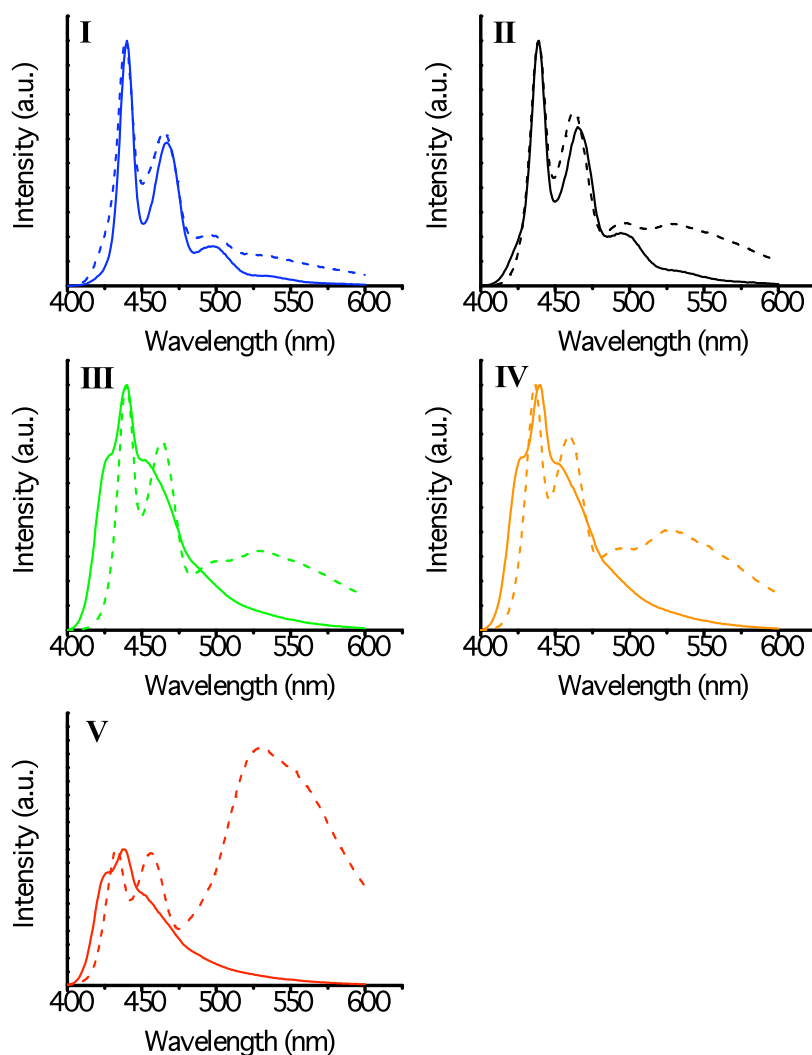


Figure 2-13 Normalized photoluminescence spectra of PFO-PPE blend thin films (*ca.* 100 nm), spin-coated from their respective solutions (I: 1-1, II: 3-1, III: 5-1, IV: 8-1, V: PFO), measured prior to (—) and following (---) annealing in air ($\lambda_{\text{ex}} = 350$ nm).

Varying the composite composition clearly influences the emission characteristics of PFO after thermal annealing. Only the PL spectra of the 1-1 and 3-1 films show spectral signatures consistent with PFO β -phase (Figure 2-13, I and II). Upon annealing in air, PFO shows the largest green:blue ratio at 2.44 and the 8-1, 5-1, 3-1, and 1-1 blends give ratios of 0.74, 0.69, 0.56 and 0.30, respectively. Increasing PPE concentration in the blends results in dramatically reduced ‘g-band’ intensity. In addition, a small red-shift (*ca.* 5 nm) in the peak maxima with higher PPE concentrations is observed. It is reasonable this spectral shift arises from a structure with a conjugation length lying between the accepted β - and γ -phase constructs, which are clearly shown

in PL spectra of the 1-1 blend and annealed neat PFO respectively. While ‘g-band’ intensity increases with annealing time, it remains reduced relative to neat PFO (Figure 2-14).

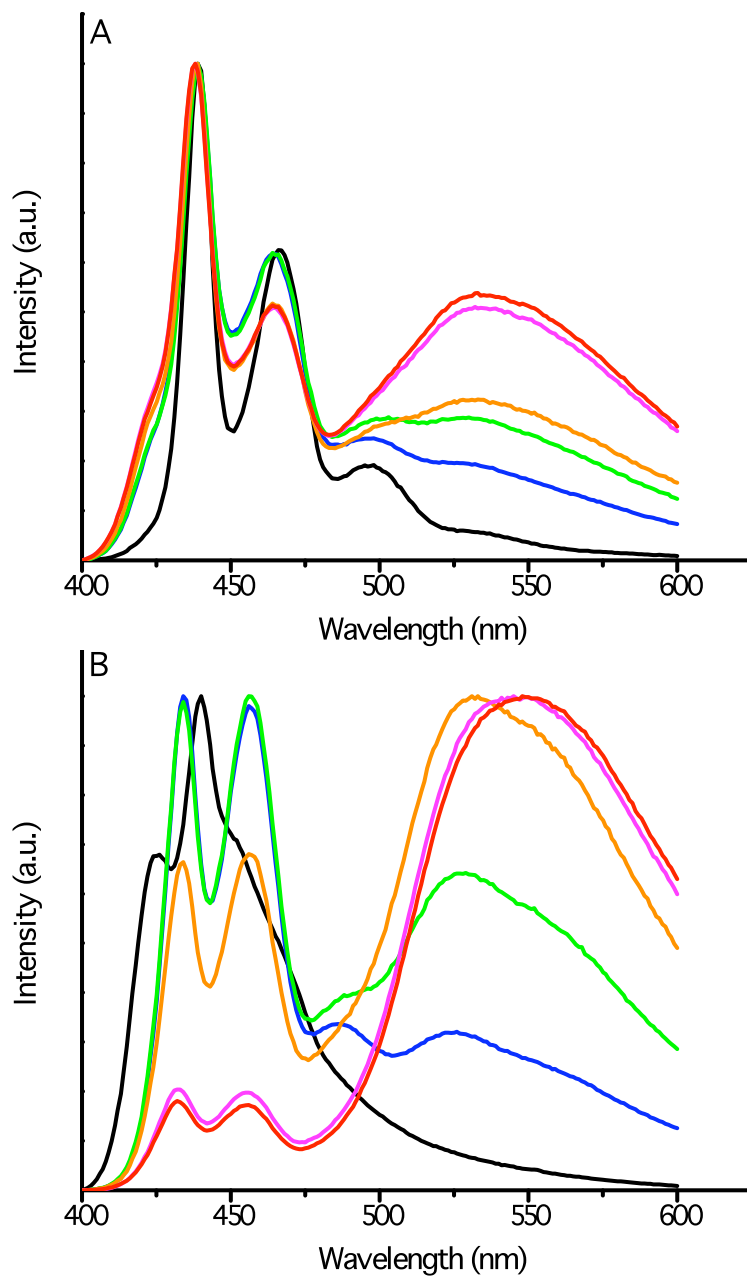


Figure 2-14: Normalized photoluminescence spectra of thin films (ca. 100nm) cast from solutions of the PFO-PPE blend (A) and PFO (B) measured prior to (black) and following

annealing in air for one hour (blue), three hours (green), five hours (orange), twenty-two hours (pink), and twenty-five hours (red) ($\lambda_{\text{ex}} = 350 \text{ nm}$).

Similar observations have been noted for other PF-based blends.²⁸ The present observations are consistent with other reports of PFO blends, including the previously mentioned work by Ahn *et al.* in which formation of a micro-encapsulation environment upon blending PFO with relatively high concentrations of a non-innocent oxadiazole electron acceptor was proposed.² All of these findings may be reasonably attributed to a minimization of fluorenone-fluorenone interaction arising from the inclusion of a non-PFO blending agent.

2.2.6 Method of Stabilization

If the PPE induced amelioration of the 'g-band' arises from a minimization of fluorenone dipole interactions, the appearance of this spectral feature should, in principle, be reversed upon exposure to PPE. In this context, PFO films containing γ -phase domains and exhibiting intense 'g-band' emission were prepared (Figure 2-15, green trace). Pure PPE was spin-coated onto these films followed by annealing in air. The blue trace in Figure 2-15 shows the emission profile for films exposed to PPE. Clearly, the 'g-band' emission intensity diminished (green:blue ratio of 0.60 vs. 1.33 prior to addition of PPE) and the spectral signature of β -phase domains appears. PPE free films showed increased green emission (Figure 2-15, red trace), leading to a ratio of 1.63. These observations are consistent with PPE inducing polymer chain reorganization leading to the formation of β -phase domains while simultaneously severing the dipole interactions between fluorenone moieties.²

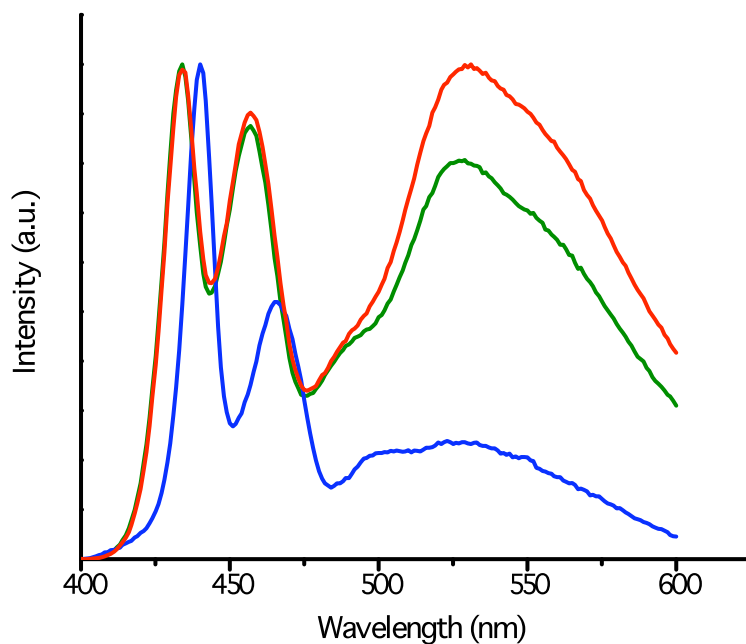


Figure 2-15 Normalized photoluminescence spectra of air-annealed PFO film (green), re-annealed in air (red), and re-annealed in air with PPE on top (blue) ($\lambda_{\text{ex}} = 350 \text{ nm}$).

2.2.7 Surface/Film Structure

AFM of spin-cast thin films of the present polymer composites show minor topographical differences; however, any chemical structural interpretation of these data can only be viewed as speculative. Prior to annealing, the 1-1 blend shows an increase in surface roughness compared to PFO and the 8-1 blend, consistent with PPE inserting itself between the PFO polymer chains. As expected the roughness of 3-1 and 5-1 blend films are intermediate to the 1-1 blend and PFO. Upon annealing, the surface features on the 1-1 blend are slightly enlarged, however this feature becomes even larger in the other films, especially PFO. Clearly the PPE incorporation improves the morphological stability of the films, consistent with presented optical analysis. PLM images show no substantial changes with the incorporation of PPE. SEM also shows films to be featureless. Furthermore, AES (Figure A2-1 - 2) shows oxygen content of the 1-1 blend to be small and uniform across the surface of the films, suggesting that these two polymers are miscible, at least when spin-coated. This miscibility gives credence to the theory that PPE is improving the spectral stability (in terms of the 'g-band') by severing the fluorenone-fluorenone

excimers. Given the importance of surface morphology in determining the performance of PLEDs and PVs the present blended system clearly presents few if any challenges.³

2.2.8 Polymer Light-Emitting Diodes

PLEDs were fabricated from PFO and the 1-1 blend. Turn-on voltages of the PFO/PPE devices, as shown in the current-voltage and light output-voltage plots (Figure 2-16 A and B), are equal to or slightly lower than for neat PFO devices. Turn-on voltages of all devices ranged from 4.5 to 6.0 volts. We do note the current increases more rapidly for the neat PFO device, likely due to the insulator nature of the PPE in the blend device.

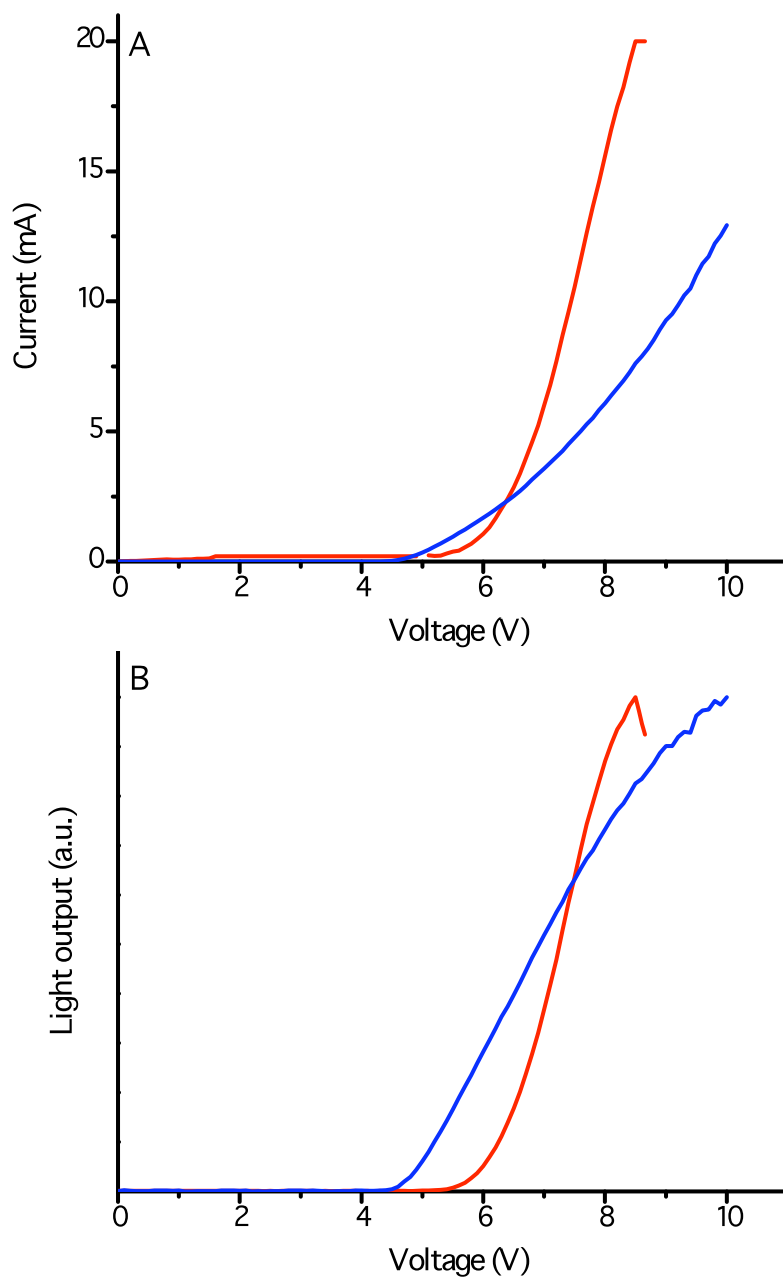


Figure 2-16 (A) Current versus voltage and (B) light output versus voltage for devices made from the 1-1 blend (blue) and PFO (red).

The electroluminescent spectra from the PFO and PFO-PPE devices are shown in Figure 2-17B. Clearly, in the absence of any thermal stressing, devices employing a PFO emissive layer show substantial ‘g-band’ character (red trace) while this emission is completely absent from the spectrum obtained for the device based upon the PFO-PPE blend (blue trace). Devices with the

A version of this chapter has been published. Sirtonski et al., 2010, J. Mater. Chem., 20:8147-8152. 39

blended emissive layer show a slight red shift in emission maximum relative to neat PFO. The Commission Internationale de l'Eclairage (CIE) x-y colour coordinates for the PFO Device were (0.232, 0.269). As expected based on the spectral differences between the blend based device and the PFO device, the PFO-PPE blend device gave CIE x-y coordinates of (0.218, 0.189), showing its more pure blue emission.

The external quantum efficiencies (EQE) are also comparable, if not identical, between the devices with the PFO and blend devices both giving a maximum EQE of about 0.016% (Figure 2-17A, See Appendix A2 for details on EQE calculation). While these numbers are low, the devices were not optimized for efficiency and were used to evaluate spectral quality. These results clearly show proof-of-concept feasibility for making functional PLEDs from PFO-PPE blends that exhibit improved luminescent purity over devices using PFO emissive layers alone.

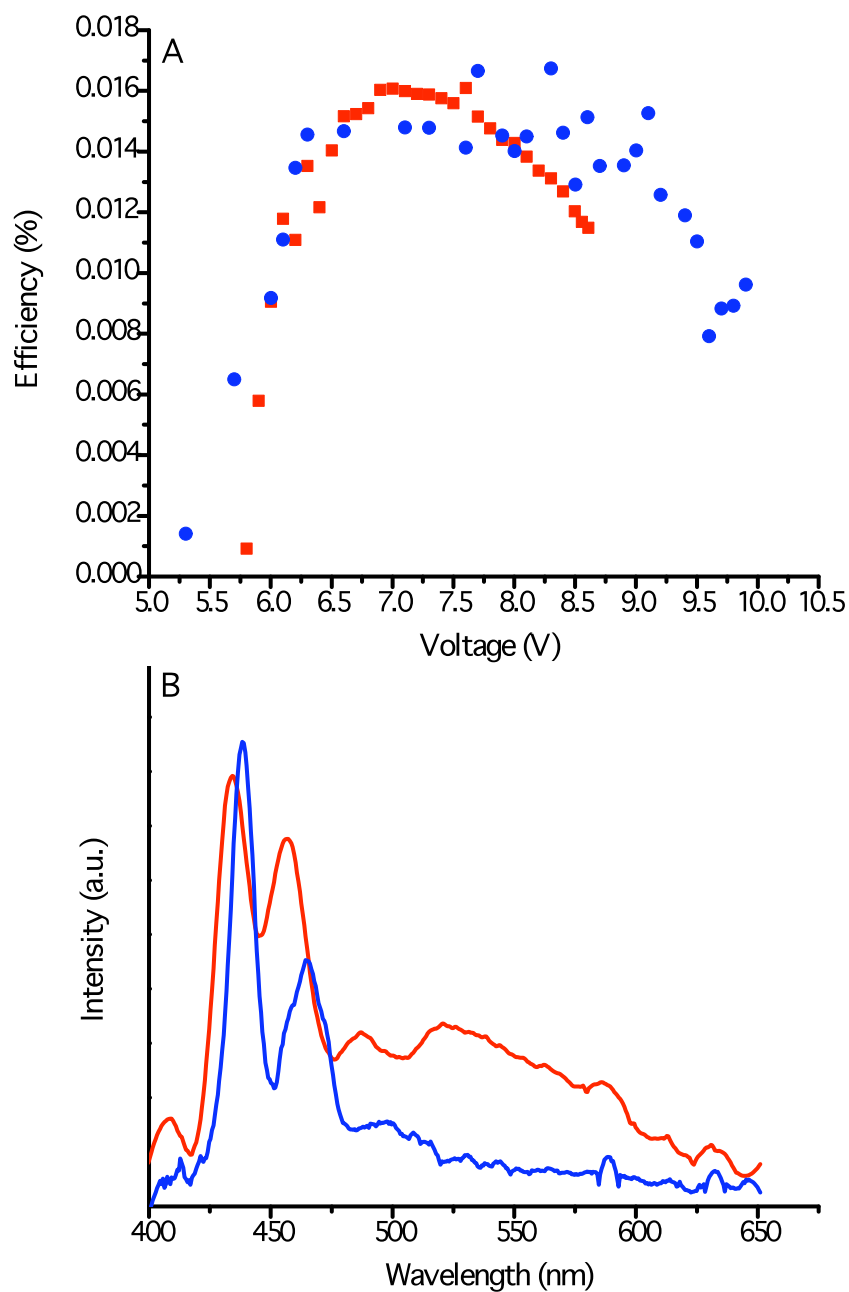


Figure 2-17 (A) External quantum efficiency versus voltage and (B) normalized electroluminescence spectra of devices made from the 1-1 blend (blue) and PFO (red).

2.2.9 Conclusions

Spin coating mixtures of PFO-PPE gives composite films with β -phase spectral features and substantially reduced 'g-band' emission. Reduced 'g-bands' were also seen for the PFO-PPO,

PFO-m-DB and PFO-p-DB blends, but to a much lesser extent than the PFO-PPE blend. It is reasonable these observations in the PFO-PPE composite arise from the lower solvating power of the system that the introduction of PPE provides, and the minimization of fluorenone-fluorenone interactions through the miscibility of the spin-coated PFO-PPE blend. Adding to the attractiveness of these composites, AFM, PLM, SEM and AES indicate no detectable phase segregation within the film structure or surface from the PPE incorporation, further suggesting miscibility. Finally, prototype PLEDs made from this composite show improved spectral features when compared to devices fabricated from pure PFO.

2.3 References

1. D. Sainova, T. Miteva, H. G. Nothofer, U. Scherf, I. Glowacki, J. Ulanski, H. Fujikawa and D. Neher, *Appl. Phys. Lett.*, 2000, **76**, 1810-1812.
2. J. H. Ahn, C. Wang, I. F. Perepichka, M. R. Bryce and M. C. Petty, *J. Mater. Chem.*, 2007, **17**, 2996-3001.
3. A. P. Kulkarni and S. Jenekhe, *Macromolecules*, 2003, **36**, 5285-5296.
4. X. Gong, P. K. Iyer, D. Moses, G. C. Bazan, A. J. Heeger and S. S. Xiao, *Adv. Funct. Mater.*, 2003, **13**, 325-330.
5. Z. Z. Denchev and N. V. Dencheva, *Polym. Int.*, 2008, **57**, 11-22.
6. L. A. Utraki, *Polymer Blends Handbook*, Springer-Verlag, 2002.
7. S. Ziaee and D. R. Paul, *J. Polym. Sci. Part B: Polym. Phys.*, 1996, **34**, 2641-2656.
8. W. M. Hess, C. R. Herd and P. C. Vegvari, *Rubber Chem. Technol.*, 1993, **66**, 329.
9. A. J. Heeger, *Chem. Soc. Rev.*, 2010, **39**, 2354-2371.
10. M. E. Joaquim, in *Synthetic Lubricants And High-Performance Functional Fluids*, eds. L. R. Rudnick and R. L. Shubkin, 1999, pp. 239-251.
11. T. Xu, D. Wu and L. Wu, *Prog. Polym. Sci.*, 2008, **33**, 894-915.
12. J. A. Grande, *Plastics Technology*, 2007, **53**, 58-63.
13. Santolubes, Santolube OS-124 MSDS, <http://www.santolubes.com/resources/tds-msds/MSDS-SANTOVAC-OS-124.pdf>, Accessed Oct. 29, 2010.
14. H. Azuma, T. Kobayashi, Y. Shim, N. Mamedov and H. Naito, *Organic Electronics*, 2007, **8**, 184-188.
15. Santolubes, Santolube OS-124 Technical Data Sheet, <http://www.santovac.com/resources/tds-msds/TDS-SANTOVAC-OS-124.pdf>, Accessed Oct. 20, 2010.

16. W. Chunwaschirasiri, B. Tanto, D. L. Huber and M. J. Winokur, *Phys. Rev. Lett.*, 2005, **94**, 107402.
17. M. Grell, D. D. C. Bradley, G. Ungar, J. Hill and K. S. Whitehead, *Macromolecules*, 1999, **32**, 5810-5817.
18. F. B. Dias, J. Morgado, A. L. Macanita, F. P. da Costa, H. D. Burrows and A. P. Monkman, *Macromolecules*, 2006, **39**, 5854-5864.
19. P. Blondin, J. Bouchard, S. Beaupre, M. Belletete, G. Durocher and M. Leclerc, *Macromolecules*, 2000, **33**, 5874-5879.
20. A. J. Cadby, P. A. Lane, M. Wohlmenannt, C. An, Z. V. Vardeny and D. D. C. Bradley, *Synth. Met.*, 2000, **111-112**, 515-518.
21. G. Ryu, R. Xia and D. D. C. Bradley, *J. Phys.: Condens. Matter*, 2007, **19**, 056205.
22. B. J. Schwartz, *Annu. Rev. Phys. Chem.*, 2003, **54**, 141-172.
23. K. L. Chan, M. Sims, S. I. Pascu, M. Ariu, A. B. Holmes and D. D. C. Bradley, *Adv. Funct. Mater.*, 2009, **19**, 2147-2154.
24. K. Becker, J. M. Lupton, J. Feldmann, B. S. Nehls, F. Galbrecht, D. Gao and U. Scherf, *Adv. Funct. Mater.*, 2006, **16**, 364-370.
25. F. Montilla and R. Mallavia, *Adv. Funct. Mater.*, 2007, **17**, 71-78.
26. R. Grisario, G. P. Suranna, P. Mastrorilli and C. F. Nobile, *Adv. Funct. Mater.*, 2007, **17**, 538-548.
27. T. A. M. Ferenczi, M. Sims and D. D. C. Bradley, *J. Phys.: Condens. Matter*, 2008, **20**, 045220.
28. B. He, J. Li, Z. Bo and Y. Huang, *Macromolecules* 2005, **38**, 6762-6766.

Chapter 3

Aromatic Ether-Dioctylfluorene Random Copolymers

3.0 Introduction

In Chapter 2, it was found blending poly(9,9-dioctylfluorene) (PFO) with polyphenyl ether (PPE) lead to improvements in PFOs spectral stability. This observation raises the question, what effect would incorporating aromatic ethers (AEs) directly and covalently into the backbone of the polyfluorene (PF) have on its spectral stability? It is expected based upon the miscibility of PFO and PPE and observations of spin-coated films that placing AE into the polymer backbone would decrease the mobility of the AE within the film. If minimizing AE mobility decreases phase separation with heating, fluorenone moieties would also be separated and the dipole interactions associated with the formation of fluorenone-fluorenone excimers responsible for deleterious green emission would be minimized. In this regard, incorporating AE blocks into the backbone could improve PFO's spectral stability. Another influence of this structure is the non-conjugated nature of AE blocks would decrease the extent of intramolecular charge transfer, isolating excitons and limiting their migration to the low energy fluorenone defects sites.

When copolymerizing fluorene with an electrically insulating moiety, effective conjugation length (ECL) must be discussed.¹ The ECL is defined as the minimum number of repeat units necessary to achieve saturation of the optical and electronic properties.² ECLs are most easily determined by oligomer studies, where oligomers of increasing lengths are prepared and characterized until optical and/or electronic saturation occurs. The first report of ECL for a PF based material (i.e., poly(9,9-dihexylfluorene) (PFH, Figure 3-1)) showed an ECL of twelve for absorption and six for photoluminescent (PL) emission.³ This apparent discrepancy was justified in the context of a proposed significant change in the polymer backbone geometry between the ground and vibronically relaxed excited states. Similar values have also been reported for PFO and correspond to absorbance and PL spectra maxima of 380 nm and 400 nm, respectively.⁴ Alternatively, ladder-poly-para-phenylene (LPPP, Figure 3-1), which may be considered a fully planar PF, has absorption and PL maxima at 438 nm and 470 nm, respectively.^{1,5} The difference in spectral properties of PF and LPPP clearly shows the effect of twisting along the polymer backbone. To date, the ECL of LPPP has not been reported, although based upon optical characterization it is clearly higher than that of PFO. Falling between PFO and LPPP, poly-2,8-indenofluorene (PIF, Figure 3-1) exhibits absorption and PL ECLs of six to seven and five to six, corresponding to spectra maxima of 416 nm and 429 nm, respectively.¹ It should be noted that PIF monomer are effectively 1.5 times the length of PFO monomers, so the ECLs of PIF should be multiplied by 1.5 to more directly compare to the ECLs of PFO. While these investigations provide insight into the optical and electronic properties of these polymers, all of the ECL

determinations were obtained by recording absorbance and PL spectra of oligomers and polymers in solution. These spectra will have blue-shifted maxima compared to thin film spectra because the polymer chain can rotate much more freely resulting in an apparent decrease of the observed ECL relative to equivalent solid state systems. As the PL maximum blue-shifts more than the absorbance maximum (i.e., PFO has solution absorbance and PL maxima of 380 nm and 400 nm, but thin film maxima of 380 nm and 425 nm) it is possible that the changes in backbone geometry are accentuated by solvation. Thus, the thin film PL ECL for PFO, PFH, and PIF may be larger than reported, and more in line with the absorbance ECL. Similar to ECL, conjugation length can be defined as the number of monomers consecutively bonded together without any defects. In this context, defects would be anything which ends the conjugation, whether an actual chemical defect or a twist in the backbone. As such conjugation length is a more accurate term in describing what is going on in copolymer films, as saturation of optical properties is not likely.

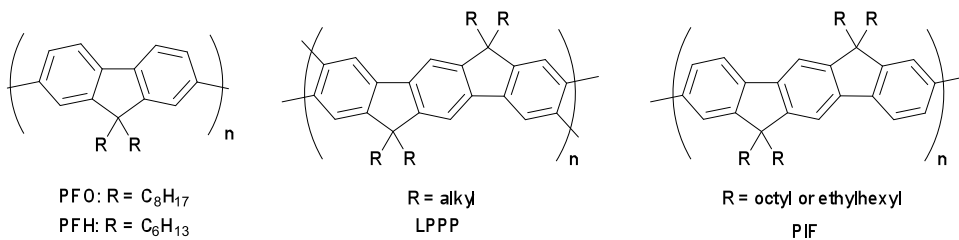
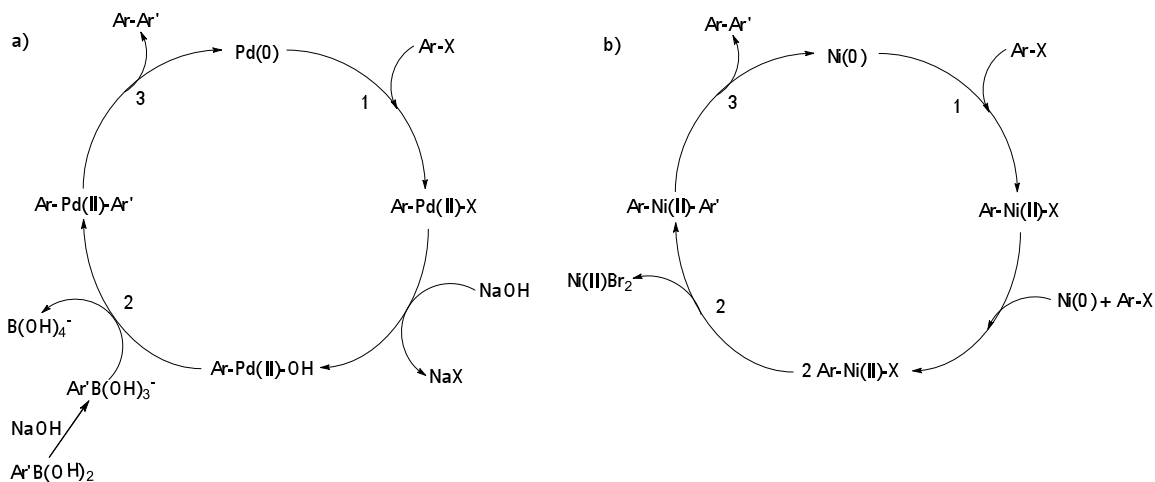


Figure 3-1 Structures of PFO, PFH, LPPP, and PIF.

The first method used to polymerize alkyl substituted fluorenes was oxidative coupling of 9,9-dihexylfluorene with FeCl_3 .⁶ While this approach was successful in affording PFH, it only yielded low molecular weight (M_n up to 5000) material, and the reaction is not regioselective, leading to structural defects. Following this first report, the Yamamoto⁷ and Suzuki-Miyaura⁸ cross-coupling reactions have come to dominate the literature reports of PF synthesis.⁹ The Suzuki-Miyaura reaction involves coupling of fluorene-diboronic acids and dihalofluorenes using a palladium catalyst (Scheme 3-1a).¹⁰ This polymerization procedure leads to polymers with a maximum M_n of tens of thousands.¹¹ Yamamoto-type reactions involve aryl-aryl coupling of dihalofluorenes using $\text{Ni}(\text{COD})_2$ in the presence of 2,2-dipyridal (BPY) (Scheme 3-1b).¹² The main advantage of the Yamamoto cross-coupling over the Suzuki-Miyaura cross-coupling is M_n s of up to 200000 can routinely be realized.¹³ However, as can be seen in Scheme 3-1b, the Ni is consumed during the reaction and results in substantial Ni impurities within the film that compromise material purity.¹⁴

Scheme 3-1 a) Generalized Suzuki-Miyaura cross-coupling reaction, and b) Generalized Yamamoto cross-coupling reaction, where Ar = aromatic group, X = halogen, 1 = oxidative addition, 2 = transmetalation, and 3 = reductive elimination (ligands not directly involved have been omitted for clarity).



One drawback of these cross-coupling reactions is their long reaction times under typical benchtop reaction conditions. These reaction times can be dramatically reduced by using microwaves. While the first reports of using microwaves in organic syntheses appeared in 1986,^{15, 16} they were not applied to PF research until 2002 when Carter demonstrated PF could be prepared in ten minutes using a microwave, rather than the typical reaction time of several days.¹⁷ Beyond the obvious advantages of shorter reaction times, the amount of side reactions were decreased and a purer product was obtained. Carter used the Yamamoto cross-coupling and demonstrated that M_n could be tuned by the addition of end-capper, with a M_n range of 5100 to 104600. The reduced reaction time arises from a variety of factors. The input energy is absorbed by the sample and solvent not the container, allowing for more direct and immediate heating.¹⁸ This is what is responsible for the so called 'microwave effect' which was believed to lower the activation energy of the reaction.¹⁹ In reality as the input energy is directly absorbed by the sample, rather than transmitted from the vessel, there is more energy available, and so the activation energy is achieved faster and easier. Higher temperatures are also available due to the increased pressure, decreasing the time required for reaction.¹⁸ Shortened reaction time is not the only advantage of using a microwave. The higher pressure associated with the reaction also allows for the use of lower boiling solvents which make product purification easier.¹⁸ The input of energy starts and stops immediately, and both the power and heating rates can be controlled,

limiting power consumption.¹⁸ The reactor can be automated and controlled externally, increasing ease of use.¹⁸ The sealed container and increased pressure also minimizes the loss of volatile reactants.¹⁸ Generally, reaction conditions are easier to measure, reproduce and scale up.¹⁸ Finally, selective heating is possible when using multi-phase systems and/or microwave active reagents/catalysts.²⁰ In addition to all of these advantages, performing Yamamoto cross-coupling reactions in a microwave allows for a one-pot, one-step reaction, eliminating the need for a separate catalyst activation step.¹⁷

This Chapter describes the preparation of a new molecule, bis(4-bromophenoxy) benzene, which was polymerized with dioctylfluorene to yield random AE-PF copolymers via both Yamamoto (PAEFO) and Suzuki-Miyaura (PAEFO-S) cross-couplings. Bis(4-bromophenyl) ether was also polymerized with dioctylfluorene via a Yamamoto cross-coupling (PAEFO-2). All three polymers show improved spectral stability compared to not only PFO, but to the PFO-PPE blend as well. In addition to being highly luminescent, PAEFO and PAEFO-2 are highly coloured and magnetic, suggesting they may find application in new heretofore unknown multifunctional devices designed to exploit these characteristics. Such multifunctional materials are of great interest and are believed to have the ability to significantly alter the design and function of future devices.²¹

3.1 Experimental

3.1.1 Chemicals

All reagents and solvents were purchased from commercial sources and used as delivered unless specified, PFO (ADS129BE: American Dye Source, Inc); 4-bromophenol, bis(4-bromophenyl) ether, 1,4-dichlorobenzene, ferrocene, aluminum chloride, ammonium hexafluorophosphate, dimethylglyoxime, N,N-dimethylformamide anhydrous 99.8% (DMF), BPY, 1,5-cyclooctadiene (COD), 5-bromo-1,3-dimethylxylene, 3,5-dimethylphenylboronic acid, 9,9-dioctylfluorene-2,7-diboronic acid bis(1,3-propanediol) ester and 9,9-dioctyl-2,7-dibromofluorene (Aldrich); bis(4-bromophenyl) ether (Alfa Aesar); ethyl ether (Fisher); potassium carbonate, toluene, concentrated HCl diluted with distilled water, chloroform, dichloromethane and acetonitrile (Caledon); celite (EMD); Ni(COD)₂, Pd(PPh₃)₄, and Al powder (Strem); η^6 -1,4-dichlorobenzene- η^5 -cyclopentadienyliron hexafluorophosphate was prepared according to literature procedures.²²

3.1.2 Procedures

Microwave syntheses were carried out with a Biotage Initiator System. Solutions used for spin-coating were prepared by dissolving PFO, PAEFO, PAEFO-2, or PAEFO-S in chloroform (0.01 g polymer per ml CHCl₃). PFO solutions were heated slightly to ensure full dissolution. Thin films were prepared by spin-coating from stock solutions onto optical grade fused quartz substrates (ESCO Products) using a Laurell Technologies Corporation model WS-400B-6NPP/LITE/AS spinner. Spinning started at 500 rpm for 5 seconds, followed by 1000 rpm for 10 seconds and finally 4000 rpm for 40 seconds.

3.1.3 Characterization

¹H NMR and ¹³C NMR spectra were recorded with a Varian Inova 300 (300 MHz) and a Varian Inova 500 (500 and 125 MHz). Elemental analysis (EA) was performed with a Carlo Erba CHNS-O EA 1108 elemental analyzer. Fourier transform infrared spectroscopy (FTIR) was carried out using a Nic-Plan FTIR Microscope attached to a Nicolet Magna 750 FTIR spectrometer. Mass spectrometry was performed on Kratos MS50G electron impact (EI) and Bruker Ultraflex extreme matrix assisted laser desorption ionization time of flight (MALDI-TOF) systems. Gel permeation chromatography (GPC) was performed using a Viscotek GPC MAX 270, calibrated against polystyrene standards at a flow rate of 0.5 ml/min with THF as the solvent. Thermogravimetric analysis (TGA) was carried out in nitrogen at a heating rate of 10 °C/min using a Perkin Elmer Pyris 1 TGA. UV-visible spectra were obtained using a Hewlett Packard 8453 UV-VIS DAD Spectrophotometer. Photoluminescence (PL) measurements were recorded with a Varian Cary Eclipse Fluorescence Spectrophotometer ($\lambda_{\text{ex}} = 350$ nm, slit width parameter = 2.5 nm). Ratios of the absolute intensities of the green and blue spectral regions were determined by integrating over the 500-600 nm range (green) and dividing by the integrated 400-500 nm range (blue). Monomer ratios were calculated by dividing the number of moles of the fluorene monomer that were added to the reaction by the number of moles of the added aromatic-ether.

3.1.4 Synthesis of Bis(4-bromophenoxy) benzene

1.00 g η^6 -1,4-dichlorobenzene- η^5 -cyclopentadienyliron hexafluorophosphate, 2.10 g 4-bromophenol, 2.26 g potassium carbonate were combined in a 50 ml round bottom flask with 10 ml DMF. The solution was heated to 50 °C for 5 hours and then allowed to stir at room temperature for 12 hours without light. This brown solution was poured into 80 ml of 10% HCl_(aq) and vacuum filtered, washing with copious amounts of ethyl ether until a dry solid was obtained

in 72 % yield. 0.86 g of the collected solid was placed in a 20 ml microwave vial with 0.95 g dimethylglyoxime, 10 ml DMF, and 10 ml acetonitrile. This vial was heated in the microwave for 12 minutes at 200°C, and then poured into 150 ml of 10% HCl_(aq). Vacuum filtration yielded a black solid that was triturated in 15 ml toluene, filtered through celite, and finally washed with 25 ml toluene. After removal of the toluene by evaporation the remaining brown solid was dissolved in a minimum volume of dichloromethane, and added dropwise to 50 ml of 90% ethanol, 10% water. After settling, this solution was vacuum filtered to get the desired flakey white solid in 29 % yield. ¹H NMR (300 MHz, CDCl₃): δ 7.43 (m, 4 H); 7.27 (s, 4 H); 6.88 (m, 4 H). ¹³C NMR (125 MHz, CDCl₃): δ 156.88, 152.56, 132.72, 120.61, 119.99, 115.56. HRMS calculated for C₁₈H₁₂Br₂O₂: 419.91837. Found: 419.91799. EA calculated for C₁₈H₁₂Br₂O₂: C, 51.46; H, 2.87; O, 7.62. Found: C, 51.37; H, 2.84; O, 9.00.

3.1.5 Synthesis of PAEFO

Predetermined amounts of 9,9-dioctyl-2,7-dibromofluorene and bis(4-bromophenoxy) benzene (Table 3-1), 0.40 g Ni(COD)₂, 0.20 g BPY, 0.16 ml COD, 5 ml DMF, and 10 ml distilled toluene were combined in a 20 ml microwave vial in an argon filled MBraun glovebox. The sealed vial was removed from the glove box and heated for 10 minutes at 230 °C in the microwave. The reaction mixture was poured into 150 ml methanol to precipitate the polymer. This solution sat overnight to allow for polymer aggregation, and then it was filtered. The solid was washed with methanol and acetone to remove remaining reactants and lower weight oligomers. The remaining solid was dissolved in toluene and refiltered. The solvent was evaporated leaving the polymer behind. MALDI-TOF MS polymer repeat unit (C₂₉H₄₀ and C₁₈H₁₂O₂): Calculated: 388.6305 and 260.2883. Found: ca. 388 amu and ca. 260 amu. ¹³C NMR (125 MHz, CDCl₃): δ 157, 152, 141, 140, 139, 128, 126, 121, 120, 119, 118, 55, 40, 31, 30, 29, 24, 23, 14.

Table 3-1 Monomer masses used and the associated monomer ratios in the Yamamoto synthesis of PAEFO.

| Run | Fluorene (g) | AE (g) | Fluorene:AE monomer ratio |
|-----|--------------|--------|---------------------------|
| 1 | 0.28 | 0.03 | 7:1 |
| 2 | 0.34 | 0.02 | 13:1 |
| 3 | 0.25 | 0.11 | 2:1 |

3.1.6 Synthesis of PAEFO-2

Predetermined amounts of 9,9-dioctyl-2,7-dibromofluorene and bis(4-bromophenyl) ether (Table 3-1), 0.40 g Ni(COD)₂, 0.20 g BPY, 0.16 ml COD, 5 ml DMF, and 10 ml distilled toluene were combined in a 20 ml microwave vial in an argon filled MBraun glovebox. The sealed vial was removed from the glove box and heated for 10 minutes at 230 °C in the microwave. The reaction mixture was poured into 150 ml methanol to precipitate the polymer. This solution sat overnight to allow for polymer aggregation, and then it was filtered. The solid was washed with methanol and acetone to remove remaining reactants and lower weight oligomers. The remaining solid was dissolved in toluene and refiltered. The solvent was evaporated leaving the polymer behind. MALDI-TOF MS polymer repeat unit (C₂₉H₄₀ and C₁₂H₈O): Calculated: 388.6305 and 168.1924. Found: ca. 388 amu and ca.168 amu. ¹³C NMR (125 MHz, CDCl₃): δ 133, 129, 123, 120, 119, 32, 30, 29, 23, 14.

Table 3-2 Monomer masses used and the associated monomer ratios in PAEFO-2 synthesis.

| Run | Fluorene (g) | AE (g) | Fluorene:AE monomer ratio |
|-----|--------------|--------|---------------------------|
| 1 | 0.23 | 0.07 | 2:1 |
| 2 | 0.26 | 0.01 | 11:1 |

3.1.7 Synthesis of PAEFO-S

1.11 g 9,9-dioctylfluorene-2,7-diboronic acid bis(1,3-propanediol) ester, 1.24 g 9,9-dioctyl-2,7-dibromofluorene, 0.08 g bis(4-bromophenoxy) benzene, 0.02 g Pd(PPh₃)₄ and 33 ml toluene were combined in a 100 ml round bottom flask in an argon filled MBraun glovebox. This leads to a fluorene:AE monomer ratio of 23:1. The flask was removed from the glovebox and placed on a Schlenk line to maintain inert atmosphere. 20 ml of degassed 2M K₂CO₃ in water was added via cannula. This mixture was heated at 80 °C for four days at which point the temperature was lowered to 50 °C. 25 μL 5-bromo-1,3-dimethylxylene, and 0.06 g 3,5-dimethylphenylboronic acid were added and the mixture was kept at 50 °C for three days, before heating it at 80 °C for an additional five hours. The reaction contents were poured into 150 ml methanol to precipitate the polymer as before. The remaining work up was identical to that reported for the microwave Yamamoto synthesis, with the exception of an additional washing of the crude product with water to remove any excess K₂CO₃. MALDI-TOF MS polymer repeat unit (C₂₉H₄₀ and C₁₈H₁₂O₂):

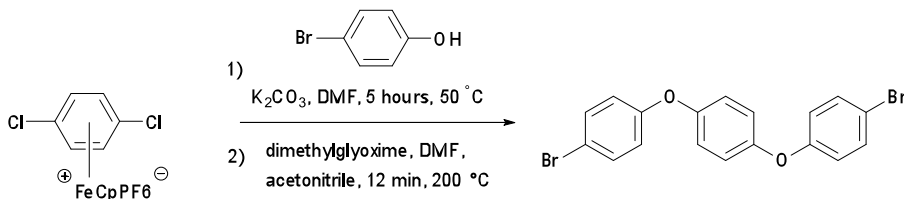
Calculated: 388.6305 and 260.2883. Found: ca. 388 amu and ca. 260 amu. ^1H NMR (500 MHz, CDCl_3): δ 7.87, 7.86, 7.79, 7.77, 7.73, 7.72, 7.70, 7.66, 7.63, 7.62, 7.52, 7.50, 7.32, 7.14, 2.14, 1.56, 1.23, 1.22, 1.16, 1.12, 0.86, 0.85, 0.84, 0.84, 0.83, 0.83, 0.82, 0.10. ^{13}C NMR (125 MHz, CDCl_3): δ 153, 152, 151, 141, 140, 137, 126, 121, 120, 55, 40, 32, 30, 29, 24, 23, 14, 1.

3.2 Results and Discussion

3.2.1 Monomer Synthesis

To incorporate aromatic ether groups into the polymer backbone of PFO (bis(4-bromophenoxy) benzene) was synthesized according to Scheme 3-2. This procedure is similar to that used by McFarlane *et al.* to synthesize AE chains on the 9 position of fluorene monomers.²³

Scheme 3-2 Synthesis of (bis(4-bromophenoxy) benzene).



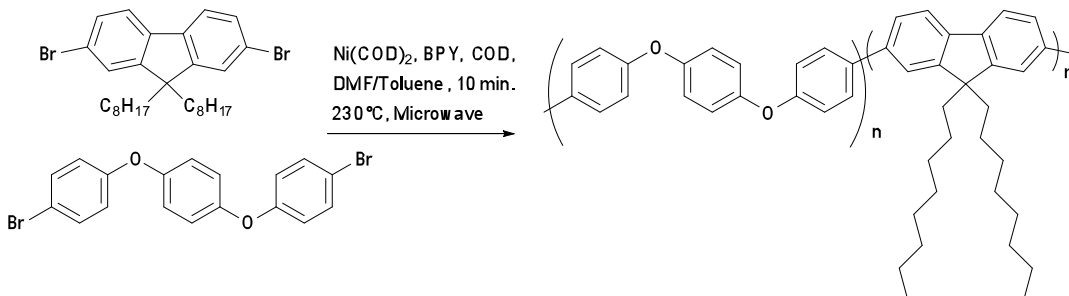
3.2.2 Monomer Characterization

EI MS, FTIR, EA, ^1H NMR and ^{13}C NMR were performed to confirm the structure of bis(4-bromophenoxy) benzene. EI MS (Figure A3-1) shows a parent peak at 419.9 as expected. EA shows an oxygen content slightly higher than predicted, but carbon and hydrogen content is consistent with the expected values. It is possible the higher oxygen content arises from water impurities also evident in the ^1H NMR spectrum. ^1H NMR (Figure A3-3) shows two distinct multiplets, centered at δ 7.43 and 6.88, and a singlet at δ 7.27. All three signals integrate to four protons as expected from the structure. The singlet is readily assigned to the four equivalent protons on the central aryl ring, while the two multiplets would correspond to the four protons next to the Br groups (δ 7.43), and the four protons next to those (δ 6.88). The ^{13}C NMR spectrum (Figure A3-4) is remarkably similar to that reported for 1,4-diphenoxybenzene.²⁴ The major difference is seen in the signal arising from the carbon bonded to Br, which shows a large decrease in shielding with a drop to δ 115.56 from δ 123.02. ^1H - ^{13}C short-range hetero-nuclear (HMQC) 2D NMR (Figure A3-5) was used to confirm assignments (Figure A3-6). Clearly, bis(4-bromophenoxy) benzene can be synthesized and purified using the method provided herein.

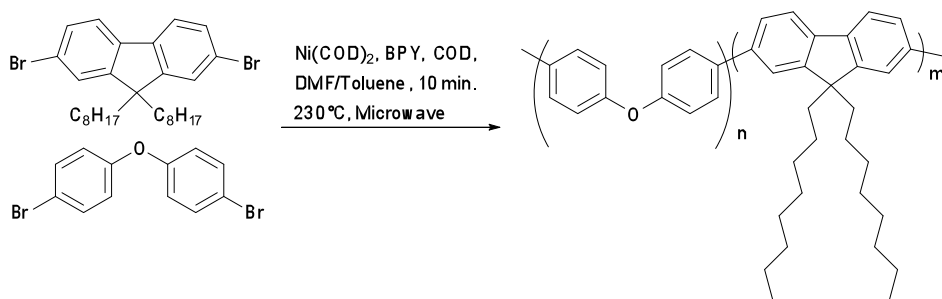
3.2.3 Polymer Synthesis

A series of random bis(4-bromophenoxy) benzene-dioctylfluorene copolymers (PAEFO) was synthesized under Yamamoto cross-coupling conditions²⁵ in a microwave²³ (Scheme 3-3). Fluorene:bis(4-bromophenoxy) benzene monomer ratios of 2:1, 7:1, and 13:1 were investigated. Another random bis(4-bromophenyl) ether-dioctylfluorene copolymer (PAEFO-2) was synthesized under identical conditions (Scheme 3-4) with fluorene:bis(4-bromophenyl) ether monomer ratios of 2:1 and 11:1. A similar random copolymer to PAEFO (PAEFO-S) was synthesized under Suzuki-Miyaura cross-coupling conditions²⁶ (Scheme 3-5) with a fluorene:bis(4-bromophenoxy) benzene monomer ratio of 23:1. Copolymers synthesized using the Yamamoto cross-coupling protocol (PAEFO and PAEFO-2) are dark blue in bulk, but are transparent when cast as a thin film, reminiscent of poly(ethylene dioxythiophene).²⁷ PAEFO-S on the other hand is light brown in bulk and transparent when cast as a thin film. Another key difference between PAEFO and PAEFO-S is microwave polymerizations yield hydrogen end-capped polymers while the addition of xylene end-capper is required for the bench-top synthesis in order to remove the bromo- and boronic ester end groups. The mass spectrum for PAEFO-S shows peaks corresponding to xylene end-capped polymer as well as polymers capped with bromine, boronic ester and combinations of those three. Further reaction with more xylene end-cappers is likely required to fully remove the bromine and boronic ester groups. Finally, no AE-AE cross-couplings were possible in this Suzuki-Miyaura reaction as only brominated AE monomer (i.e., no boronic acid functionalized AE) was used. Thus while the monomer ratio in PAEFO-S is substantially lower than the other copolymers, it may have a similar fluorene conjugation length, due to the AE moieties being spread out within the polymer chain.

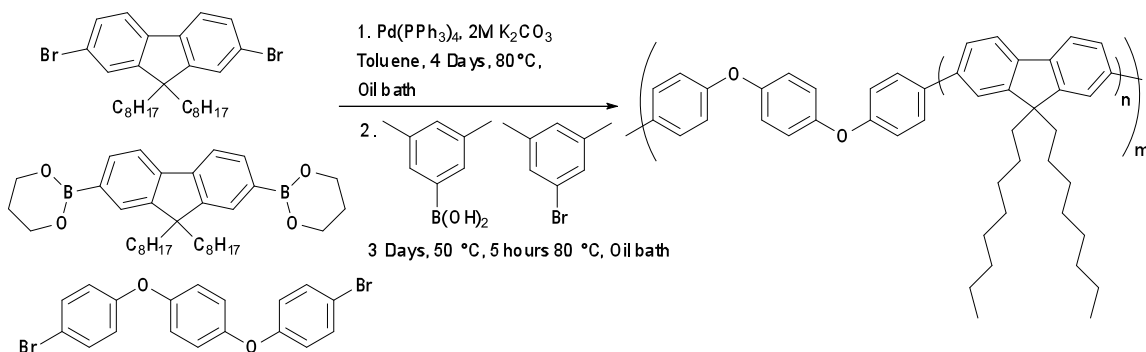
Scheme 3-3 Synthetic route to PAEFO.



Scheme 3-4 Synthetic route to PAEFO-2.



Scheme 3-5 Synthetic route to PAEFO-S.



3.2.4 Polymer Characterization

A detailed examination of the EA may provide some insight into the polymerizations. For example, if the oxygen content is higher than expected based upon the starting monomer ratios, it is reasonable to conclude the AE monomer reacted faster than the fluorene monomer; the opposite conclusion can be drawn if the oxygen concentration is low. Beyond providing information that bromine and boronic esters remain on the polymer chains of PAEFO-S, the EA for this polymer give little information, and will not be discussed further.

If solvent and/or other reagents remain in the polymer after work-up, elemental analyses will be affected (as seen with water in Section 3.2.2). As none of the mass percent totals found add up to 100% it is clear impurities made up of elements other than C, H and O persist in all of the polymers prepared here. Nitrogen and sulphur were not found by EA; however it is reasonable some nickel or bromine remain at trace levels. Given this limitation, only generalized conclusions will be drawn. All three PAEFO copolymers have higher than expected oxygen content and lower carbon and hydrogen contents. This observation suggests the fluorene:AE ratio in the film may be slightly lower than predicted by monomer ratios. However as the hydrogen content of these three

polymers is closer to what is predicted than the carbon content; some of this variability is clearly due to impurities. Oxygen content for the two PAEFO-2 copolymers is significantly higher than predicted. This suggests bis(4-bromophenyl) ether reacts faster than bis(4-bromophenoxy) benzene. However, these observations are speculative, and so NMR should provide a better understanding.

Table 3-3 EA calculated and found for each polymer based on fluorene:AE monomer ratios.

| Polymer | Monomer Ratio | Calculated | | | Found | | |
|---------|---------------|------------|-------|-------|-------|-------|------|
| | | C | H | O | C | H | O |
| PFO | 1:0 | 89.63 | 10.37 | 0 | | | |
| PAE | 0:1 | 83.06 | 4.65 | 12.29 | | | |
| PAEFO | 2:1 | 87.98 | 8.94 | 3.08 | 85.88 | 8.54 | 4.24 |
| PAEFO | 7:1 | 89.05 | 9.87 | 1.07 | 84.57 | 9.65 | 2.59 |
| PAEFO | 13:1 | 89.30 | 10.09 | 0.60 | 85.77 | 10.01 | 3.22 |
| PAEFO-S | 23:1 | 89.44 | 10.21 | 0.35 | 79.28 | 9.42 | 1.68 |
| PAE-2 | 0:1 | 85.69 | 4.79 | 9.59 | | | |
| PAEFO-2 | 2:1 | 88.92 | 9.38 | 1.69 | 72.37 | 8.10 | 5.22 |
| PAEFO-2 | 11:1 | 89.48 | 10.16 | 0.36 | 55.83 | 13.35 | 6.98 |

While the incorporation of metallic nickel into the polymers will broaden an NMR spectrum, some general structural information may be obtained. ^1H NMR of 2:1 PAEFO clearly shows seven broad peaks centered at δ 7.82, 7.69, 7.59, 7.13, 2.11, 1.15, and 0.83. This spectrum looks remarkably similar to that reported by Lee *et al.*²⁸ for 2-bromo-9,9-di-n-hexylfluorene, with the addition of the peaks at δ 7.59 and 7.13, suggesting these arise from AE moieties. Based upon the monomer NMR, δ 7.59 corresponds to the four protons closest to the polymer linkage points, and δ 7.13 arises from the remaining eight protons. As the peak at δ 7.59 overlaps with signals at δ 7.82 and 7.69 it can't be fully separated. Setting the integration of the three upfield peaks (the alkyl protons) to 80 (corresponding to two fluorene moieties) gives integration for δ 7.13 of eight,

corresponding to one AE unit. The three downfield peaks then have an integration of sixteen, four from the AE, and the other twelve from two fluorene moieties. This strongly suggests the fluorene:AE ratio in the polymer is the same as the monomer ratio used for polymerization, and while this contradicts the elemental analysis results, it should be more reliable. Similar results were found for 7:1 PAEFO and 13:1 PAEFO (Table 3-4). There are four fewer AE protons in the PAEFO-2 copolymers, so the upfield peak in the aromatic region should integrate to four rather than eight. In 2:1 PAEFO-2 this peak partially overlaps with the solvent peak making integration difficult. Setting the integration on this peak to four leads to a ratio of 2:1 according to the peaks from the alkyl chains. However the other aromatic peak suggests the ratio is closer to 1:1. Most likely the ratio for 2:1 PAEFO-2 is closer to 1:1, suggesting that bis(4-bromophenyl) ether reacts better/faster than bis(4-bromophenoxy) benzene. The peak overlap seen in 2:1 PAEFO-2 is accentuated in 11:1 PAEFO-2 as more nickel was used in the polymerization. As with 2:1 PAEFO-2, it is likely that 11:1 PAEFO-2 has more AE in the backbone than is suggested by the monomer ratio. Due to the variety of end-groups in PAEFO-S no similar information can be gained, though many of the peaks are at about the same chemical shift as those in the PAEFO copolymer.

Table 3-4 Monomer ratios for each PAEFO and PAEFO-2 copolymer combined with molar ratios for each as determined from the integration of the ^1H NMR spectra.

| Polymer | Fluorene:AE monomer ratio | NMR calculated Fluorene:AE ratio |
|---------|---------------------------|----------------------------------|
| PAEFO | 2:1 | 2:1 |
| PAEFO | 7:1 | 7:1 |
| PAEFO | 13:1 | 13:1 |
| PAEFO-2 | 2:1 | $\leq 2:1$ |
| PAEFO-2 | 11:1 | $\leq 11:1$ |

Molecular weight information for the copolymers was determined by MALDI-TOF MS and GPC (See Appendix A3). GPC showed 2:1 PAEFO to have a number-average molecular weight (M_n) of 22071 and a weight-average molecular weight (M_w) of 34085 with a polydispersity index (PDI = M_w/M_n) of 1.5. Determining the degree of polymerization (number of monomer units bonded together in a polymer chain)²⁹ from these numbers is very difficult because two different

monomers must be considered. Table 3-5 shows approximate number of monomer units that would correspond to these molecular weights while also maintaining a two to one molar ratio. As can be seen in Table 3-5 it can be estimated that the 2:1 PAEFO copolymer averages between 42 and 65 fluorene units and between 22 and 34 AE units, leading to average degree of polymerization from 64 to 99. Bradley *et al.*³⁰ have shown that GPC overestimates molecular weight values by about 2.7, though this is largely ignored in the literature as the numbers should all be overestimated by the same amount. In addition, it is reasonable to expect GPC of a copolymer to overestimate molecular weight values by a different amount than it would for either of the homo-polymers. For both of these reasons no corrections were made to M_n and M_w values. MALDI-TOF MS was employed to confirm the repeat units correspond to those calculated for each polymer (388 and 260 for PAEFO and PAEFO-S; 388 and 168 for PAEFO-2). MS also shows well resolved peaks up to about 6000 amu for all Yamamoto cross-coupled copolymers, suggesting little difference in molecular weight from batch to batch. PAEFO-S has a slightly lower molecular weight (MS shows well resolved peaks to about 5000 amu) than the Yamamoto cross-coupled copolymers consistent with previous studies (*vide supra*).

Table 3-5 Estimated average number of fluorene and AE monomer units per 2:1 PAEFO chain.

| | Found | Fluorene units | AE units | Calculated Molecular Weight | Calculated fluorene:AE molar ratio |
|-------|-------|----------------|----------|-----------------------------|------------------------------------|
| M_n | 22071 | 42 | 22 | 22020 | 2.1:1 |
| M_w | 34085 | 65 | 34 | 34060 | 2.0:1 |

Thermogravimetric analysis (TGA) of the polymers is almost identical to that of PFO (Figure 3-2), showing inclusion of AE linkages does not degrade the thermal stability of PFO. In fact, the three PAEFO copolymers show an onset of weight loss slightly higher than PFO. The PAEFO-2 copolymers show an onset of weight loss at a lower temperature than PFO, but the bulk of weight loss is at the same temperature as PAEFO, suggesting the early weight loss is due to monomers or oligomers remaining in the bulk polymer. PAEFO-S also shows an onset of weight loss lower than PFO, though this is minor. As PAEFO-S is the only polymer without fluorene moieties at the ends of the polymer it is possible the weight loss is initially due to the end-groups coming off, and then shifting to normal PAEFO decomposition mechanisms. As discussed in Chapter 2, the

primary cause of weight loss in all these polymers is likely due to thermal decomposition rather than evaporation as there is some residue remaining after the measurement.

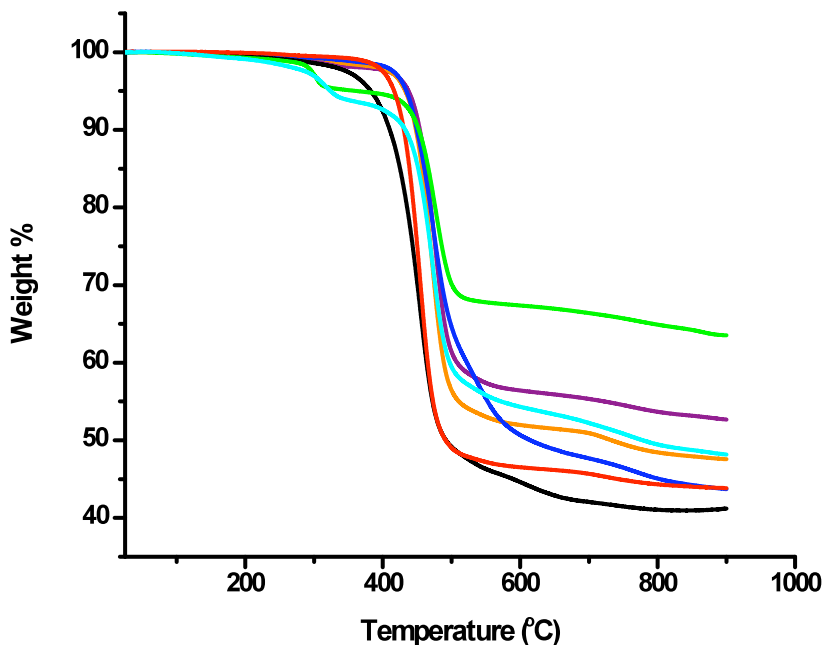


Figure 3-2 TGA curves of PAEFO (2:1 blue trace, 7:1 purple trace, and 13:1 orange trace), PAEFO-2 (2:1 cyan trace, and 11:1 green trace), PAEFO-S (black trace), and PFO (red trace) under a N₂ atmosphere at a heating rate of 10 °C/min.

3.2.5 Absorption/Emission spectra

To evaluate the optical spectroscopy (i.e., UV-vis absorption and PL), thin films of the polymer were spin-cast onto quartz substrates from CHCl₃ (1% w/v) solutions. The UV-vis absorption spectra of all the copolymers are very similar to the spectrum for PFO, showing a broad absorbance over the UV region (Figure 3-3). The difference is the copolymer absorbance spectra show a blue shift from 380 nm in neat PFO to 354 nm as the AE content is increased (See Table 3-6). PAEFO and PAEFO-2, both synthesized with monomer ratios of 2:1 have nearly identical absorbance with peaks at 354 nm and 358 nm, respectively. 7:1 PAEFO has the next most blue-shifted absorbance with a maximum at 374 nm. 13:1 PAEFO, 11:1 PAEFO-2, and PAEFO-S all have identical absorbance maxima at 378 nm. These observations (shorter wavelength absorption with higher AE content) fit with the inclusion of AE moieties shortening the conjugation length of the fluorene units along the polymer. As discussed earlier (See Section 3.0), the closer the

conjugation length is to the ECL, the smaller the difference in absorbance. Of course, it should also be noted that because the present copolymers exhibit a random structure there are likely segments of varying length along the polymer chain.

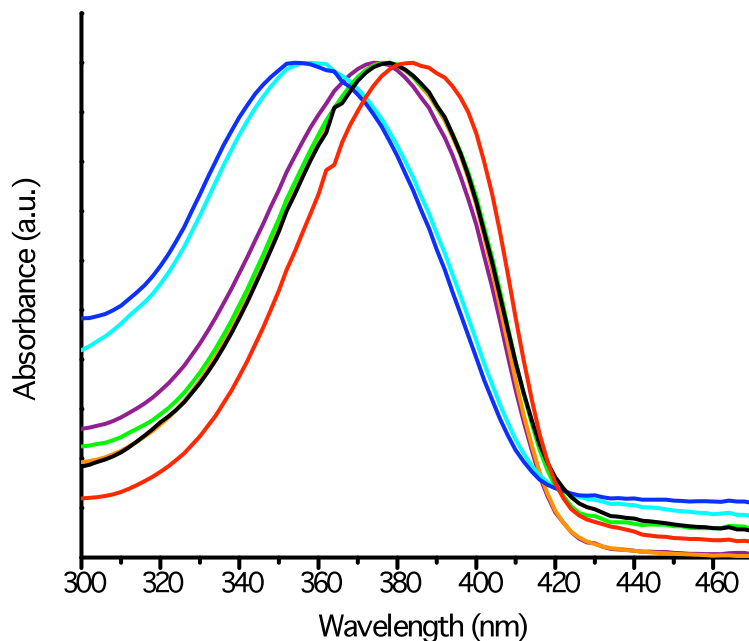


Figure 3-3 Normalized UV-vis absorbance spectra of a representative PFO film (red trace), representative PAEFO films (2:1 blue trace, 7:1 purple trace, and 13:1 orange trace), representative PAEFO-2 films (2:1 cyan trace, and 11:1 green trace), and a representative PAEFO-S film (black trace).

Table 3-6 Absorbance and emission spectra maxima as measured for all Polymers (emission maxima for α -phase PFO in brackets).

| Polymer | λ_{abs} max (nm) | λ_{em} max (nm) |
|------------|---------------------------------|--------------------------------|
| PFO | 380 | 440 (425) |
| 2:1 PAEFO | 354 | 420 |
| 7:1 PAEFO | 374 | 422 |
| 13:1 PAEFO | 378 | 424 |

| | | |
|--------------|-----|-----|
| 2:1 PAEFO-2 | 358 | 421 |
| 11:1 PAEFO-2 | 378 | 422 |
| PAEFO-S | 378 | 421 |

Consistent with the absorbance spectra, a red-shift is seen in the PL spectra as AE content is decreased (Figure 3-4). The PL maxima range from 420 nm with the higher AE content (2:1 PAEFO) to 424 nm (13:1 PAEFO). 7:1 PAEFO has a PL maximum half way in between at 422 nm, as does 11:1 PAEFO-2. 2:1 PAEFO-2 is closer to 2:1 PAEFO with a maximum at 421 nm. These observations support the conclusion drawn from the absorbance measurements that the AE moieties are shortening the conjugation length of the fluorene in the polymer. The one copolymer that does not fit is PAEFO-S as it has an emission maximum at 421 nm suggesting a conjugation length similar to the 2:1 PAEFO-2. Its absorbance maximum at 378 nm suggests it has the longest conjugation length of all the copolymers. A possible explanation for this observation is there may be a larger variation in conjugation lengths for PAEFO-S impacting the optical properties. It is also possible the chain end groups play a role, however additional systematic studies are required to confirm what role they play. If it is assumed the reports of PF ECL are accurate in the thin film (*vide supra*), then 2:1 PAEFO, with an absorbance maximum at 354 nm and an emission maximum at 420 nm, would have a conjugation length of about four fluorene units.³ Conjugation lengths for the other copolymers can be estimated to be at values between four and six fluorene units. The observation that the absorbance maxima of the different polymers fall over a larger range than the PL spectra supports the hypothesis that there are significant changes in the backbone geometry between the ground state and the vibronically relaxed excited state of the polymers and further suggests that these changes are not solely due to solution effects.

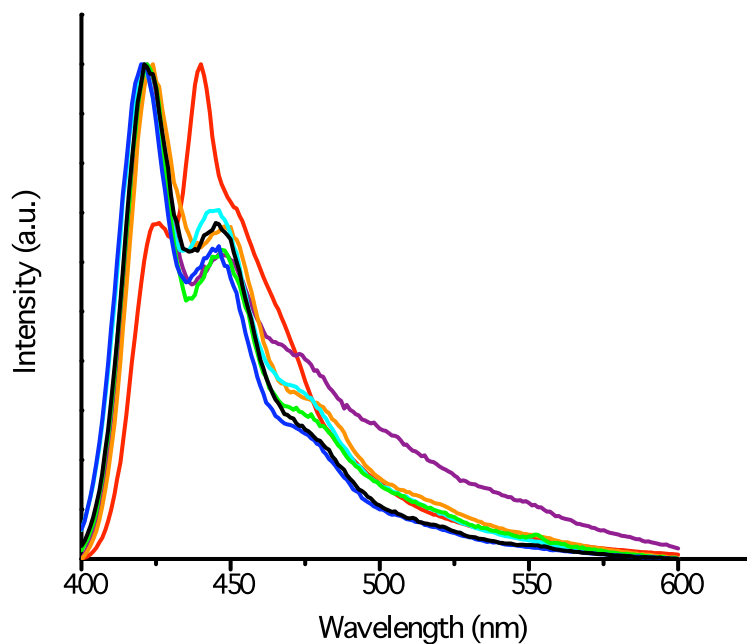


Figure 3-4 Normalized PL spectra of representative PFO (red trace), PAEFO (2:1 blue trace, 7:1 purple trace, and 13:1 orange trace), PAEFO-2 (2:1 cyan trace, and 11:1 green trace), and PAEFO-S (black trace) films ($\lambda_{\text{ex}} = 350$ nm).

3.2.6 Phase Stability

Upon thermal heating in a nitrogen environment, no spectral changes are observed in the UV-vis absorbance spectra of all the present copolymers indicating improved spectral stability over PFO which shows the appearance of a new feature at ca. 420 nm (Figure 3-5). This feature is characteristic of γ -phase formation within the film (See Chapter 1).

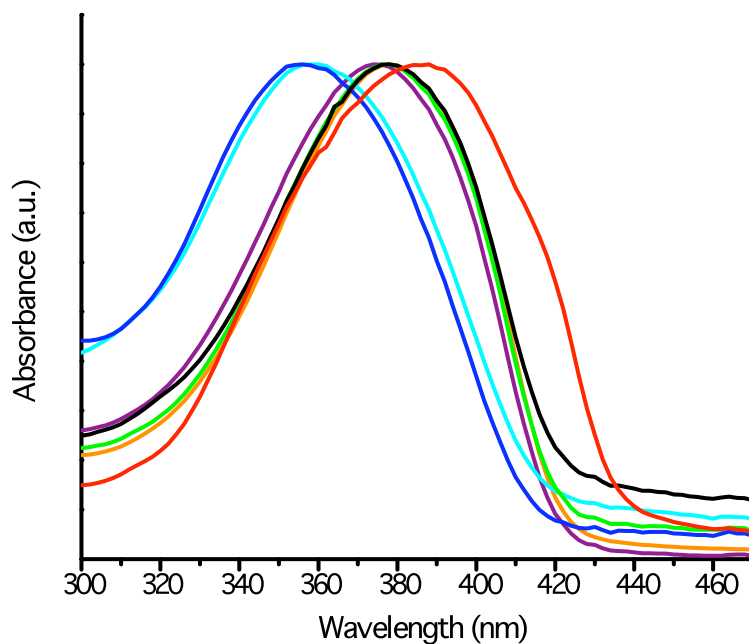


Figure 3-5 Normalized UV-vis absorbance spectra of representative PFO (red trace), PAEFO (2:1 blue trace, 7:1 purple trace, and 13:1 orange trace), PAEFO-2 (2:1 cyan, and 11:1 green trace), and PAEFO-S (black trace) films all measured following heating at 140 °C in a nitrogen environment.

Similar to the absorbance spectra, PL spectra of the copolymers show no change after heating in nitrogen for up to 19 hours at 140 °C. To show this clearly, PL spectra of a 2:1 PAEFO film taken before and after annealing are plotted and compared to an equivalent PFO film exposed to the identical conditions (Figure 3-6). As expected, and unlike the copolymers, PFO PL exhibits a shift from 425 nm (often referred to as α -phase PFO) to 435 nm (or γ -phase PFO). A reasonable explanation for the phase stability of the present copolymers is found by applying a proposal by Da Como *et al.* who investigated how chain length affects phase stability.³¹ They found that in order for PFO to adopt γ - or β -phases, it was necessary for the polymer chain to be at least eight monomer units long. As all of the AE-fluorene copolymers appear to have conjugation lengths of less than eight fluorene units, we conclude that the conjugation length is the determining factor in the phase stability. Careful examination of this report further suggests the conjugation lengths of γ -phase and β -phase PFO are eight and nine, respectively. This proposal and our observations suggest that α -phase PFO has a PL conjugation length of seven units, rather than six as previously reported.³ As the copolymers conjugation lengths are proposed to be between four and six, while

the optical spectra are still blue-shifted relative to PFO, it would appear that α -phase PFO has an ECL of seven units.

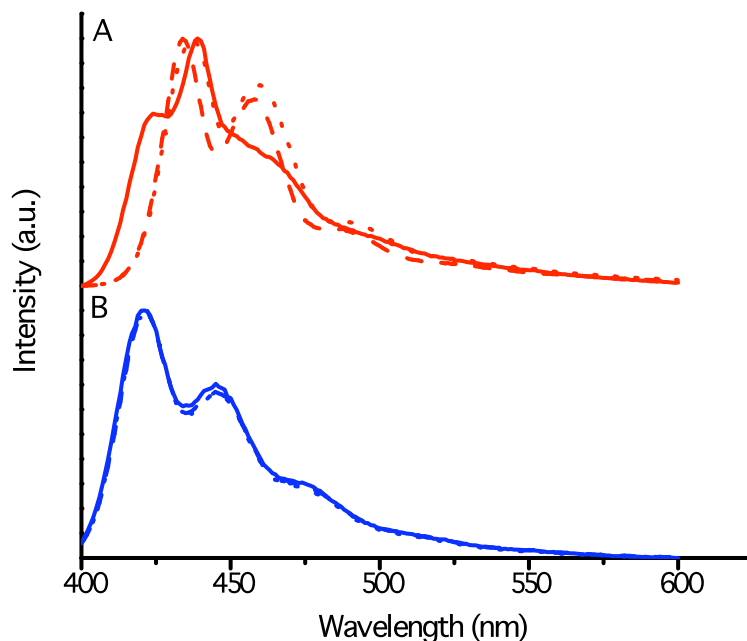


Figure 3-6 Normalized PL spectra of representative PFO (A-red traces) and PAEFO (B-blue traces) thin films (ca. 100 nm) measured prior to (—) and following heating for 1 hour (---), and 20 hours (····) in nitrogen ($\lambda_{\text{ex}} = 350$ nm).

3.2.7 Spectral Stability in the Presence of Oxygen

Unlike PFO, and similar to heating in a nitrogen environment, heating copolymer films in air yields no spectral changes indicative of changes in polymer structure (i.e., α -phase emission remains regardless of stressing) (Figure 3-7). Furthermore in three of these copolymer films (2:1 PAEFO, 2:1 PAEFO-2, and PAEFO-S) there is no detectable green emission after heating the film for 1 hour at 140 °C in air; the ratio of green (500 - 600 nm) to blue (400 - 500 nm) light (Table 3-7) shows virtually no change for these three copolymers after one hour (See section 3.1.3). The other three copolymers (7:1 and 13:1 PAEFO and 11:1 PAEFO-2) show a slight increase in green emission (integrated intensity ratios of 0.24, 0.23, and 0.21), but still substantially less than what is seen for PFO with an integrated intensity ratio of 0.55. While the integrated intensity ratio for 7:1 PAEFO shows no change after annealing it is clear from the

spectra that there is a change, and that the ratio after heating is more directly comparable to the other polymers.

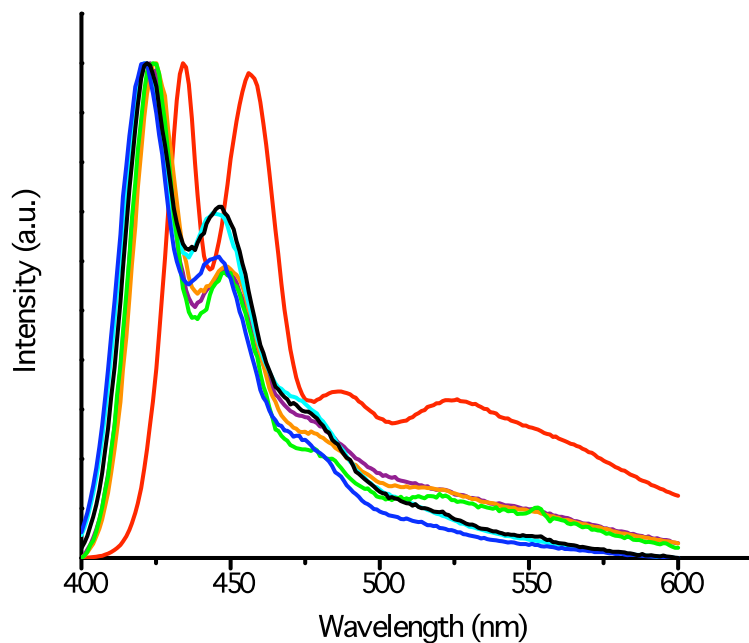


Figure 3-7 Normalized PL spectra of representative PFO (red trace), PAEFO (2:1 blue trace, 7:1 purple trace, and 13:1 orange trace), PAEFO-2 (2:1 cyan trace, and 11:1 green trace), and PAEFO-S (black trace) films measured following heating for 1 hour in air ($\lambda_{\text{ex}} = 350\text{nm}$).

Table 3-7 Integrated intensity ratios for each of the polymers studied.

| Polymer | Integrated intensity ratio by heating time | | | |
|-------------|--|--------|---------|----------|
| | 0 Hour | 1 Hour | 5 Hours | 20 Hours |
| PFO | 0.12 | 0.55 | 2.30 | |
| 2:1 PAEFO | 0.08 | 0.08 | 0.18 | 0.28 |
| 7:1 PAEFO | 0.25 | 0.24 | 0.94 | |
| 13:1 PAEFO | 0.13 | 0.23 | 1.79 | |
| 2:1 PAEFO-2 | 0.10 | 0.10 | 0.20 | 0.87 |

| | | | | |
|--------------|------|------|------|------|
| 11:1 PAEFO-2 | 0.12 | 0.21 | 1.39 | |
| 23:1 PAEFO-S | 0.08 | 0.11 | 0.29 | 0.49 |

After heating in air for five hours at 140 °C, the PL spectra of the various copolymers can be better distinguished, especially for the lower AE content PAEFO and PAEFO-2 copolymers (Figure 3-8). The ‘g-band’ now completely dominates the PL of PFO, with an intensity ratio of 2.30. While all of the copolymers have smaller ‘g-bands’, 7:1 PAEFO, 13:1 PAEFO, and 11:1 PAEFO-2 exhibit increased green emission with ratios of 0.94, 1.79, and 1.39, respectively. Clearly incorporation of AE linkages into the backbone of PFO drastically increases its spectral stability, and the more AE is incorporated, the better the improvement.

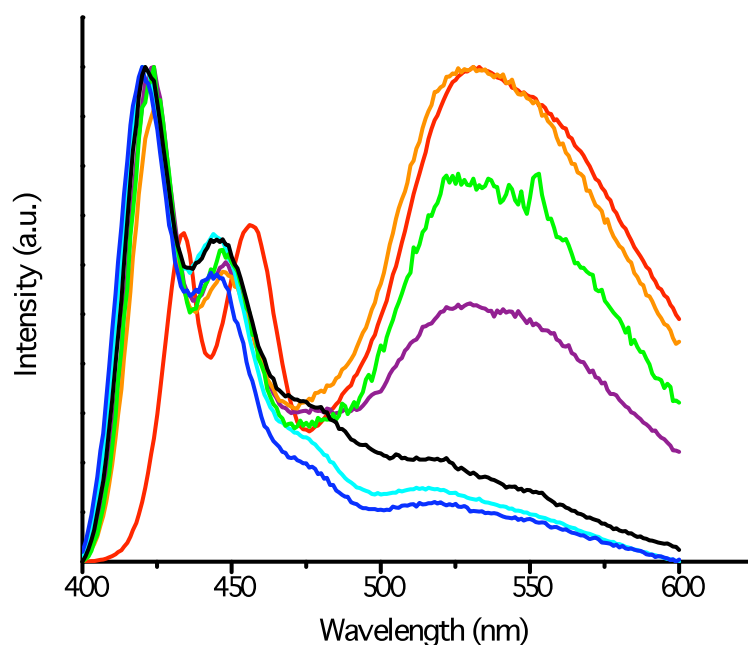


Figure 3-8 Normalized PL spectra of representative PFO (red trace), PAEFO (2:1 blue trace, 7:1 purple trace, and 13:1 orange trace), PAEFO-2 (2:1 cyan trace, and 11:1 green trace), and PAEFO-S (black trace) films measured following heating for 5 hours in air ($\lambda_{\text{ex}} = 350\text{nm}$).

To better distinguish between 2:1 PAEFO, 2:1 PAEFO-2 and PAEFO-S, these three films were further heated at 140 °C in air for 15 hours (making it 20 hours total). The PL shows significant differences between the spectral stability for these three copolymers (Figure 3-9). 2:1 PAEFO has

the smallest ‘g-band’ with a ratio of 0.28, followed by PAEFO-S at 0.49, and lastly 2:1 PAEFO-2 at 0.87. While these ‘g-bands’ are all clearly visible, they are still significantly lower than what is seen for PFO after only five hours. In fact 2:1 PAEFO and PAEFO-S have smaller ‘g-bands’ after 20 hours than PFO does after 1 hour.

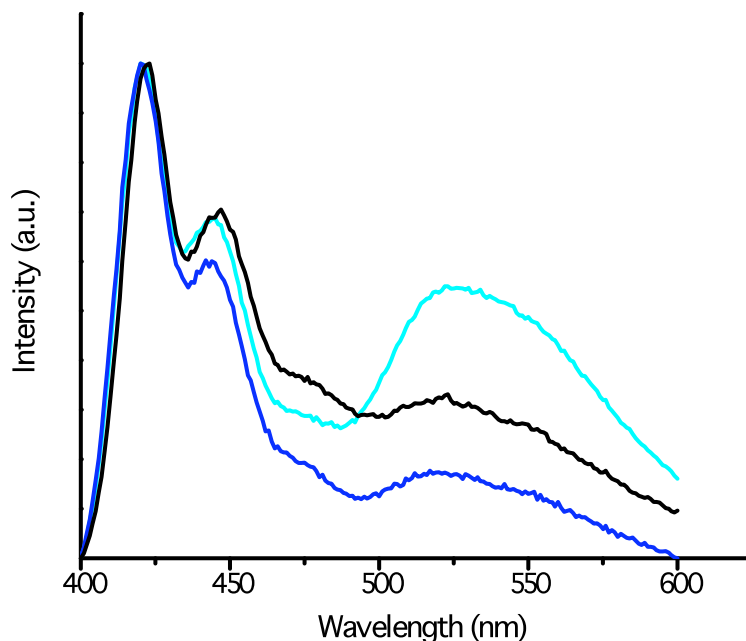


Figure 3-9 Normalized PL spectra of representative 2:1 PAEFO (blue trace), 2:1 PAEFO-2 (cyan trace), and PAEFO-S (black trace) films measured following heating for 20 hours in air ($\lambda_{\text{ex}} = 350\text{nm}$).

3.2.8 Method of Spectral Improvement

Incorporating AEs into the polymer backbone clearly improves the spectral stability of PFO, but how does it compare to the PFO-PPE blend discussed in Chapter 2? After five hours of heating a PFO-PPE blend film at 140 °C a green to blue ratio of 0.76 can be observed in the PL. While this is lower than what is seen for 13:1 PAEFO, 11:1 PAEFO-2, and 7:1 PAEFO, it is higher than the equivalent ratios for 2:1 PAEFO-2, PAEFO-S, and 2:1 PAEFO. It is also higher than what is seen for 2:1 PAEFO and PAEFO-S after 20 hours. These observations are consistent with our blend proposal that the AEs are severing the fluorenone-fluorenone dipole interactions. The improvement over the PFO-PPE blend could be caused by the nature of PPE. As a viscous liquid, PPE would be able to migrate within the film, especially upon heating; this is not the case for

covalently linked AE in the polymer backbone. Given the mobility of the PPE in a blend, more fluorenone-fluorenone interactions could develop in a blended system with prolonged heating, while the high relative PPE concentration would still prevent most of these excimers from forming. In the copolymers, the AE moieties are unable to migrate through the film, and so are better able to prevent fluorenone-fluorenone interactions. Furthermore, as the amount of AE used in the polymer is increased these moieties have a greater likelihood of separating any fluorenone defects which form within the film. Finally incorporation of non-conjugated AE moieties into the polymer backbone limits intramolecular charge transfer, helping to prevent excitons from travelling to any fluorenone defects formed upon heating.

The one copolymer that does not fit this trend is PAEFO-S, which had a low AE monomer content, but fairly high spectral stability. One possible explanation is the absence of nickel in the polymerization. It has been suggested that nickel remaining from the Yamamoto cross-coupling reaction will help catalyze the formation of fluorenone defects within the film.¹¹ Thus by using the Suzuki-Miyaura cross-coupling, with its palladium catalyst, to synthesize the polymer, fewer fluorenone moieties are formed upon thermal treatment. Another possibility is unlike the microwave syntheses, the bench-top synthesis required the use of endcappers to terminate the chains. Furthermore, the MALDI-TOF MS clearly shows bromine and boronic ester end-groups are still present on many chains. These groups may also work to sever fluorenone-fluorenone interactions, thus decreasing the observed 'g-band'.

3.2.9 Magnetism/Conductance

In addition to dramatically improving the spectral stability, PAEFO responds to a permanent magnet (Figure A3-26). This offers the possibility of new heretofore unknown multifunctional materials/devices. The most likely source of the observed magnetism is Ni incorporation into the polymer as a result of the polymerization process. Qualitatively, it is observed that using greater amounts of nickel catalyst in the polymerization leads to a material with a higher magnetic response. 11:1 PAEFO-2 had the highest amount of nickel coupling agent used in the reaction and qualitatively responds to exposure to a permanent magnet most readily. In addition EA (*vide supra*) of this copolymer showed carbon content to be significantly lower than expected, possibly due to increased amount of nickel. XPS was performed on the polymer film to confirm the presence of nickel (Figure A3-27); however even after 80 scans there is only slight shift in the baseline at 855 eV, consistent with trace Ni(0). In addition of the magnetic response, films of copolymers prepared by Yamamoto cross-coupling in a microwave appear dark blue. This colour

is reminiscent of the widely used transparent conducting/hole injecting polymer PEDOT:PSS,²⁷ and bears further investigation.

3.2.10 Conclusions

A new molecule, (bis(4-bromophenoxy) benzene), was synthesized and incorporated into the backbone of a dioctyl PF in four different fluorene:AE monomer ratios (2:1, 7:1, 13:1, 23:1). The polymer incorporating the 23:1 ratio (PAEFO-S) was synthesized via the Suzuki-Miyaura cross-coupling mechanism on a bench-top, while the other three polymers (PAEFO) were synthesized via the Yamamoto cross-coupling reaction in a microwave. Another AE-fluorene copolymer (PAEFO-2) was synthesized similarly to PAEFO, only using bis(4-bromophenyl) ether instead of bis(4-bromophenoxy) benzene with two different monomer ratios (2:1, 11:1). Conjugation lengths of these six polymers were found to range from four to six fluorene units, with closer fluorene:AE monomer ratios leading to lower conjugation lengths. As the conjugation length is less than what is required for γ - or β -phases to appear no phase changes were evident upon thermal treatment of copolymer films. When compared to PFO these new polymers show significantly improved spectral stability with no phase changes evident and drastically reduced green emission upon heating in air. This reduction in the 'g-band' is more pronounced with decreased monomer ratios (i.e. more AE in the polymer), and when the aromatic ether content is high enough (2:1 PAEFO and 2:1 PAEFO-2) this reduction is more than what was seen for the PFO-PPE blend discussed in Chapter 2. PAEFO-S did not fit this trend, as it had a low AE content and a significantly reduced 'g-band'. This observation can be explained by the absence of Nickel in the reaction mixture and possibly by the interference of end-groups that are not present in the other polymers. While the presented Suzuki-Miyaura synthesis appears to provide polymers with the best stability it is significantly more time consuming, and needs more work to fully remove bromine and boronic ester groups. Furthermore, PAEFO and PAEFO-2 have another advantage; incorporation of Ni into the polymer through the polymerization procedure leads to magnetic properties that can be exploited for future applications.

3.3 References

1. S. Setayesh, D. Marsitzky and K. Mullen, *Macromolecules*, 2000, **33**, 2016-2020.
2. U. Scherf and K. Mullen, *Synthesis*, 1992.
3. G. Klaerner and R. D. Miller, *Macromolecules*, 1998, **31**, 2007-2009.
4. A. Monkman, C. Rothe, S. King and F. Dias, *Adv. Poly. Sci.*, 2008, **212**, 187-225.
5. U. Scherf and K. Mullen, *Macromolecules*, 1992, **25**, 3546-3548.

6. M. Fukada, K. Sawada and K. Yoshino, *J. Polym. Sci. Part A: Polym. Chem.*, 1993, **31**, 2465-2471.
7. M. F. Semmelhack, P. M. Helquist and L. D. Jones, *J. Am. Chem. Soc.*, 1971, **93**, 5908-5910.
8. N. Miyaura, T. Yanagi and A. Suzuki, *Synth. Commun.*, 1981, **11**, 513.
9. A. C. Grimsdale and K. Mullen, *Adv. Polym. Sci.*, 2006, **199**, 1-82.
10. A. A. C. Braga, N. H. Morgon, G. Ujaque, A. Lledos and F. Maseras, *J. Organomet. Chem.*, 2006, **691**, 4459-4466.
11. U. Scherf and E. J. W. List, *Adv. Mater.*, 2002, **14**, 477-487.
12. T. Yamamoto, S. Wakabayashi and K. Osakada, *J. Organomet. Chem.*, 1992, **428**, 223-237.
13. H. G. Nothofer, A. Meisel, T. Miteva, D. Neher, M. Forster, M. Oda, G. Lieser, D. Sainova, A. Yasuda, D. Lupo, W. Knoll and U. Scherf, *Macromol. Symp.*, 2000, **154**, 139-148.
14. S. B. Jhaveri and K. R. Carter, *Chem. Eur. J.*, 2008, **14**, 6845-6848.
15. R. Gedye, F. Smith, k. Westaway, H. Ali, L. Baldisera, L. Laberge and J. Rousell, *Tetrahedron Lett.*, 1986, **27**, 279-282.
16. R. J. Giguere, T. L. Bray, S. M. Duncan and G. Majetich, *Tetrahedron Lett.*, 1986, **27**, 4945-4948.
17. K. R. Carter, *Macromolecules*, 2002, **35**, 6757-6759.
18. T. L. Ngoc, B. A. Roberts and C. R. Strauss, in *Microwaves in Organic Synthesis*, ed. A. Loupy, Wiley VCH, Weinheim, 2006.
19. R. Sanghi, *Resonance*, 2000, **5**, 77-81.
20. M. Hajek, in *Microwaves in Organic Synthesis*, ed. A. Loupy, Wiley-VCH, Weinheim, 2006.
21. K. Salonitis, J. Pandremenos, J. Paralikas and G. Chryssolouris, *Int. J. Adv. Manuf. Technol.*, 2010, **49**, 803-826.
22. I. U. Khand, P. L. Pauson and W. E. Watts, *J. Chem. Soc. C*, 1968, 2261-2265.
23. S. L. McFarlane, D. G. Piercey, L. S. Coumont, R. T. Tucker, M. D. Fleishauer, M. J. Brett and J. G. C. Veinot, *Macromolecules*, 2009, **42**, 591-598.
24. AIST, SDBS: p-diphenoxybenzene, http://riodb01.ibase.aist.go.jp/sdbs/cgi-bin/direct_frame_top.cgi, Accessed Nov. 11, 2010.
25. T. Yamamoto, A. Morita, Y. Miyazaki, T. Maruyama, H. Wakayama, Z.-h. Zhou, Y. Nakamura and T. Kanbara, *Macromolecules*, 1992, **25**, 1214-1223.

26. A. Suzuki, *Pure Appl. Chem.*, 1994, **66**, 213-222.
27. J. C. Simpson, K. Rueter and S. Kirchmeyer, in *Conjugated Polymers: Theory, Synthesis, Properties, and Characterization*, eds. T. A. Skotheim and J. R. Reynolds, CRC Press, 2007.
28. J.-I. Lee, G. Klaerner and R. D. Miller, *Chem. Mater.*, 1999, **11**, 1083-1088.
29. C. E. Carraher, *Seymour/Carraher's Polymer Chemistry*, CRC Press, 2008.
30. M. Grell, D. D. C. Bradley, X. Long, T. Chamberlain, M. Inbasekaran, E. P. Woo and M. Soliman, *Acta Polym.*, 1998, **49**, 439-444.
31. E. Da Como, E. Scheler, P. Strohsriegl, J. M. Lupton and J. Feldmann, *Appl Phys A*, 2009, **95**, 61-66.

Chapter 4

Conclusion

4.0 Conclusions

In a recent review Grimsdale *et al.* state that polyfluorenes (PFs) are the best candidate not only for blue emission but, when used in copolymers, for all other emissive layers.¹ However they exhibit significant spectral instabilities, including slight changes in wavelengths emitted (due to phase changes) and the appearance of a new green emissive band or ‘g-band’ when exposed to thermal stressing. While there is still some debate as to the exact cause of the ‘g-band’, oxidation leading to fluorenone defects is essential.^{2, 3} Because of the promise of PF polymers, much work has gone into ameliorating these problems. Most of this work has focused on incorporating functional groups at the PF 9 position that are thermally and oxidatively stable.⁴⁻⁷ Other methods have also been shown to improve the spectral stability of PF based systems including monomer purification,⁸ polymer blending,⁹⁻¹¹ nanoparticle doping,^{12, 13} copolymerization,^{14, 15} and incorporation of sterically demanding groups.^{16, 17} Some of these methods (e.g., monomer purification) were also done to prevent or minimize oxidation, while others (e.g., blending) were done to prevent excimer formation. Still others (e.g., sterically demanding groups) have been used to prevent both oxidation and excimer formation. Recently aromatic ethers (AEs) have been found to be good candidates for functionalization at the 9-position of PF due to their high thermal and oxidative stability.^{18, 19} No work though has been done using AEs in any other manner to improve the spectral stability of PFs. To this end, AEs have been combined with PF in two different ways (blending and copolymerization) with very similar results.

Three different AE based polymers (PPO, PSU and PPE) and three other AE monomers (DE, m-DB and p-DB) were blended with PFO with varying results (see Chapter 2). Blending with PSU and DE offered no improvements to the spectral stability of PFO. On the other hand it was seen that thin films cast from solutions blending PFO with PPO, PPE, m-DB, and p-DB had improved spectral stability with decreased ‘g-bands’. Blending with PPE, m-DB and p-DB was further found to induce β -phase formation within the films, and this phase was maintained after heating. Of the four blends with improved spectral stabilities, PPE was found to have the biggest reduction in the ‘g-band’. Further studies showed that PPE inclusion in a film already containing fluorenone defects still decreases the ‘g-band’ strongly supporting the theory presented by the Bradley group^{3, 20, 21} that it is fluorenone-fluorenone excimers and not fluorenone alone that yields the ‘g-band’.

Chapter 3 introduced three different PFO-AE copolymers. Two different AE monomers were used, one of which (bis(4-bromophenyl) ether) was commercially available, while the other

(bis(4-bromophenoxy) benzene) was first synthesized using iron-mediated nucleophilic-aromatic-substitution.¹⁹ These two monomers were randomly copolymerized with 2,7-dibromo-9,9-dioctylfluorene via the Yamamoto cross-coupling in a microwave at varying monomer ratios yielding PAEFO-2 and PAEFO, respectively. ¹H NMR confirmed the ratio of fluorene to AE in the polymer corresponded to the monomer ratios used in the polymerizations. These polymers were also found to exhibit substantially improved spectral stability compared to PFO, with the degree of stability related to the amount of AE present in the polymer (i.e., more AE, better stability). Not only did the prepared copolymers exhibit reduced 'g-bands', they also showed phase stability. The lack of phase changes has been attributed to the length of the fluorene segments within the polymer, and the decreased 'g-band' to the ability of the AE moieties to limit the formation of fluorenone-fluorenone excimers. The polymers with a 2-1 fluorene-AE molar ratio were further found to have smaller 'g-bands' than the PFO-PPE blend when exposed to identical heating conditions. This is most likely due to the fact that the AE units within the copolymer are unable to move in the same way PPE can. In addition to exhibiting improved spectral stability these polymers are also blue in colour (though they are transparent in thin film) and magnetic. These properties may lead to new applications, further increasing their functionality.

Bis(4-bromophenoxy) benzene was also copolymerized with 2,7-dibromo-9,9-dioctylfluorene and 9,9-dioctylfluorene-2,7-diboronic acid bis(1,3-propanediol) ester via the Suzuki-Miyaura cross-coupling yielding PAEFO-S. This polymerization was not performed in the microwave and so required a longer reaction time and the addition of xylene end-capping groups. MALDI-TOF MS showed that bromine, boronic ester and xylene were all present and as a result information gained from NMR analysis was limited. PAEFO-S also showed very high spectral stability, especially when considering the low AE content. This spectral stability was attributed to two factors: First, no AE-AE couplings are possible, so even with a much higher fluorene:AE monomer ratio compared to the PAEFO and PAEFO-2 copolymers, the fluorene segments are of similar size. Second, nickel is not used in the Suzuki-Miyaura cross-coupling, and so would not be present in PAEFO-S films. As nickel is believed to promote fluorenone formation, there would be less fluorenone in PAEFO-S after heating than the other copolymers. As such, there would be less fluorenone-fluorenone excimers to separate, leading to a decrease in 'g-band'.

4.1 Future Work

4.1.1 Polyfluorene/Aromatic Ether Blends

While the PAEFO copolymers have better spectral stability than the PFO-PPE blend, β -phase emission could not be induced. Given the proposed applications of β -phase PF,²² further study of these blends is desirable. While not straightforward, a crystal structure of the PFO-PPE blend would be beneficial to definitively show any fluorenone-AE interactions. Techniques such as small-angle neutron-scattering (SANS) may provide information about how PPE and PFO are interacting in solution, allowing any fluorenone-AE interactions to be probed.

Another system that should be explored is blending PPE with fluorene based oligomers that already contain fluorenone, possibly starting with the ones used by Chan *et al.*³ A study of this type could further prove the 'g-band' is in fact dependent on interchain interactions. Oligomers are much easier to characterize, and so should provide for a better understanding of related polymer systems.²³

In addition to these studies that are aimed at basic material understanding, more work should be done to evaluate the device application of these material systems. While PLED devices were fabricated, they were not optimized. Furthermore, as these blends induce β -phase regions within PFO, work can be done to study their usefulness in lasing devices.

4.1.2 Aromatic Ether-Dioctylfluorene Random Copolymers

As was seen, PAEFO-S exhibited better spectral stability than was expected given its low AE content. However full polymerization was not achieved and would be one of the first goals of future work. Microwave procedures for Suzuki-Miyaura cross-couplings are available in the literature²⁴ and would be one possible way to achieve high molecular weight materials that are more directly comparable to PAEFO. Another possibility is increased reaction time and temperature, especially after addition of end-cappers. Once this is done varying the monomer ratios will allow for a series to be studied similar to PAEFO and PAEFO-2.

The dark blue colour of the Yamamoto cross-coupled polymers bears further investigation. As mentioned in Chapter 3, no absorption was seen over the visible spectrum for thin films or solutions of these polymers. This demands the question as to what leads to this colour if not absorbance of visible light? Comparing PAEFO to PEDOT:PSS may provide some insight. When a solution of PEDOT:PSS is diluted enough to be able to be mostly transparent with a slight blue

tinge the UV-vis absorbance shows a slight broad absorbance in the visible region (Figure 4-1). PAEFO on the other hand shows no visible absorbance when mostly transparent with a slight black tinge (Figure 4-1). However PAEFO may still absorb near IR light, contributing to the colour and showing it is conductive, so near IR absorbance measurements should be taken. If this is the case other conductance measurements such as four-point probe, will prove useful.

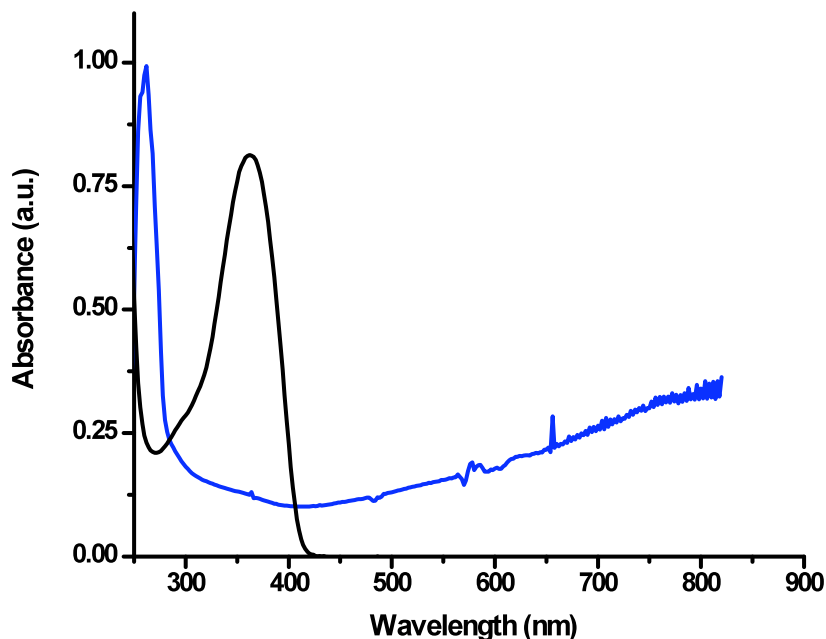


Figure 4-1 UV-vis absorbance of PEDOT:PSS (blue trace) and PAEFO (black trace).

The magnetism of these dark blue polymers also bears further investigation. While it is reasonable that nickel is the cause of the observed magnetism this needs to be confirmed and better understood. One technique that could be used to confirm the presence of nickel is inductively coupled plasma MS (ICP-MS), although the nickel would need to be removed from the polymer before ICP-MS could be done. One way to do this is to use a muffle furnace to burn off the polymer, hopefully without losing the nickel, and then dissolving what is remaining in nitric acid, however large amounts of polymer may be needed in order to get enough nickel for detection. As increasing the $\text{Ni}(\text{COD})_2$ used in the polymerization lead to polymers that were qualitatively more magnetic, further increases should lead to polymers with higher nickel content, which should then allow for easier characterization as techniques like XPS may then be able to detect the nickel and provide information as to its oxidation state. Regardless of the cause,

magnetic susceptibility measurements should be acquired. Finally, coating a polymer film onto an electrode and running electrochemistry measurements may provide information about the nickel and how conductive the films are.

From the present studies, it is clear microwave polymerization is necessary for the formation of deeply coloured magnetic materials. Using the Yamamoto cross-coupling reaction to synthesize PAEFO outside of a microwave leads to a polymer with more similarity to PAEFO-S as it is not dark blue or magnetic. MALDI-TOF MS (Figure A4-1) also shows the product to not be fully polymerized with bromine still present on the polymer chains. Similar to PAEFO-S, full polymerization needs to be done first, although the solution discussed for PAEFO-S to use a microwave would be counter-productive in this case. Increasing the reaction time, especially after addition of the xylene end-cappers, is likely the best option. Once full polymerization can be achieved, a series of polymers with varied fluorene-AE monomer ratios could be synthesized and studied. Such polymers would likely be smaller than the microwave produced ones, and have a higher PDI. Determining their spectral stability may provide insight into the mechanism of fluorenone formation. If for example, they are more spectrally stable than PAEFO, it would suggest that the use of a microwave is detrimental to oxidative stability. Also, if nickel can be seen in these films by XPS, ICP-MS or other technique, then it would be clear that the high pressures and temperatures affordable in the microwave lead to changes in the nickel, bringing about the magnetism.

As mentioned with the blends, oligomer studies tend to provide a better understanding. As such, oligomers containing the same fluorene and AE monomer units could be synthesized and studied using all of the above mentioned techniques. Furthermore, oligomers containing fluorene, AE, and fluorenone could also be studied allowing for full control of the extent of oxidation. In addition to all the already mentioned analyses, and as with the blends, SANS may provide more information about the interactions between fluorenone and AE units.

PLED devices are another obvious future endeavour, including both prototype devices and optimization of the same. New applications may also be found that will combine the luminescent and magnetic properties of these polymers. Finally, if these polymers turn out to be conductive, then even more potential applications will present themselves.

4.1.3 Aromatic Ether Macrocyclic Fluorenes

A wide variety of AE functionalized fluorene monomers can be synthesized using the method reported by McFarlane *et al.*¹⁹ which should exhibit improved spectral stability compared to PFO. Cyclic AE groups are one such variety which may also increase fluorenes' functionality as such polymers may be useful as sensors.^{25, 26} Two methodologies for synthesizing AE macrocycle containing fluorene monomers have been attempted. One is to synthesize the macrocycle directly at the 9-position of the fluorene, while the other was to synthesize an AE cycle and then attach it to the fluorene at the 9-position.

Direct syntheses of three different AE macrocycle fluorene monomers were attempted. In all cases MIBC was first synthesized and collected according to literature procedures (Scheme 4-1).¹⁹ Bisphenol-A (BPA), biphenol (BP), and 4,4-diphenoxy diphenyl ether were then reacted (individually) with MIBC to form the three AE macrocycle fluorenes (CAEF-1, CAEF-2, and CAEF-3, respectively - See Figure 4-2). To help promote macrocycle synthesis, the different AE linkers were added slowly to a dilute MIBC solution (DMF as the solvent). Electrospray MS (ES MS) of the three products show mass/charge peaks at 563, 542, and 550, for CAEF-1, CAEF-2, and CAEF-3, respectively (Figure A4-2 to A4-4). These mass to charge ratios were promising as they correspond to the expected doubly charged molecules. However, after removal of the FeCp units in CAEF-2, multiple products are seen (Figure 4-3). While the desired macrocycle is one of the products there are many more which would need to be separated before studies could continue. Some of these products (CAEF-2-A and CAEF-2-C) show that the MIBC was not completely pure, and that in some cases only partial synthesis of MIBC was accomplished. Once separation is achieved, many of these monomers could be studied to determine their optical properties. For example, CAEF-2-A and CAEF-2-B could be polymerized with dioctylfluorene leading to PFs bridged by AE's at the 9-position. This would add to the PFO-PPE blends and the PAEFO copolymers. Finally, going back to one of the motivations for this project, once polymers, or possibly oligomers, are synthesized, studies can be done to test their usefulness as sensors.

Scheme 4-1 Synthesis of MIBC.

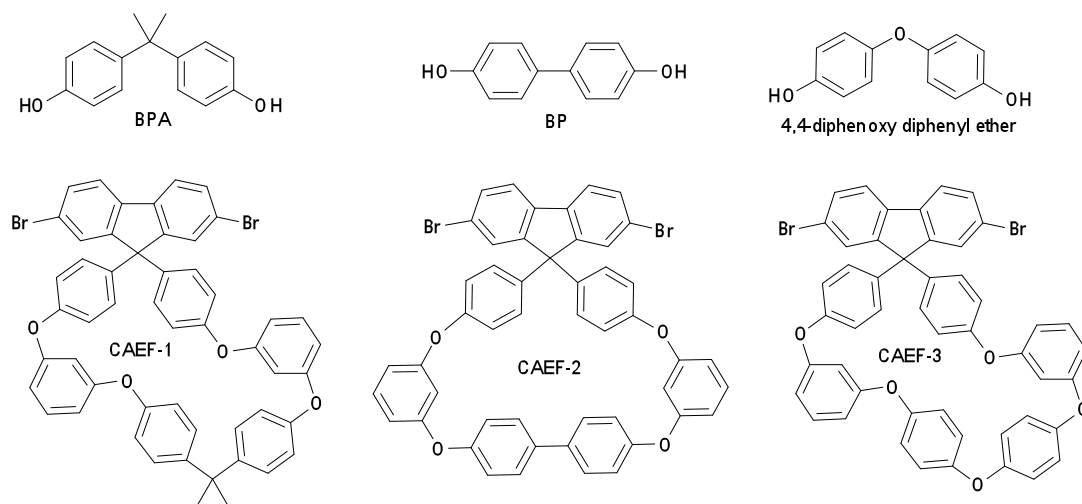
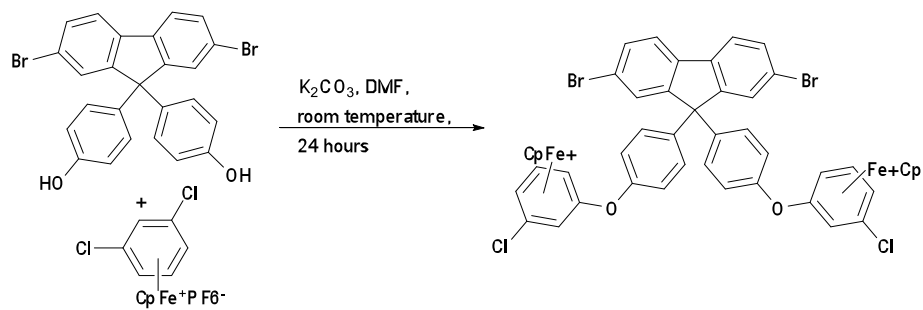


Figure 4-2 Structures of BPA, BP, 4,4-diphenoxy diphenyl ether, CAEF-1, CAEF-2, and CAEF-3.

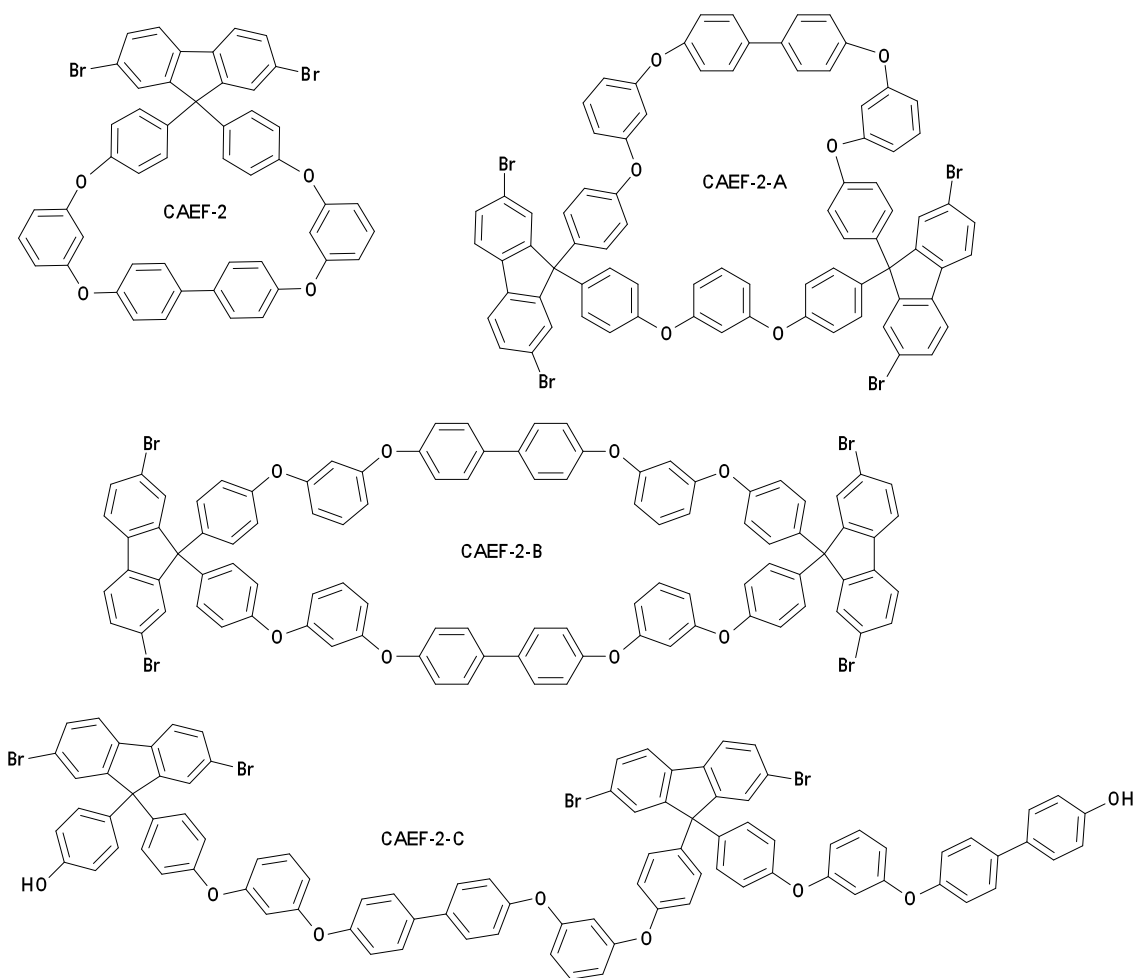


Figure 4-3 Proposed structures of some of the main actual products obtained from the attempted synthesis of CAEF-2 (See Figure A4-5 for MALDI-TOF MS).

Similarly to the direct AE macrocycle fluorene, syntheses of three different AE macrocycles were attempted. η^6 -1,3-dichlorobenzene- η^5 -cyclopentadienyliron hexafluorophosphate was reacted with BPA, BP and hydroquinone to form CAE-1, CAE-2, and CAE-3, respectively (Figure 4-4). As with the CAEFs, ES MS shows mass/charge peaks that correspond to the expected doubly charged molecules (Figure A4-6 to A4-8). While this is promising it does not necessarily show the true products and, same as with the CAEFs, after removal of the FeCp units from CAE-1 multiple products are seen by MALDI-TOF MS. However the peaks are all 303 m/Z apart, suggesting that macrocycles of various sizes were formed (Figure 4-5). The next step after removal of the FeCp units would be to separate the different products using chromatography techniques like size-exclusion chromatography. CAEFs could then be synthesized using the

procedure reported by McFarlane *et al.*¹⁸ for AESFX, followed by polymerization. These polymers could then be studied for their spectral stability and potential application in sensors.

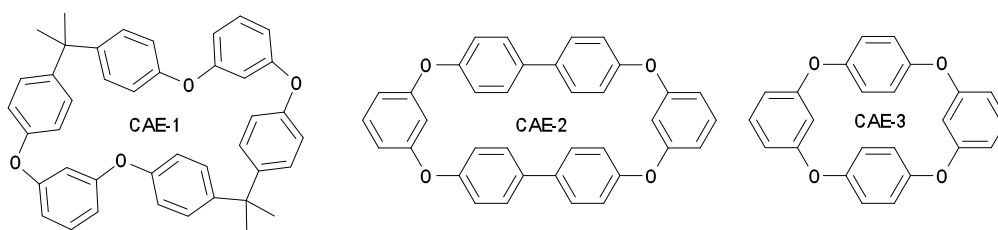


Figure 4-4 Structures CAE-1, CAE-2, and CAE-3.

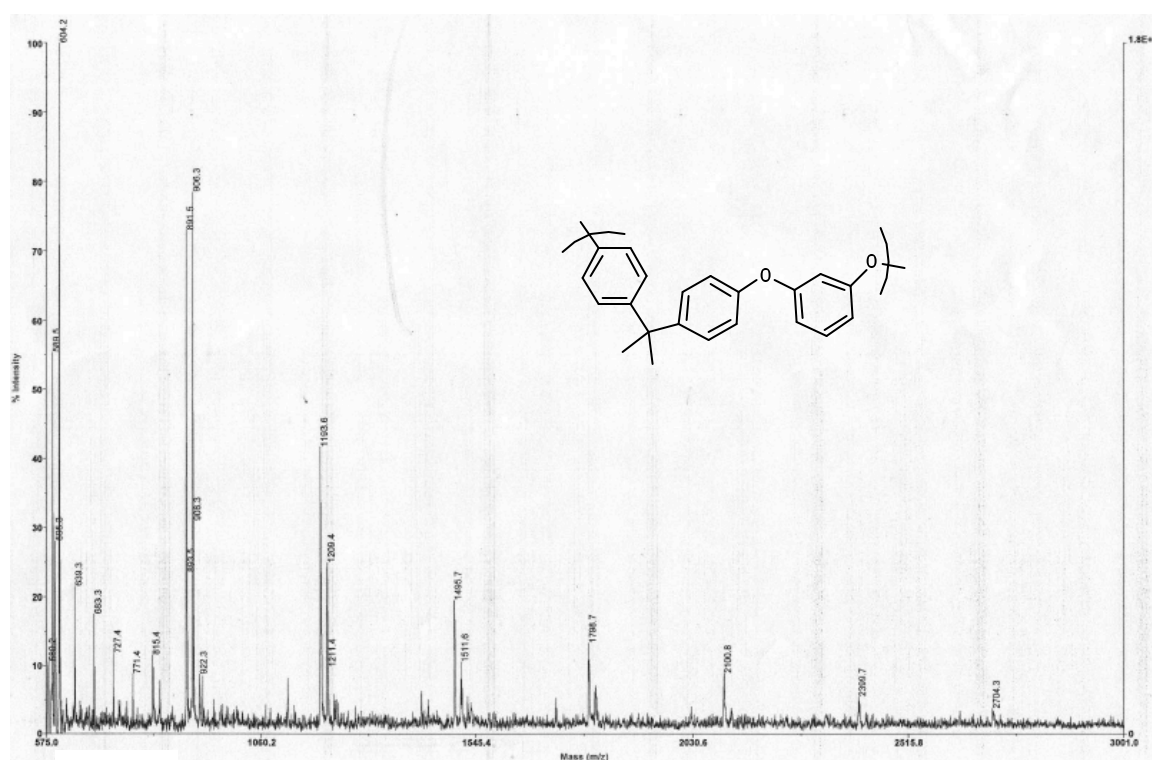


Figure 4-5 MALDI-TOF MS of CAE-1 with macrocycle repeat unit in the inset.

4.1.4 Trispirobifluorene-Fluorene Random Copolymers

The discovery that preventing oxidation is not necessary to maintain blue emission opens up a plethora of new options to stabilize the optical properties of PFs. On such possibility is found in a trispirobifluorene molecule previously synthesized by Moll *et al.* (Figure 4-6).²⁷ With bromine moieties at the 2,7 positions on both fluorene rings, this molecule could act as a cross-linker unit within PF. As the fluorene units in trispirobifluorene are perpendicular, two PF chains can be crosslinked together that are at 90 degrees to each other. In so doing interchain interactions

should be minimized, preventing fluorenone moieties from forming excimers. In fact there is a report by Yu *et al.*²⁸ which showed that trispirobifluorene centered oligomers exhibit no green emission after heating in air.

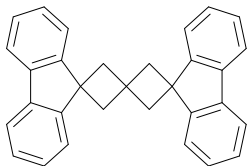
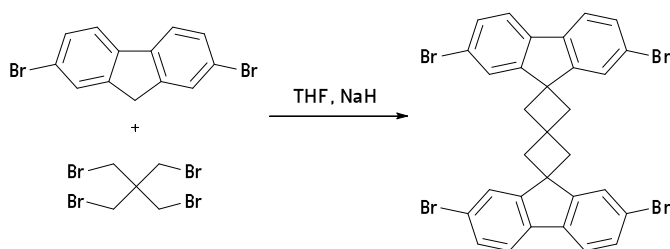


Figure 4-6 Trispirobifluorene.

With this report in mind tetrabrominated trispirobifluorene was synthesized from 2,7-dibromofluorene and pentaerythrityl tetrabromide according to literature procedures (Scheme 4-2).²⁷ This compound was subsequently copolymerized with 9,9-dioctylfluorene to form PSFO using the Yamamoto cross-coupling procedure found in Chapter 3 (for MALDI-TOF MS see Figure A4-9). Low trispirobifluorene concentrations were used (relative to 9,9-dioctylfluorene) in order to maintain product solubility. Immediate solution (CHCl_3 as the solvent) PL measurements show the expected blue colour with an emission maximum at 450 nm (Figure 4-7). However, PL measurements of spin-coated thin films of PSFO show an intense green emissive peak similar to oxidized PFO (Figure 4-7).

Scheme 4-2 Synthesis of trispirobifluorene monomer.



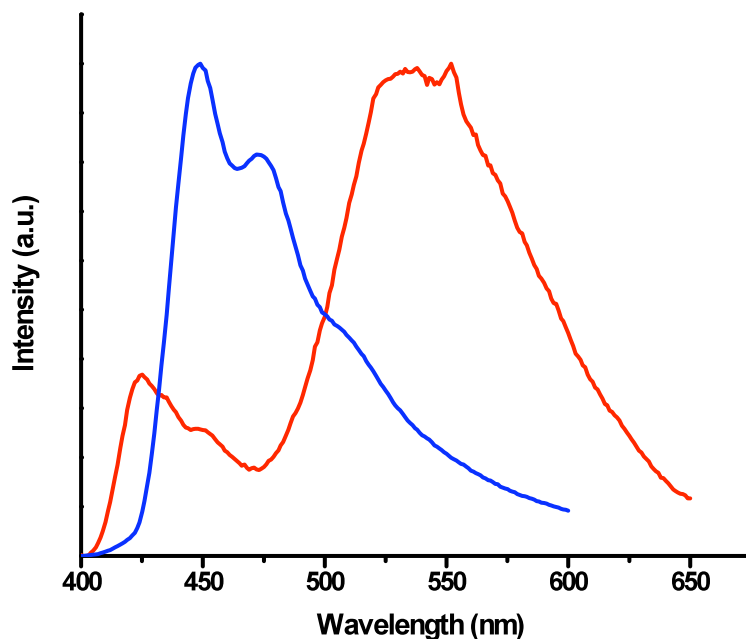


Figure 4-7 PL spectra of PSFO measured in CHCl_3 solution (blue trace) and thin film (red trace) ($\lambda_{\text{ex}} = 350 \text{ nm}$).

Unlike PFO, no heating in air is required to bring about the ‘g-band’, suggesting another mechanism of oxidation is at play. One possible pathway to fluorenone formation in PSFO is due to the four membered rings. These spiro linkages are highly strained and may be able to spontaneously break apart allowing oxygen to come in and form fluorenone. These fluorenone moieties would be in close proximity to each other further increasing the likelihood of excimer formation, thus very few would be needed for the ‘g-band’ to dominate. Similarly to what was found with the PAEFO copolymers, nickel incorporated into the polymer film may work to catalyze this fluorenone formation. As Yu *et al.*²⁸ did not use nickel in the preparation of their oligomers, this may also explain why they did not see the ‘g-band’. Another explanation is found by a closer examination of their report. All their PL measurements were done in solution, and at concentrations similar to those used by the Bradley group to show that fluorenone-fluorenone excimers are the cause of PFs ‘g-band’.³ Clearly no stability information can be attained about fluorene based systems in this manner, although this report by Yu *et al.*²⁸ has been used to back-up a claim that another fluorene based material is oxidatively stable.²⁹

Despite the lack of positive results, PF copolymers containing trispirobifluorene deserve further study. Increasing the size of the rings in the spiro linkages may overcome the strain, leading to a more stable monomer unit while still minimizing interchain interactions. A synthetic method towards increasing the size of the spiro linker (synthesising tetrakis(2-bromoethyl) methane) can be found in the literature.³⁰ Other bifluorenes could also be used as copolymer units in a similar manner, including CAEF-2-A and CAEF-2-B (shown above), and spirobifluorene³¹ (Figure 4-8). Numerous other new bifluorene monomers could also be synthesized and studied. Once a stable bifluorene unit can be found, it can be copolymerized with dialkylfluorenes leading to PFs that are potentially spectrally stable. While these polymers may find immediate use in light emitting devices, oligomer studies are crucial to fully understand these materials. As mentioned earlier, exact composition is easier to determine when working with oligomers, and thus better characterization is possible. Clearly there are almost limitless possibilities for fluorene based research.

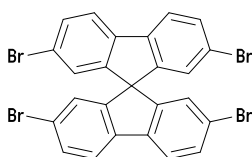


Figure 4-8 Spirobifluorene.

4.2 References

1. A. C. Grimsdale, K. L. Chan, R. E. Martin, P. G. Jokisz and A. B. Holmes, *Chem. Rev.*, 2009, **109**, 897-1091.
2. K. Becker, J. M. Lupton, J. Feldmann, B. S. Nehls, F. Galbrecht, D. Gao and U. Scherf, *Adv. Funct. Mater.*, 2006, **16**, 364-370.
3. K. L. Chan, M. Sims, S. I. Pascu, M. Ariu, A. B. Holmes and D. D. C. Bradley, *Adv. Funct. Mater.*, 2009, **19**, 2147-2154.
4. G. Kwag, E. Park and S. N. Lee, *J. Appl. Polym. Sci.*, 2005, **96**, 1335-1340.
5. J. Liu, J. Zou, W. Yang, H. Wu, C. Li, B. Zhang, J. Peng and Y. Cao, *Chem. Mater.*, 2008, **20**, 4499-4506.
6. N. Cocherel, C. Poriel, L. Vignau, J.-F. Bergamini and J. Rault-Berghelot, *Org. Lett.*, 2010, **12**, 452-455.
7. Y.-H. Tseng, P.-I. Shih, C.-H. Chien, A. K. Dixit, C.-F. Shu, Y.-H. Liu and G.-H. Lee, *Macromolecules*, 2005, **28**, 10055-10060.

8. M. R. Craig, M. M. De Kok, J. W. Hofstraat, A. P. H. J. Schenning and E. W. Meijer, *J. Mater. Chem.*, 2003, **13**, 2861-2862.
9. A. P. Kulkarni and S. Jenekhe, *Macromolecules*, 2003, **36**, 5285-5296.
10. D. Sainova, T. Miteva, H. G. Nothofer, U. Scherf, I. Glowacki, J. Ulanski, H. Fujikawa and D. Neher, *Appl. Phys. Lett.*, 2000, **76**, 1810-1812.
11. J. H. Ahn, C. Wang, I. F. Perepichka, M. R. Bryce and M. C. Petty, *J. Mater. Chem.*, 2007, **17**, 2996-3001.
12. J. H. Park, Y. T. Lim, O. O. Park, J. K. Kim, J.-W. Yu and Y. C. Kim, *Chem. Mater.*, 2004, **16**, 688-692.
13. C.-H. Yang, C. J. Bhongale, C.-H. Chou, S.-H. Yang, C.-N. Lo, T.-M. Chen and C.-S. Hsu, *Polymer*, 2007, **48**, 116-128.
14. U. Giovanella, M. Pasini, S. Destri, W. Porzio and C. Botta, *Synth. Met.*, 2008, **158**, 113-119.
15. F.-I. Wu, D. S. Reddy and C.-F. Shu, *Chem. Mater.*, 2003, **15**, 269-274.
16. S. Setayesh, A. C. Grimsdale, T. Weil, V. Enkelmann, K. Mullen, F. Meghdadi, E. J. W. List and G. Leising, *J. Am. Chem. Soc.*, 2001, **123**, 946-953.
17. J. Lee, H.-J. Cho, B.-J. Jung, N. S. Cho and H.-K. Shim, *Macromolecules*, 2004, **37**, 8523-8529.
18. S. L. McFarlane, L. S. Coumont, D. G. Piercey, R. McDonald and J. G. C. Veinot, *Macromolecules*, 2008, **41**, 7780-7782.
19. S. L. McFarlane, D. G. Piercey, L. S. Coumont, R. T. Tucker, M. D. Fleishauer, M. J. Brett and J. G. C. Veinot, *Macromolecules*, 2009, **42**, 591-598.
20. M. Sims, D. D. C. Bradley, M. Ariu, M. Koeberg, A. Asimakis, M. Grell and D. G. Lidzey, *Adv. Funct. Mater.*, 2004, **14**, 765-781.
21. T. A. M. Ferenczi, M. Sims and D. D. C. Bradley, *J. Phys.: Condens. Matter*, 2008, **20**, 045220.
22. A. Monkman, C. Rothe, S. King and F. Dias, *Adv. Poly. Sci.*, 2008, **212**, 187-225.
23. K. Mullen and G. Wegner, *Electronic Materials: The Oligomer Approach*, Wiley-VCH, Weinheim, 1998.
24. K. Olofsson, P. Nilsson and M. Larhed, in *Microwaves in Organic Synthesis*, ed. A. Loupy, Wiley-VCH, Weinheim, 2006.
25. M. Yu, F. He, Y. Tang, S. Wang, Y. Li and D. Zhu, *Macromol. Rapid Commun.*, 2007, **28**, 1333-1338.
26. X.-H. Zhou, J.-C. Yan and J. Pei, *Macromolecules*, 2004, **37**, 7078-7080.

27. O. P. Y. Moll, T. L. Borgne, P. Thuery and M. Ephritikhine, *Tetrahedron Lett.*, 2001, **42**, 3855-3856.
28. S. Yu, H. Lin, Z. Zhao, Z. Wang and P. Lu, *Tetrahedron Lett.*, 2007, **48**, 9112-9115.
29. L. Li, C. Xu and S. Li, *Tetrahedron Lett.*, 2010, **51**, 622-624.
30. G. R. Newkome, V. K. Gupta, R. W. Griffin and S. Arai, *J. Org. Chem.*, 1987, **52**, 5480-5482.
31. D. Katsis, Y. H. Geng, J. J. Ou, S. W. Culligan, A. Trajkovska, S. H. Chen and L. J. Rothberg, *Chem. Mater.*, 2002, **14**, 1332-1339.

Appendix 2 (A2)

In all of the PFO-PPE blend solutions the PFO concentration was maintained at 1 % w/v. The PFO-PVQ blend reported by Kulkarni et al. was prepared in such a way that the PFO concentration changed. They first prepared separate PFO and PVQ solutions, and then mixed a predetermined quantity of each to get the blend solution. Thus the PFO concentration changed from blend to blend, making comparisons between the different blend concentrations harder.

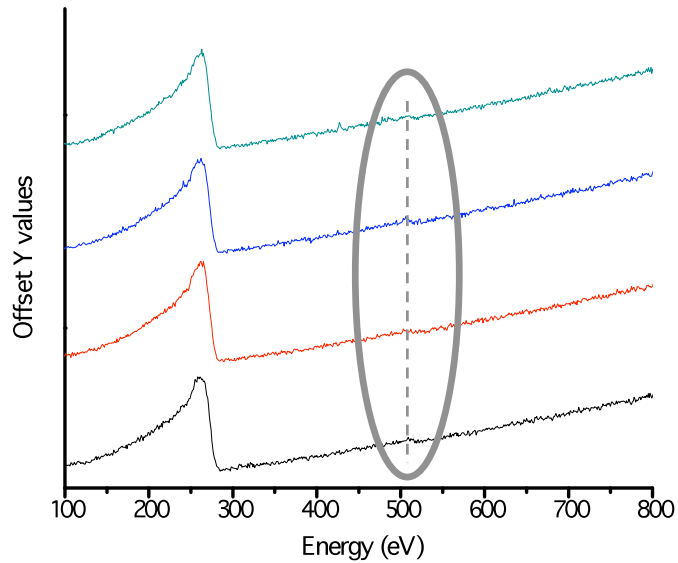


Figure A2-1 Stacked AES spectra measured at four different points on thin film cast from 1-1 blend, showing carbon peak at ca. 260 nm, and a weak oxygen peak at ca. 510 nm (highlighted by the grey oval/dotted line).

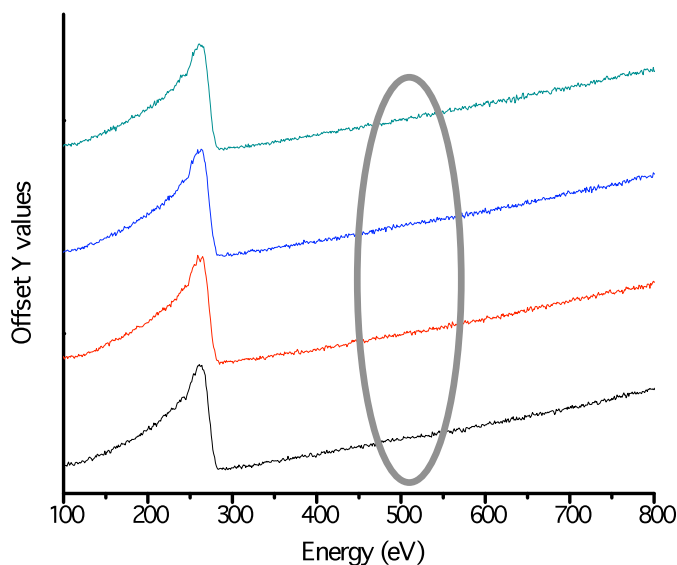


Figure A2-2 Stacked AES spectra measured at four different points on thin film cast from PFO, showing a carbon peak at ca. 260 nm, and no oxygen peak (highlighted by the grey oval).

External quantum efficiency (EQE) by definition is the ratio of the number of photons emitted per electron injected. The number of electrons per second injected is easily calculated from the measured current as one ampere (A) measures the injection of 6.6241×10^{18} electrons per second. The number of photons emitted per second requires more work, but can be calculated from the measured spectrum. The intensity is measured at each wavelength in units of watts (W) per meter (m) squared steradian (sr). Assuming one sr, and that the detector is a square centimeter, the intensity at each wavelength can be converted to units of energy per second using the formula $(\text{W}/\text{m}^2 \cdot \text{sr}) \cdot (1 \text{ m}/100 \text{ cm})^2 \cdot 1 \text{ sr}$. This can then be divided by the energy of a photon to calculate the number of photons emitted at that wavelength (formula: $(x \text{ J/s}) / (hc/\lambda)$ where x = the value calculated from the intensity, $h = 6.626 \times 10^{-34} \text{ J}\cdot\text{s}$, $c = 2.99 \times 10^8 \text{ m/s}$, and λ = wavelength in m). The number of photons per second at each wavelength can then be summed, providing the total number of photons emitted per second, and divided by the number of electrons injected per second. Multiplying this number by 100 gives the EQE in percent.

Appendix 3 (A3)

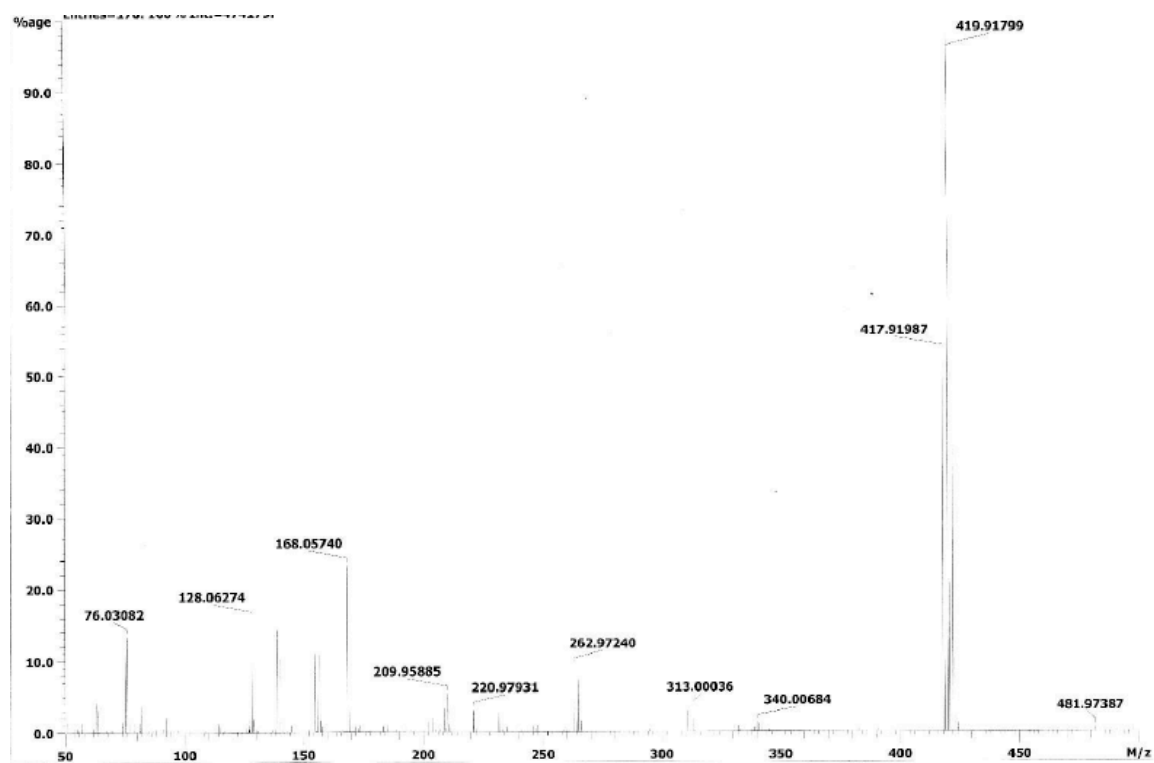


Figure A3-1 EI MS of bis(4-bromophenoxy) benzene.

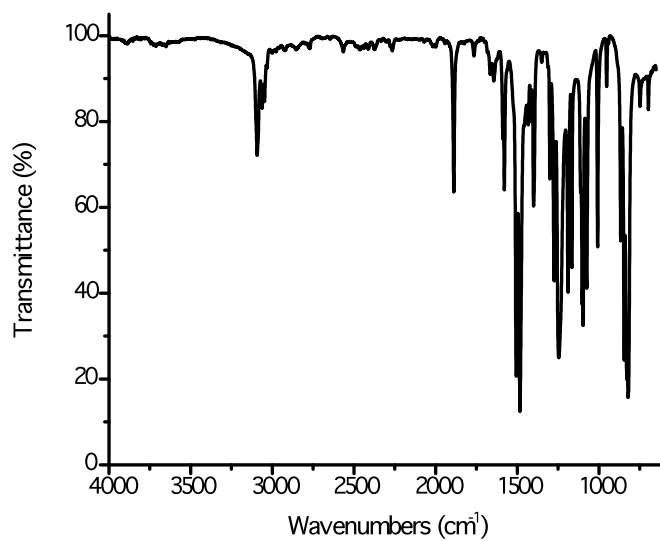


Figure A3-2 FTIR spectrum of bis(4-bromophenoxy) benzene.

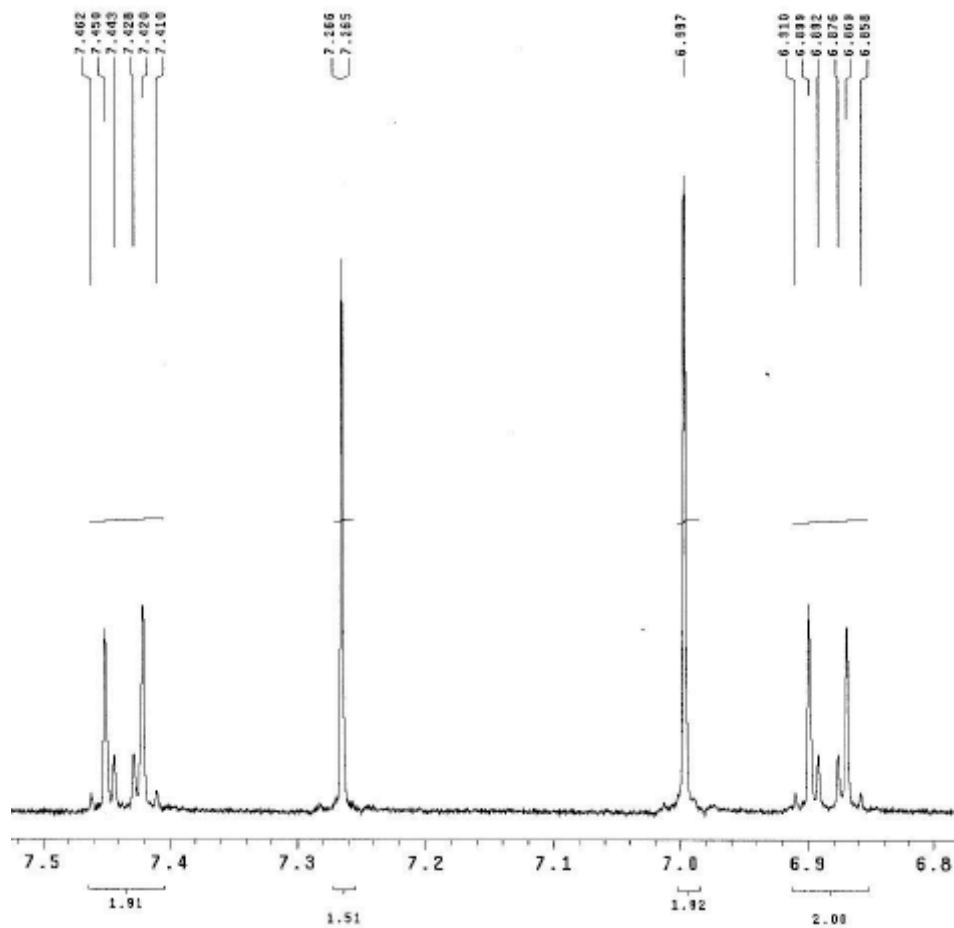


Figure A3-3 ^1H NMR spectrum of bis(4-bromophenoxy) benzene.

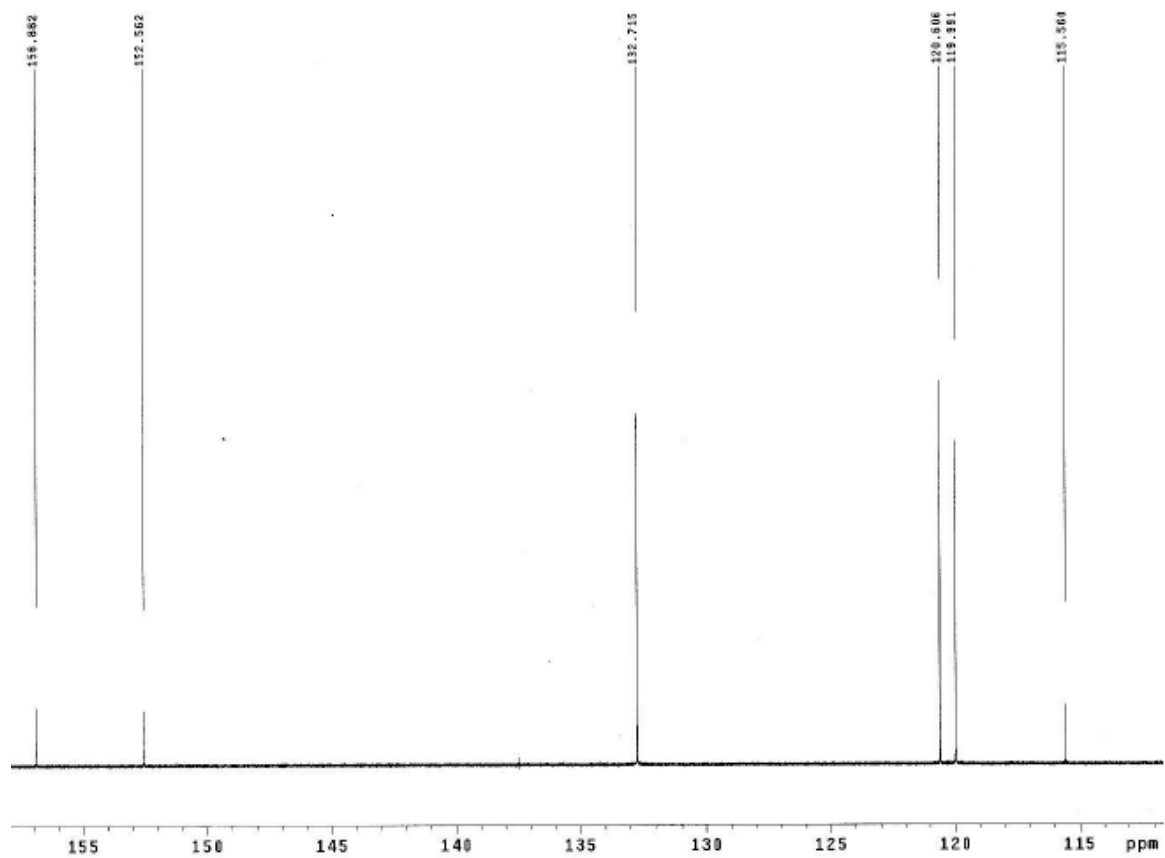


Figure A3-4 ^{13}C NMR spectrum of bis(4-bromophenoxy) benzene.

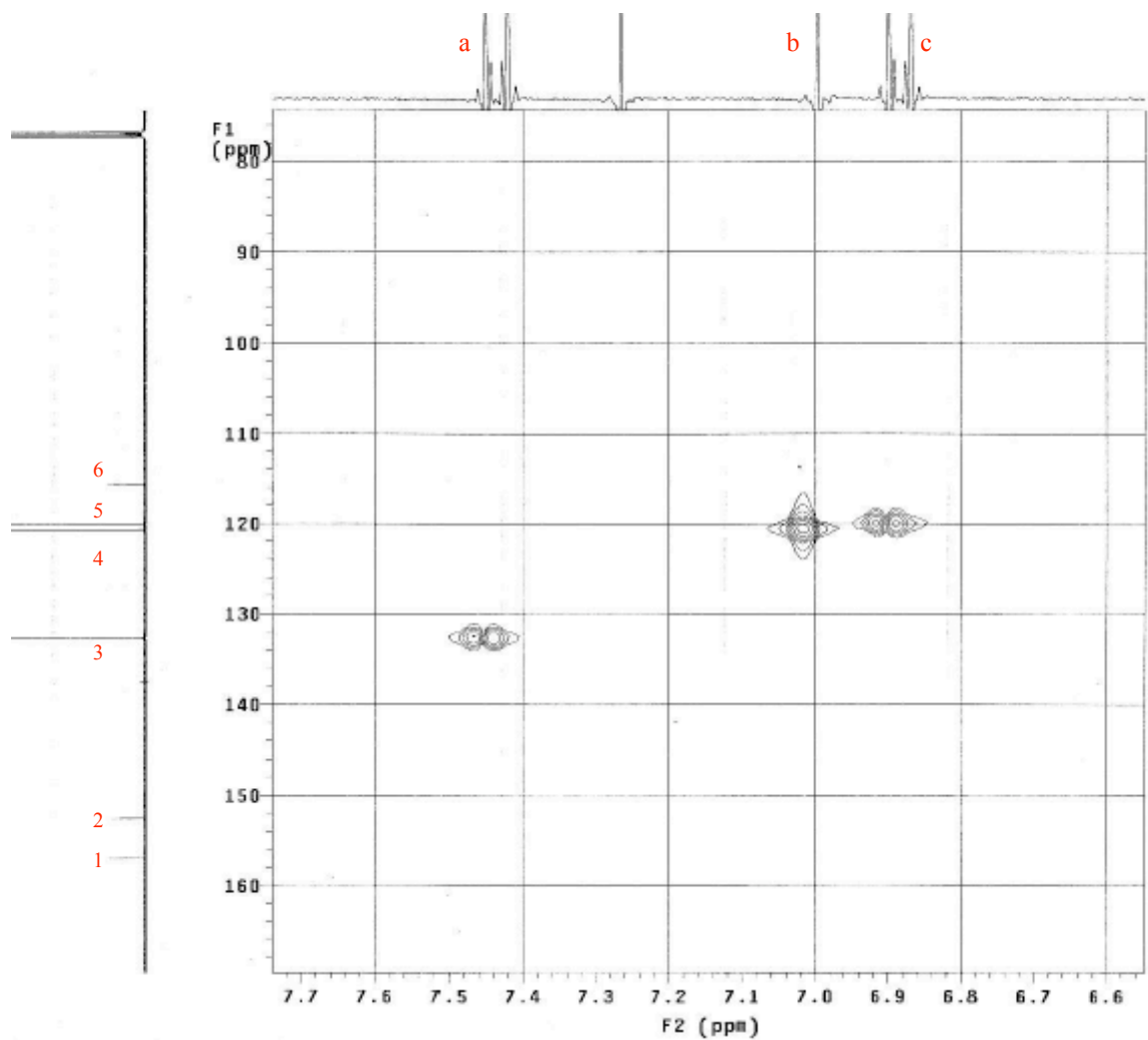


Figure A3-5 HMQC 2D NMR spectrum of bis(4-bromophenoxy) benzene.

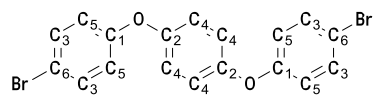


Figure A3-6 Bis(4-bromophenoxy) benzene with ^{13}C NMR assignments shown. ^1H NMR assignments are as follows: a protons are bonded to C_3 's, b protons are bonded to C_4 's, and c protons are bonded to C_5 's.

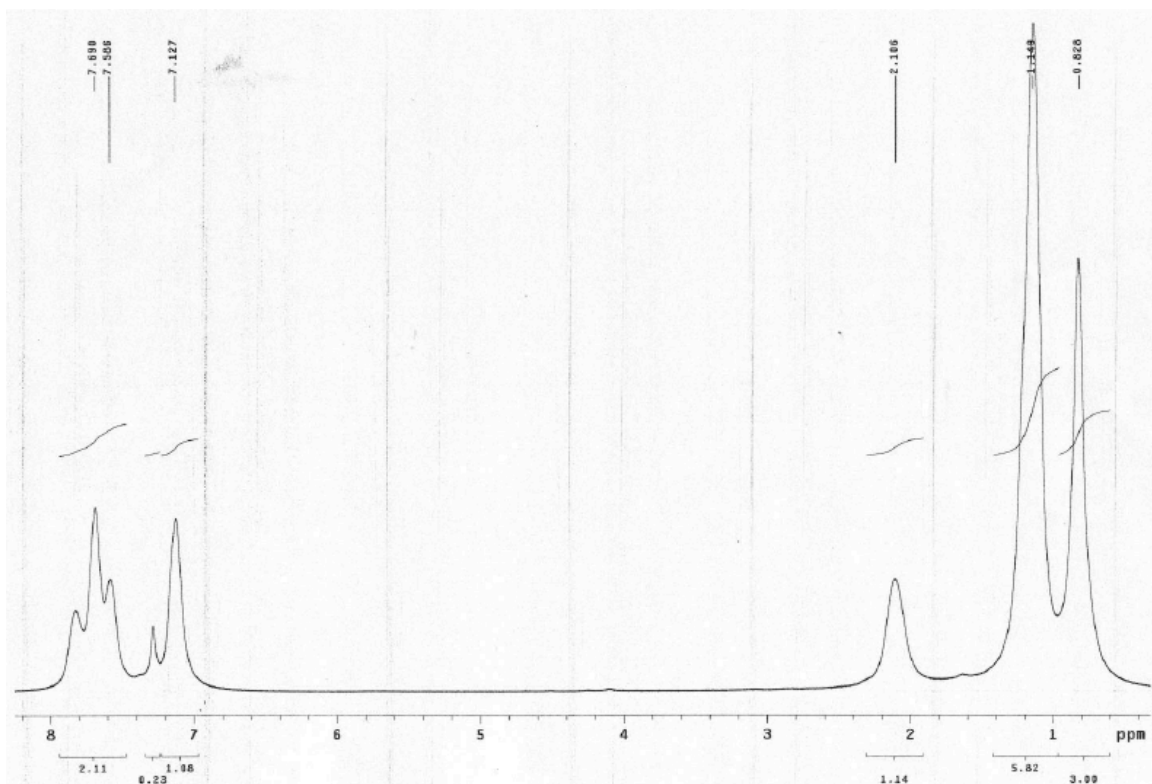


Figure A3-7 ^1H NMR spectrum of 2:1 PAEFO.

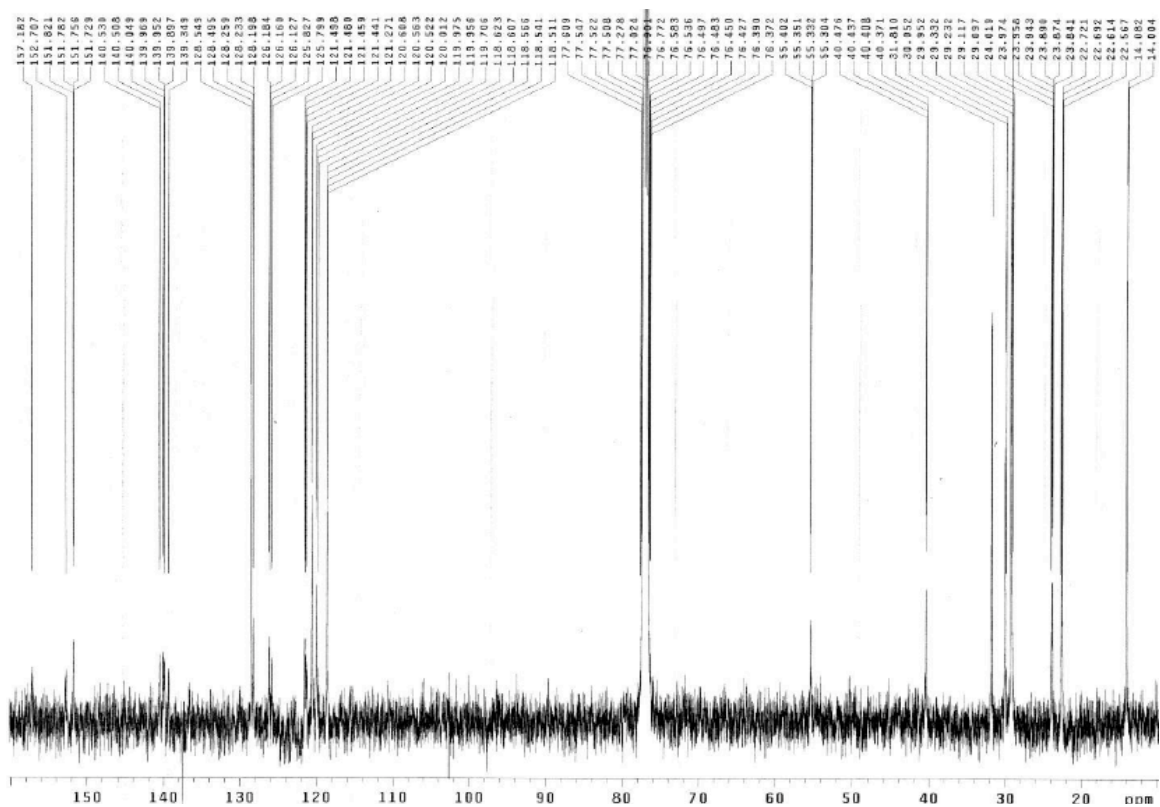


Figure A3-8 ^{13}C NMR spectrum of 2:1 PAEFO.

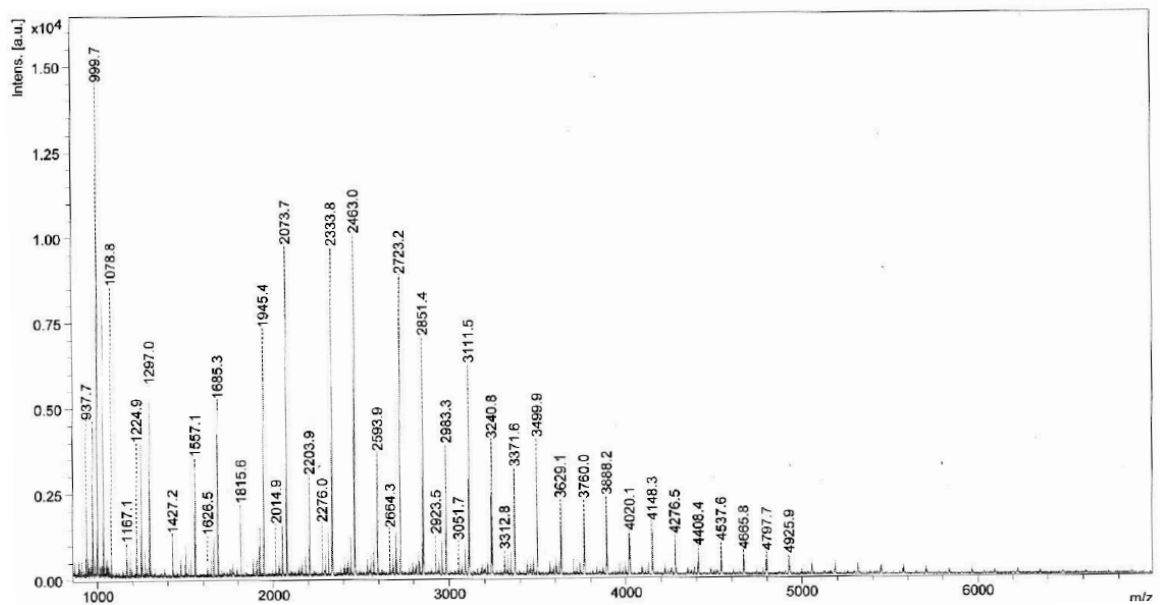


Figure A3-9 MALDI-TOF MS of 2:1 PAEFO.

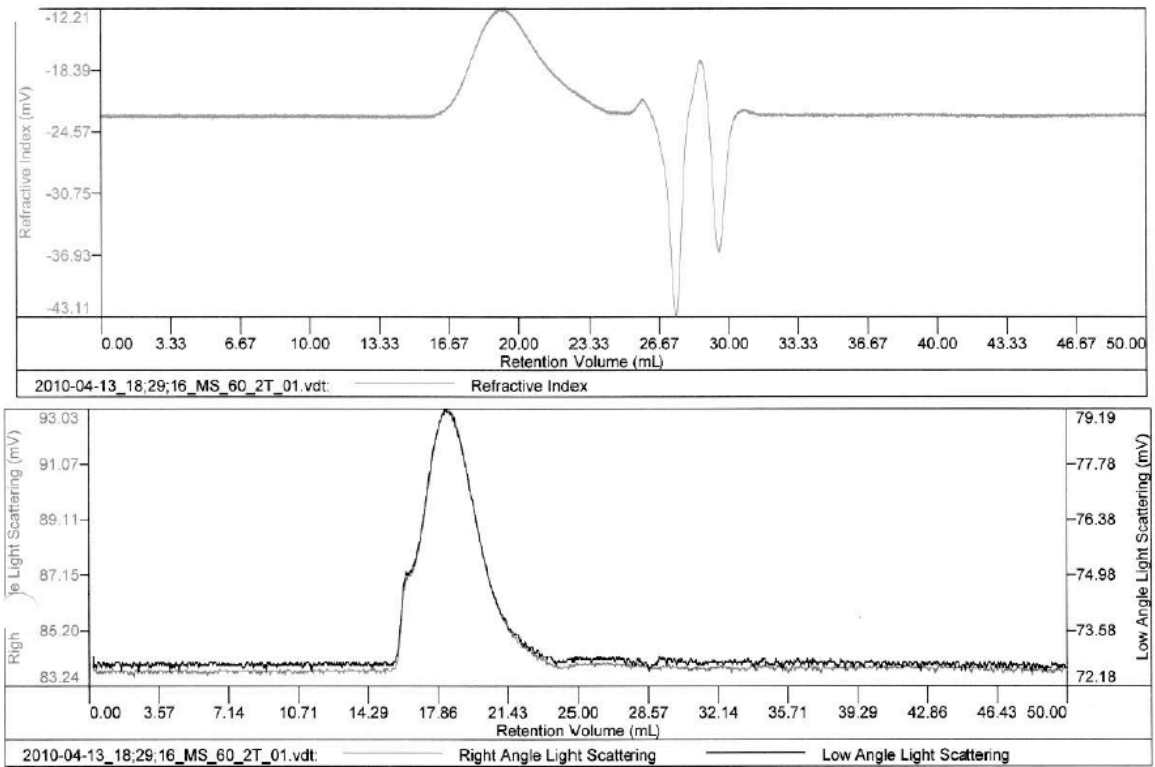


Figure A3-10 GPC of 2:1 PAEFO.

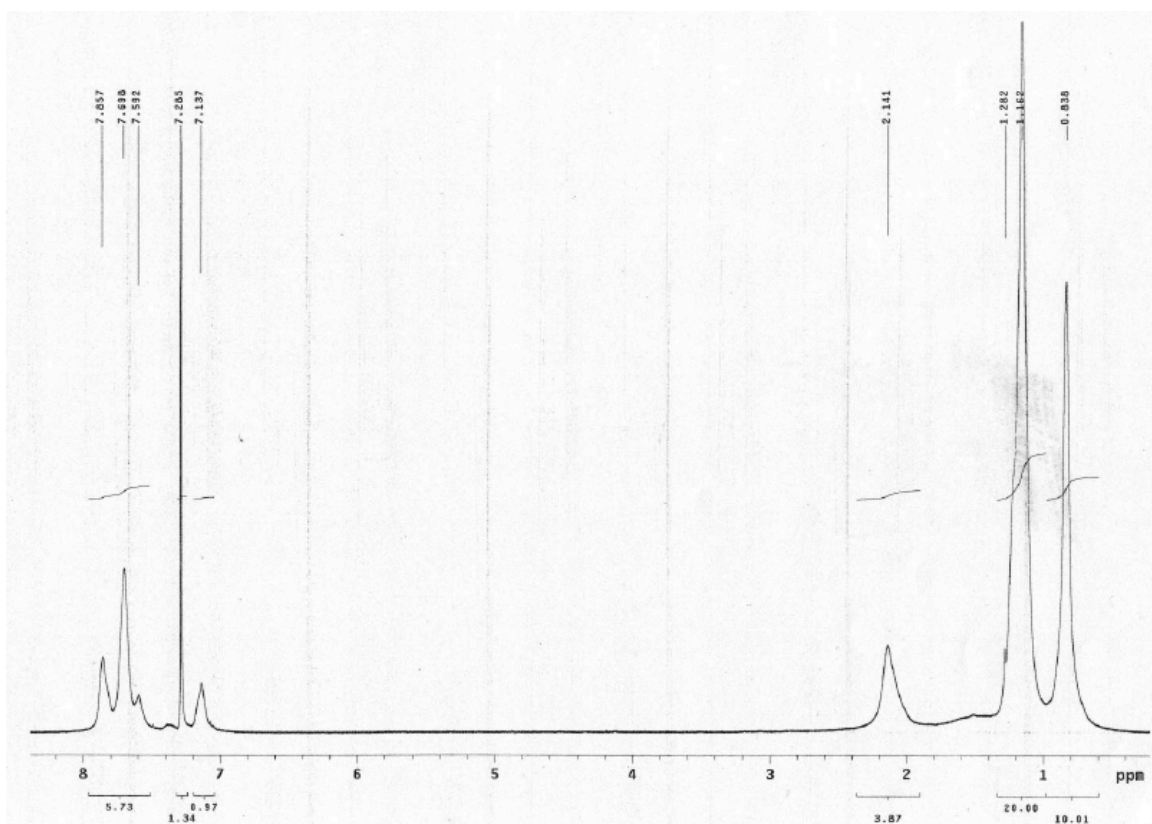


Figure A3-11 ^1H NMR spectrum of 7:1 PAEFO.

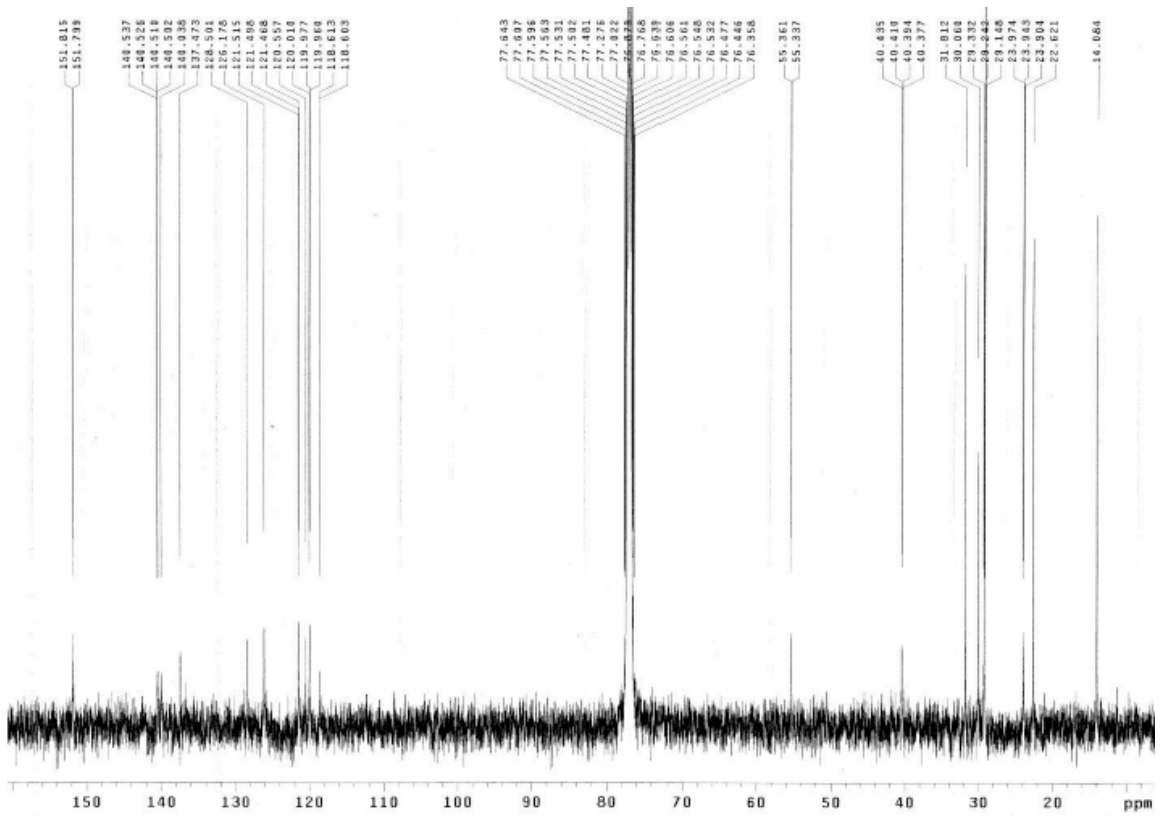


Figure A3-12 ¹³C NMR spectrum of 7:1 PAEFO.

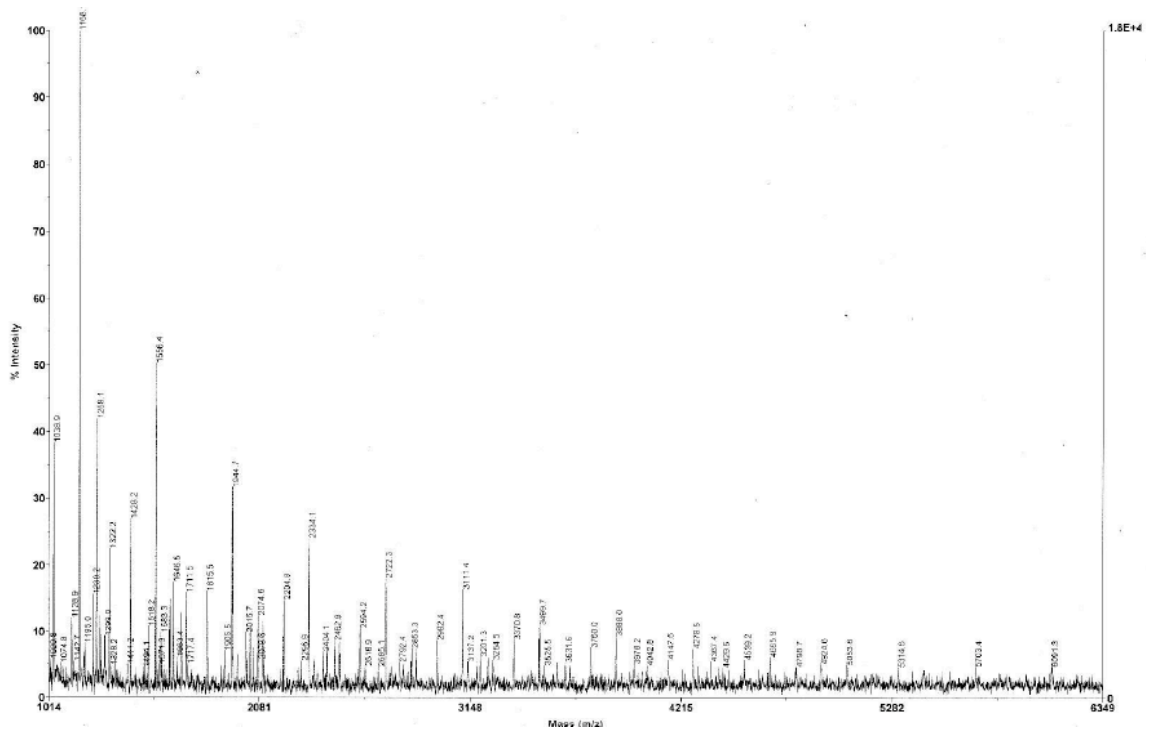


Figure A3-13 MALDI-TOF MS of 7:1 PAEFO.

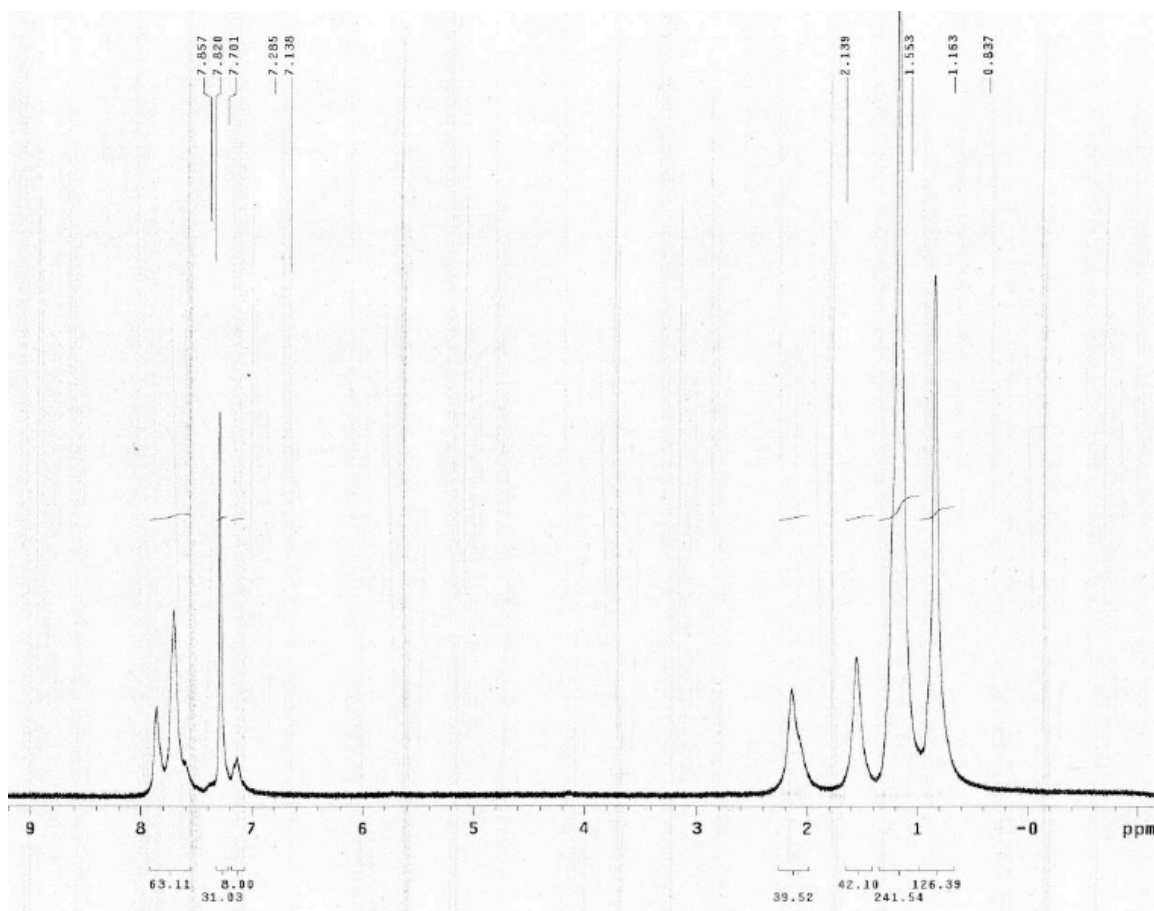


Figure A3-14 ^1H NMR spectrum of 13:1 PAEFO.

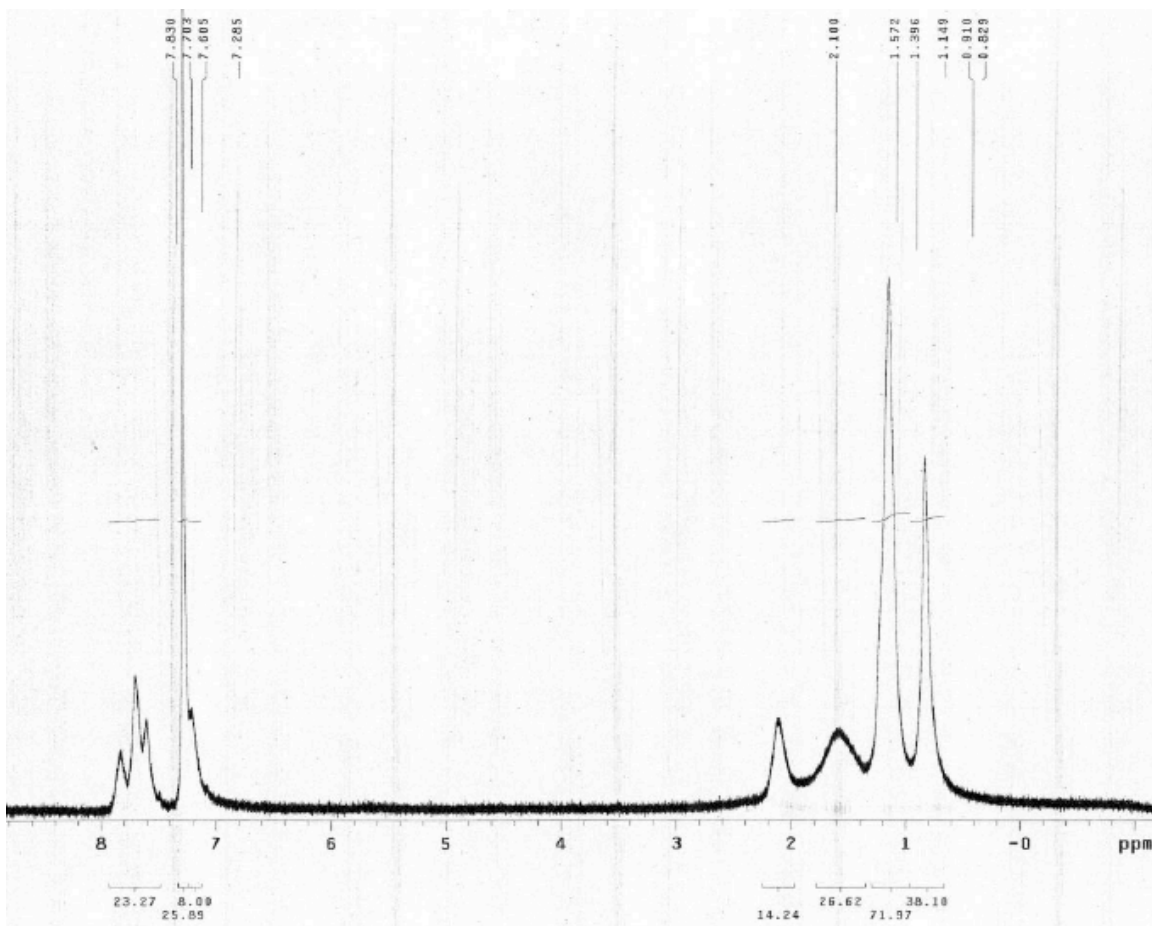


Figure A3-17 ^1H NMR spectrum of 2:1 PAEFO-2.

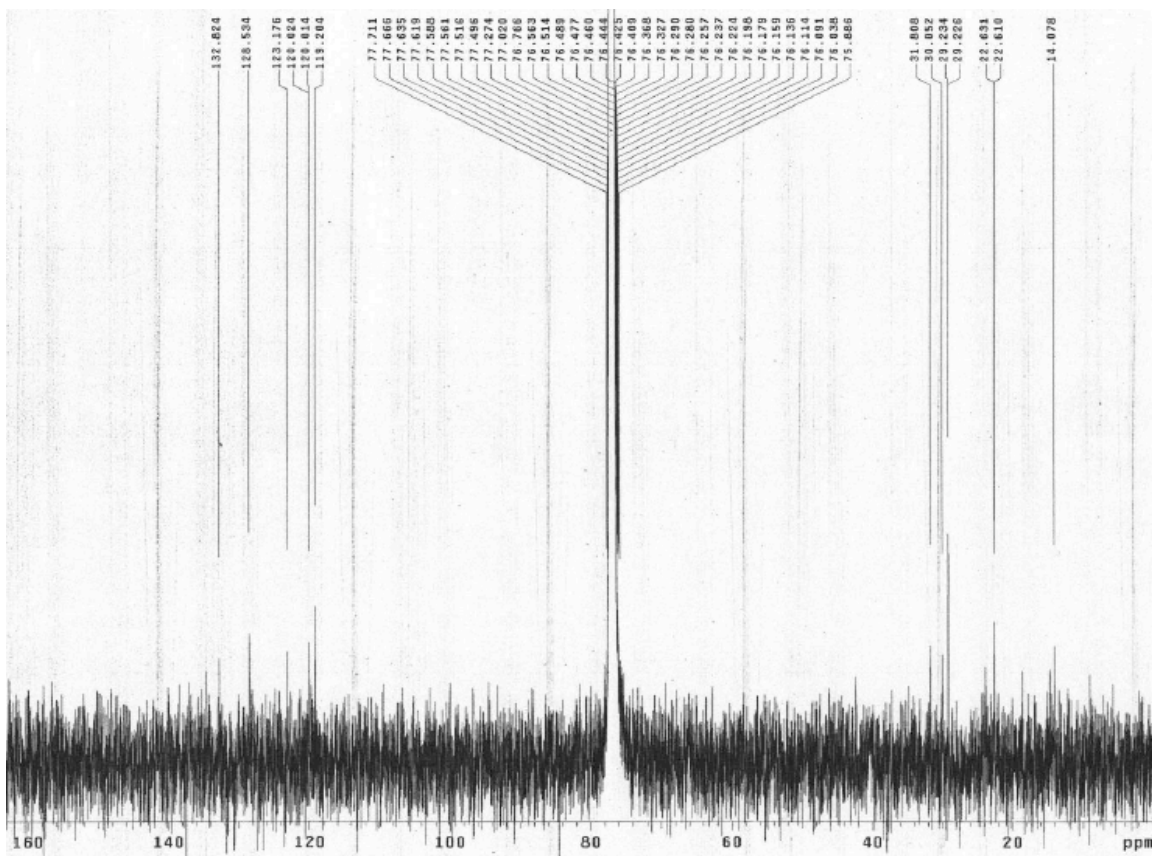
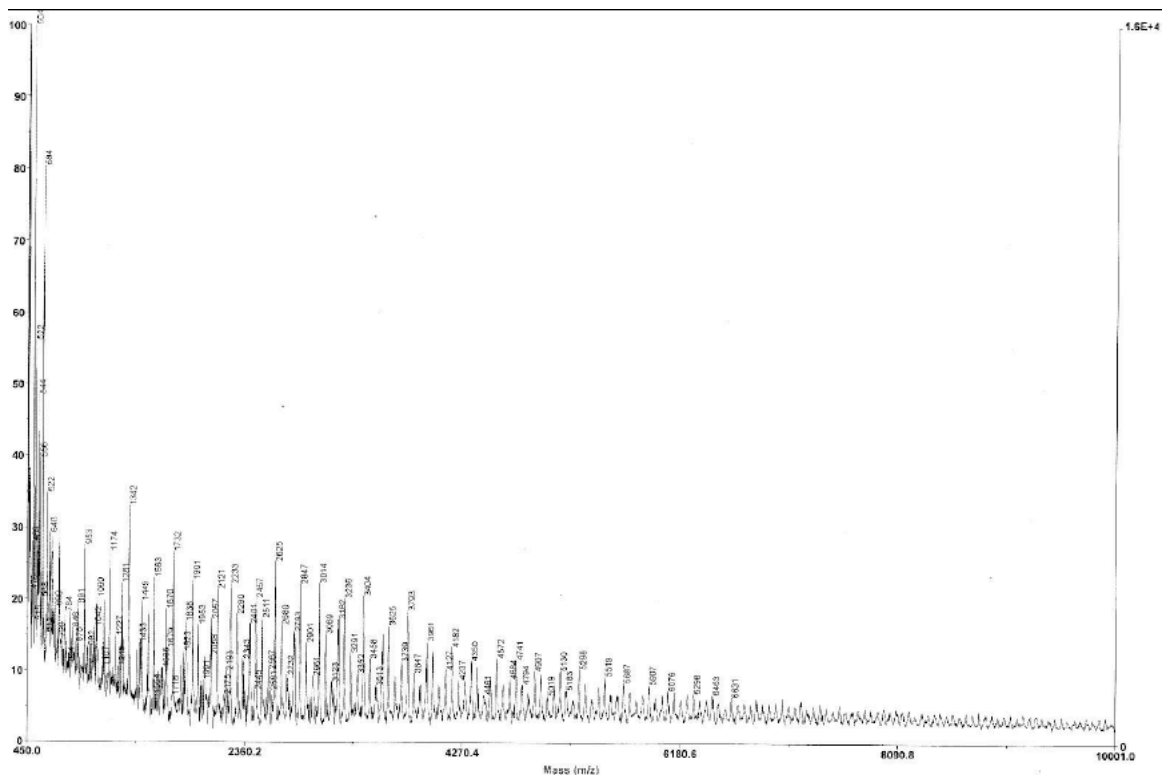


Figure A3-18 ^{13}C NMR spectrum of 2:1 PAEFO-2.



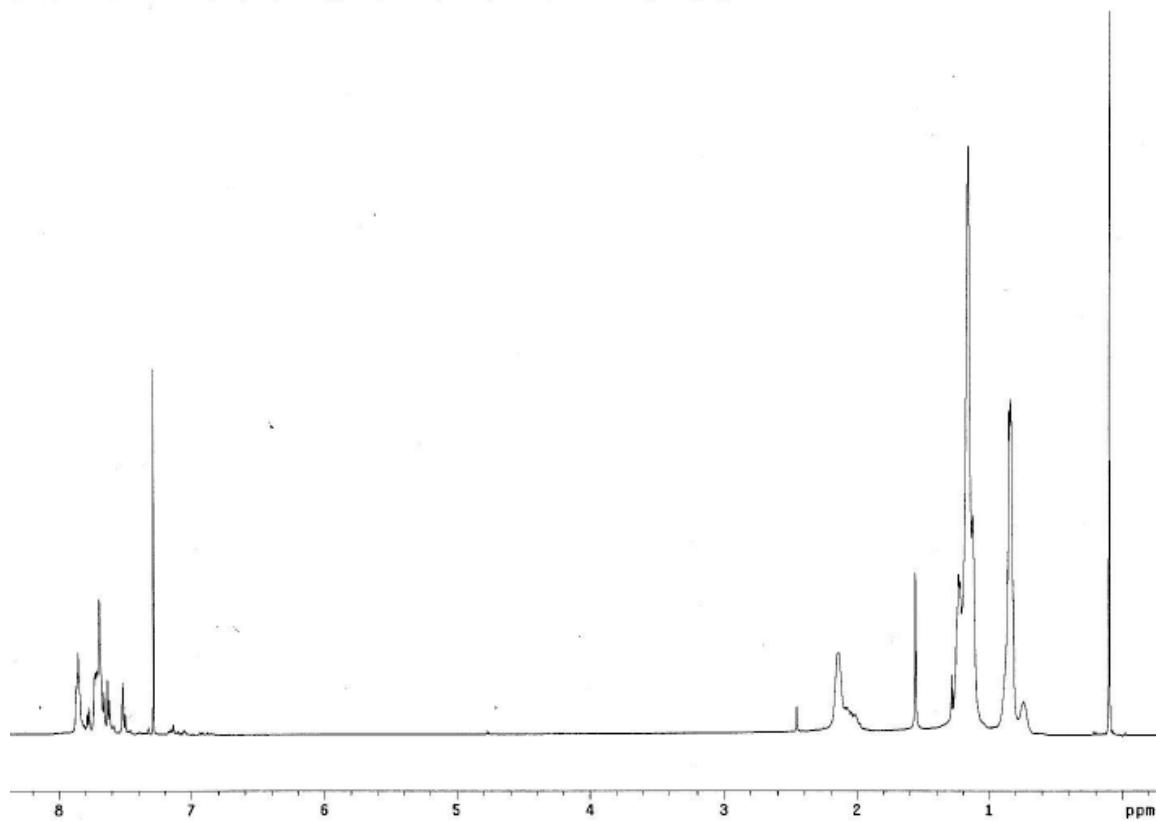


Figure A3-23 ^1H NMR spectrum of PAEFO-S.

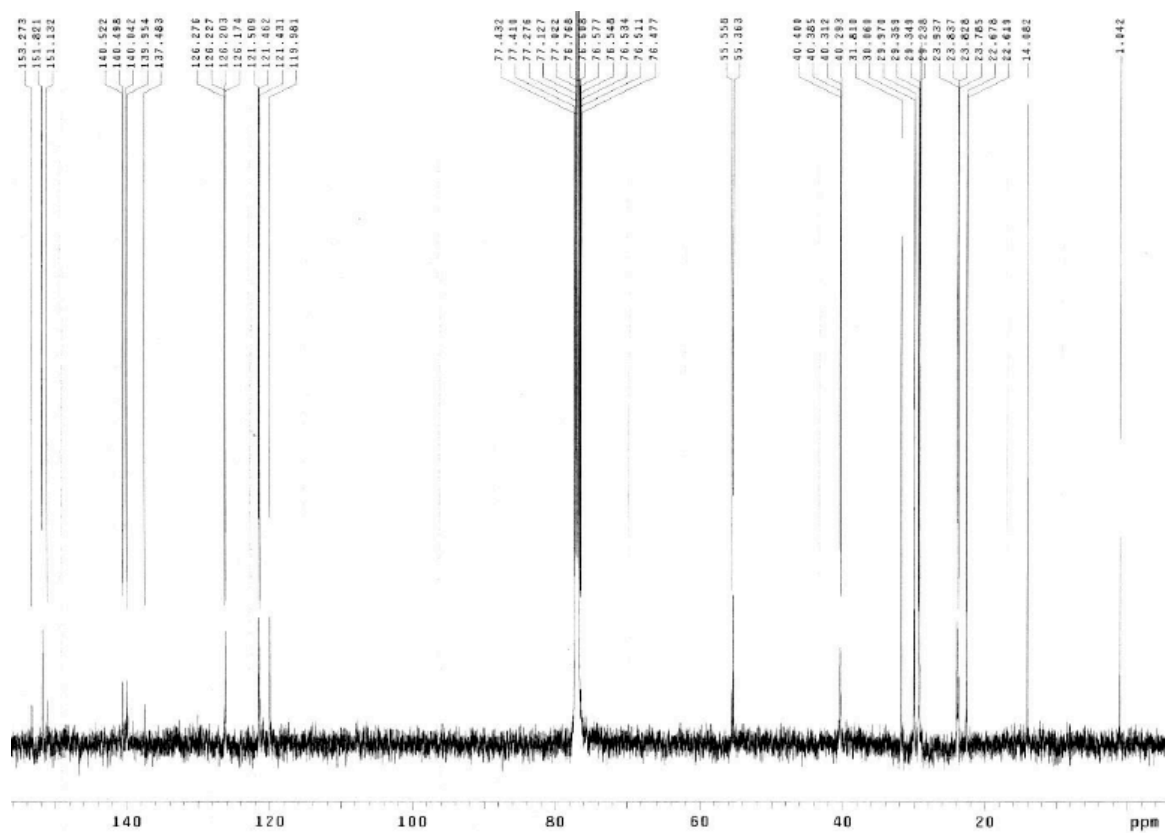


Figure A3-24 ^{13}C NMR spectrum of PAEFO-S.

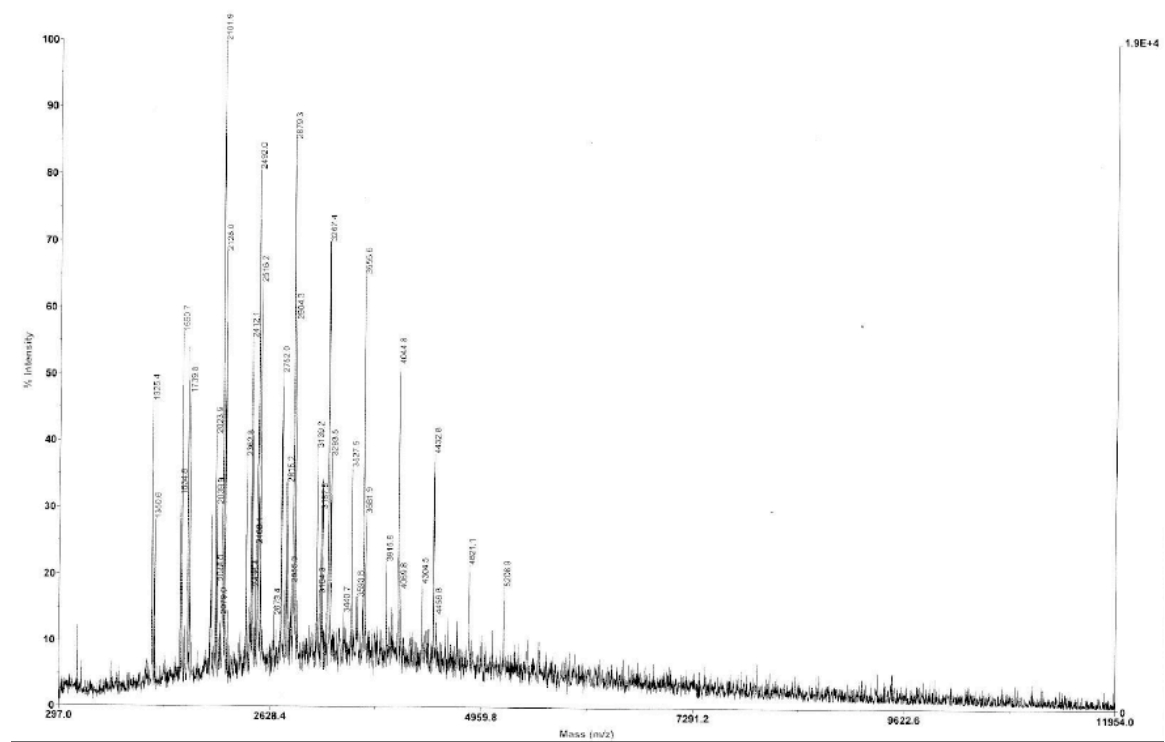


Figure A3-25 MALDI-TOF MS of PAEFO-S.



Figure A3-26 Photograph demonstrating the magnetic properties in PAEFO.

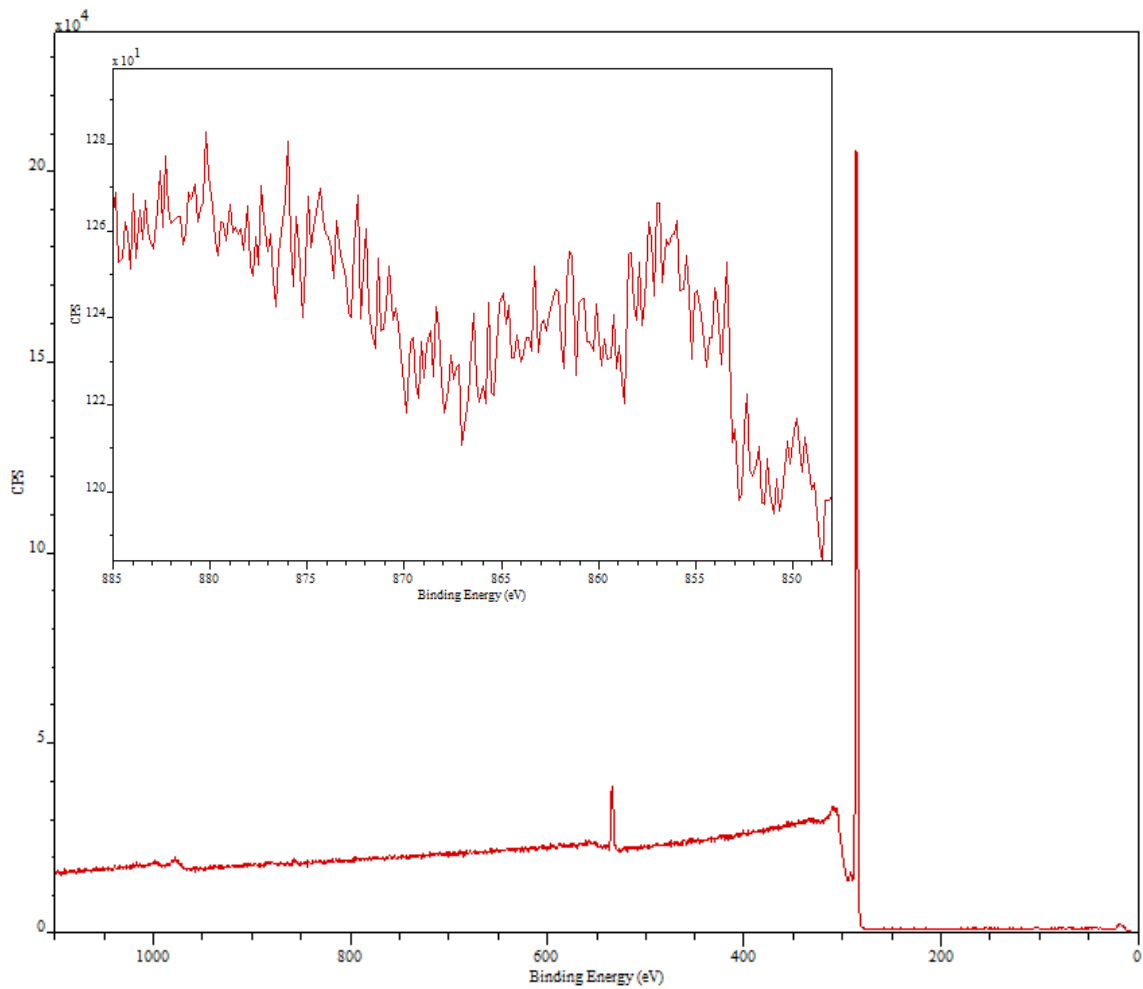


Figure A3-27 XPS of 11:1 PAEFO-2 showing region for Ni(0) in the inset.

Appendix 4 (A4)

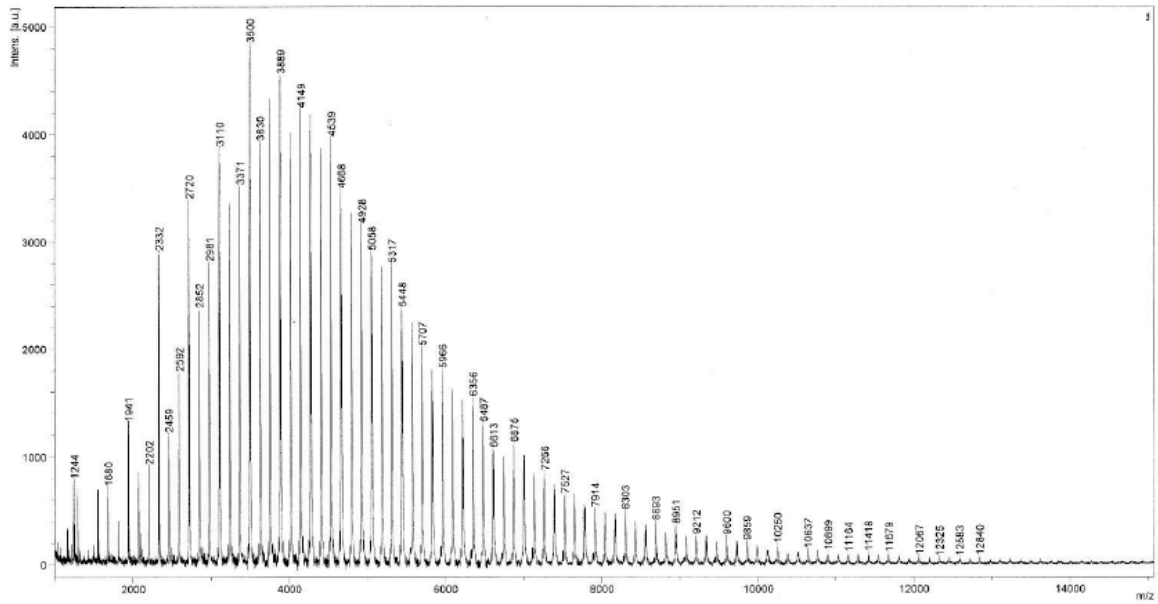


Fig. A4-1 MALDI-TOF MS of PAEFO synthesized without the use of a microwave.

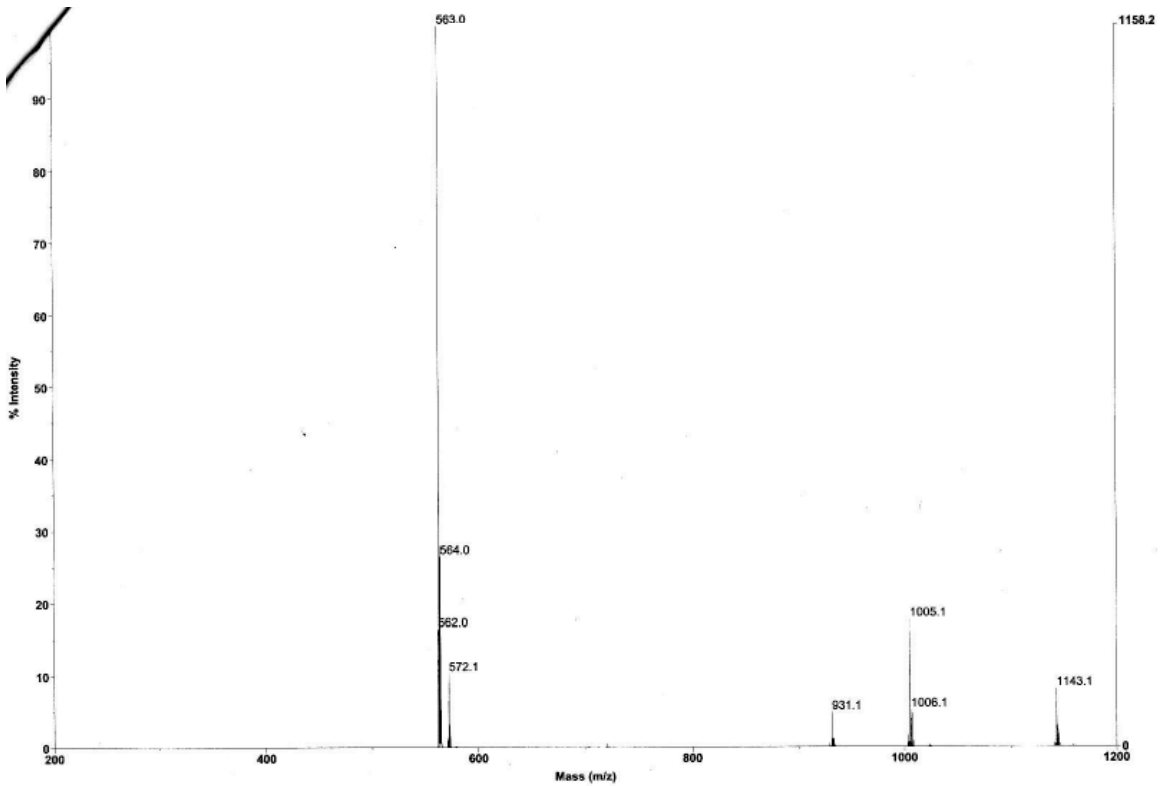


Fig. A4-2 ES MS of CAEF-1.

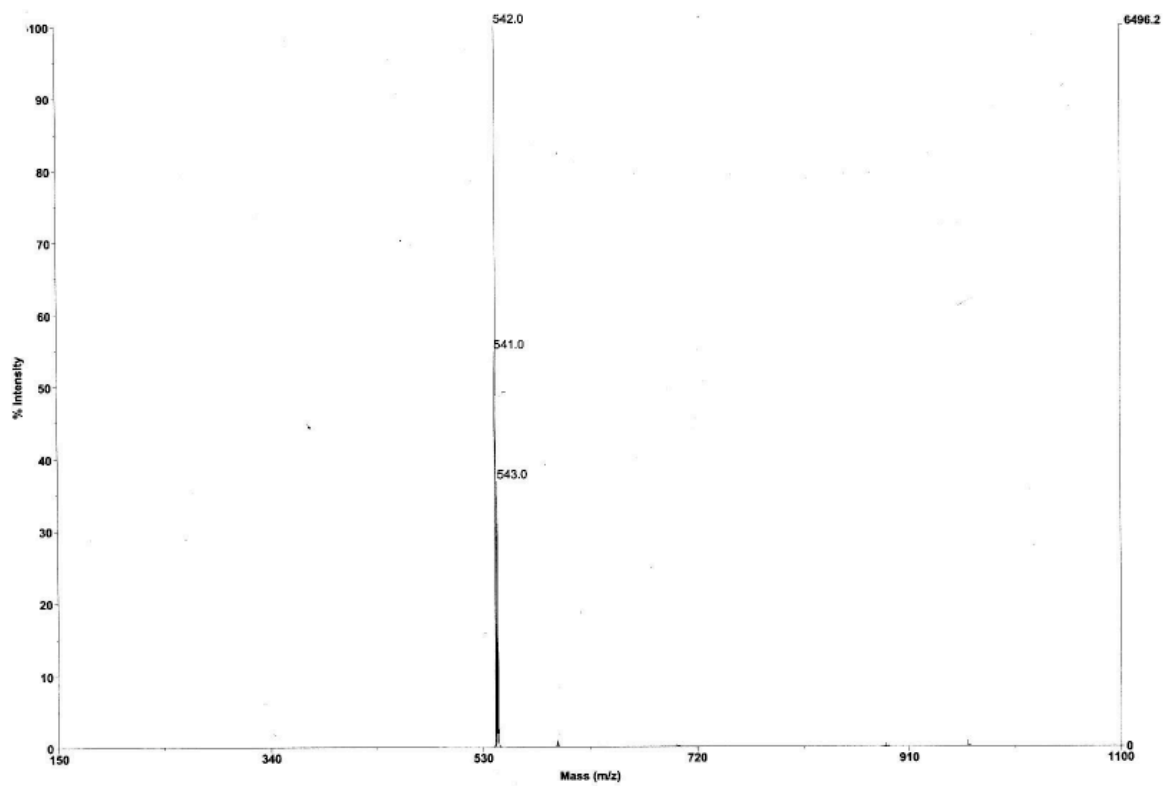


Fig. A4-3 ES MS of CAEF-2.

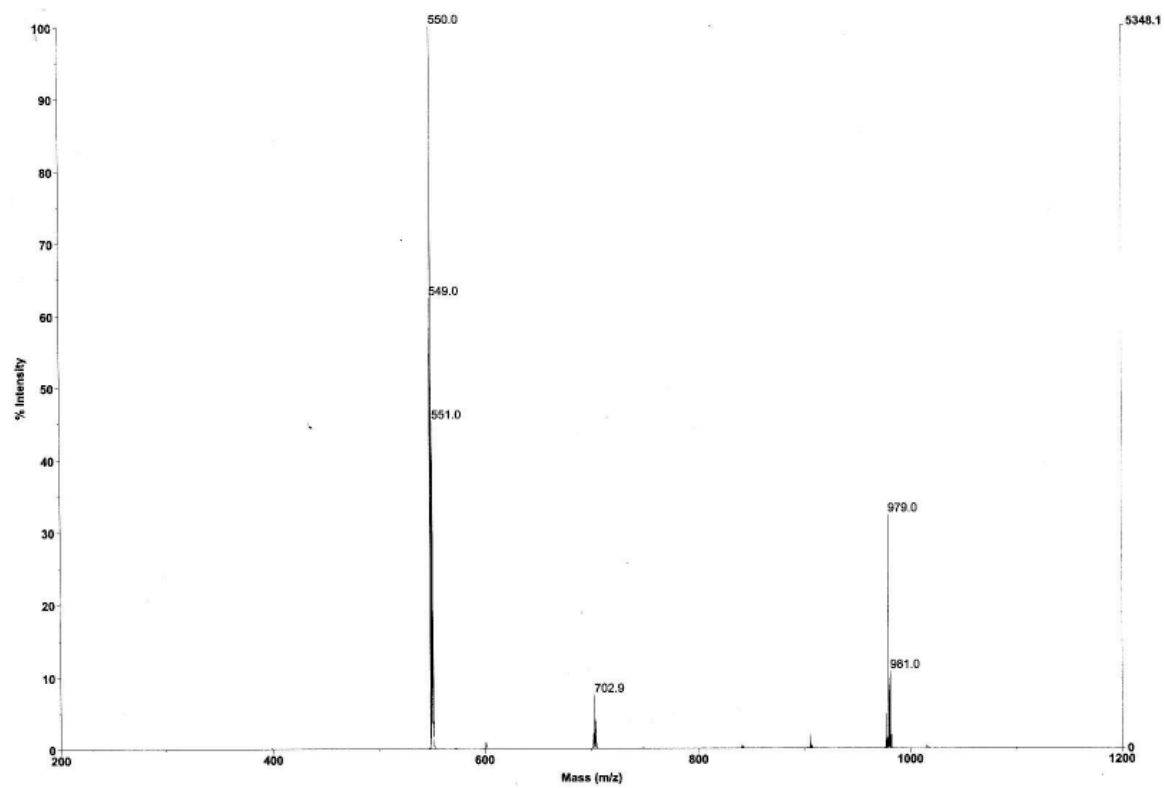


Fig. A4-4 ES MS of CAEF-3.

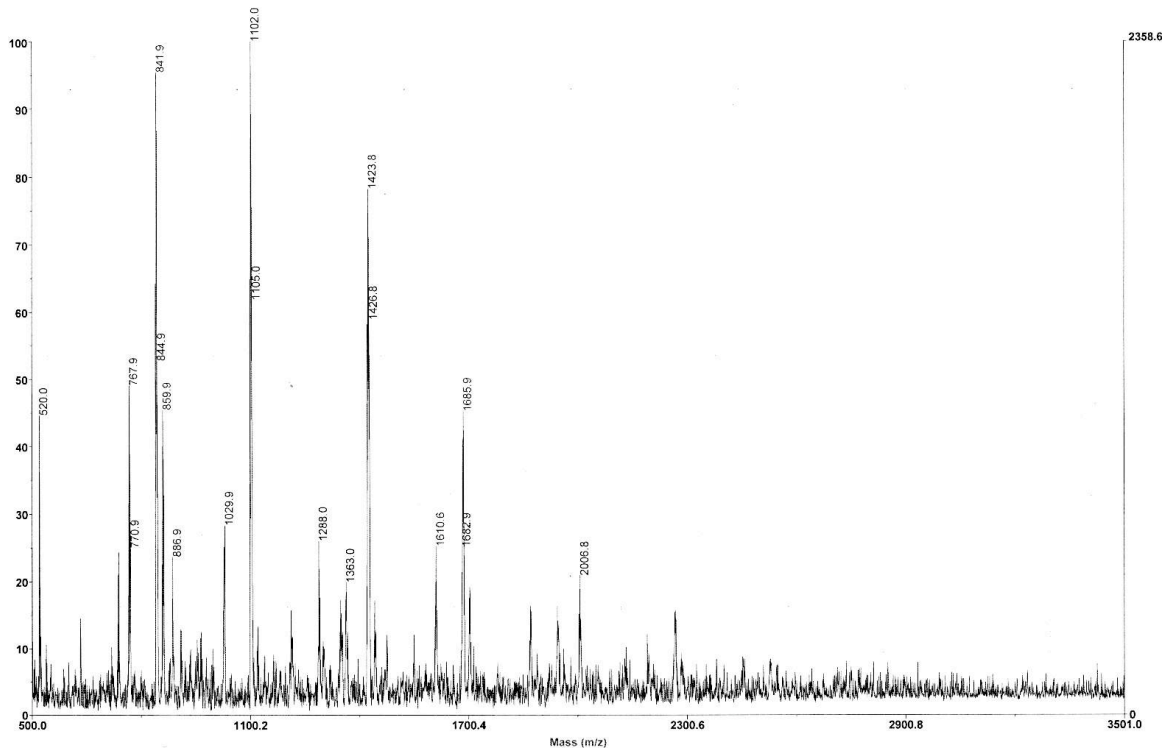


Fig. A4-5 MALDI-TOF MS of CAEF-2.

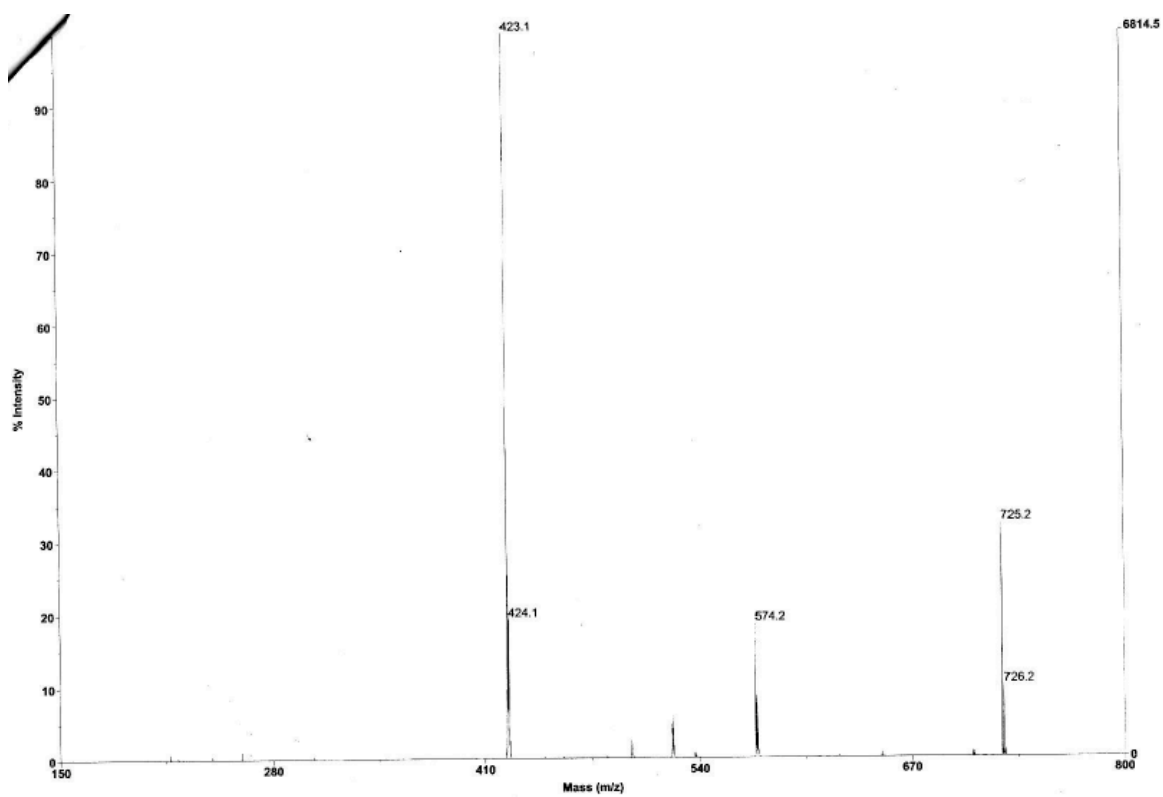


Fig. A4-6 ES MS of CAE-1.

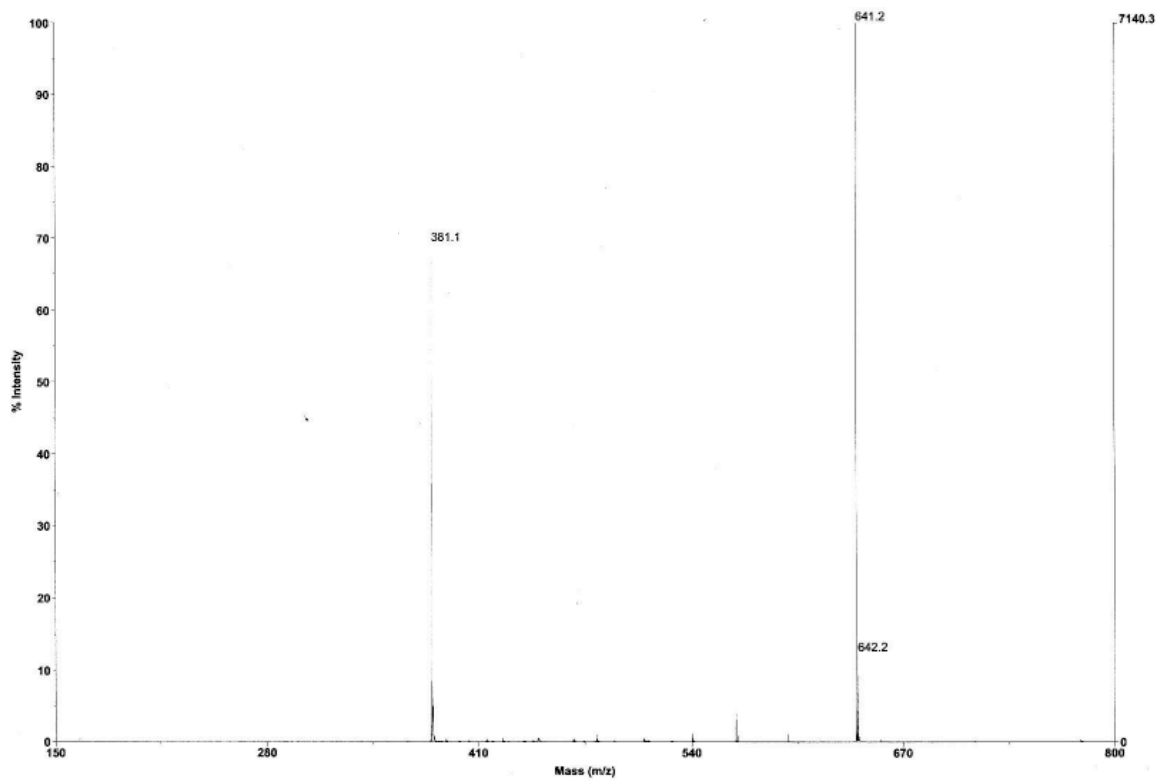


Fig. A4-7 ES MS of CAE-2.

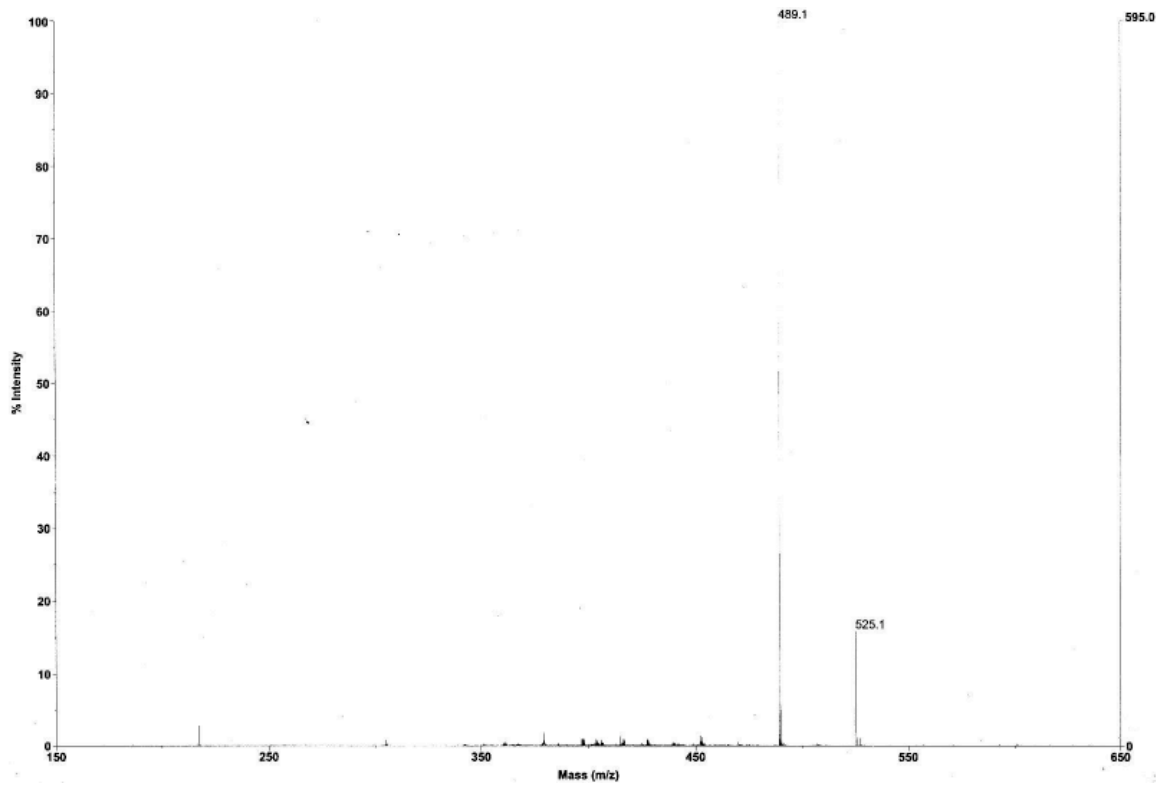


Fig. A4-8 ES MS of CAE-3.

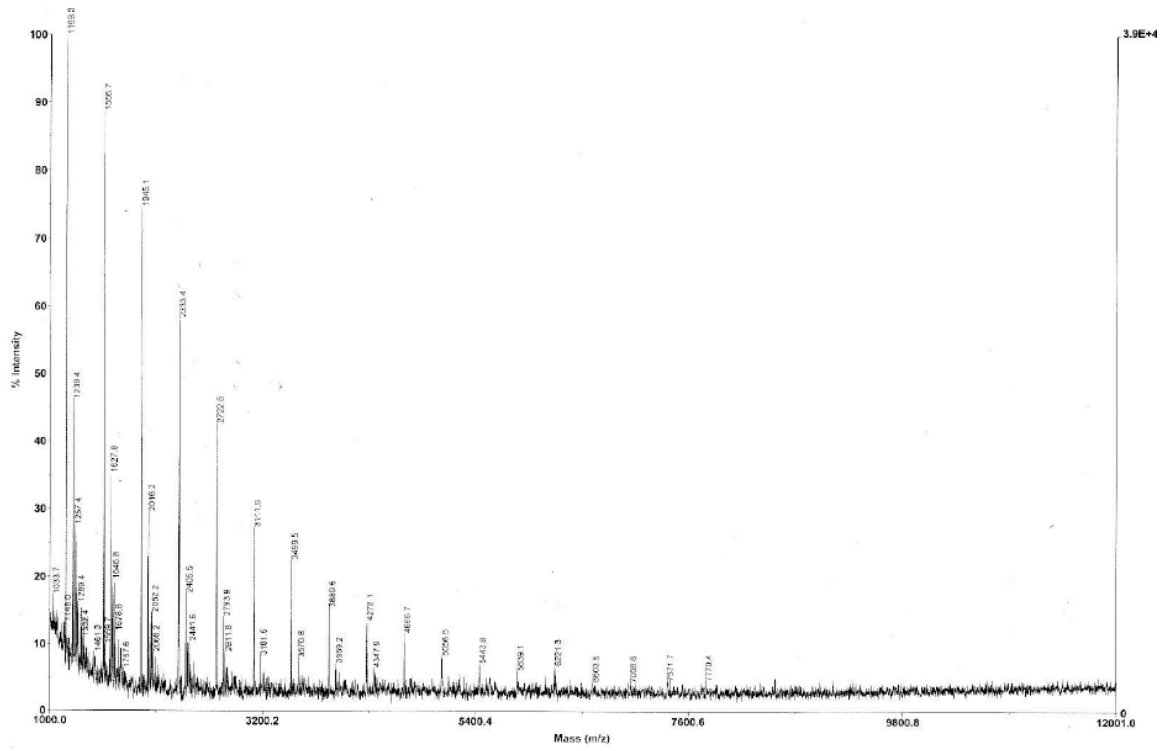


Fig. A4-9 MALDI-TOF MS of PSFO.